

Copyright

by

Jai-Pil Choi

2003

**The Dissertation Committee for Jai-Pil Choi Certifies that this is the  
approved version of the following dissertation:**

**ELECTROGENERATED CHEMILUMINESCENCE WITH  
AMINE AND BENZOYL PEROXIDE COREACTANTS:  
REACTIVITY AND REACTION MECHANISM STUDIES**

**Committee:**

---

Allen J. Bard, Supervisor

---

Eric V. Anslyn

---

Keith J. Stevenson

---

David A. Vanden Bout

---

Arumugam Manthiram

**ELECTROGENERATED CHEMILUMINESCENCE WITH  
AMINE AND BENZOYL PEROXIDE COREACTANTS:  
REACTIVITY AND REACTION MECHANISM STUDIES**

**by**

**Jai-Pil Choi, B.S., M.S.**

**Dissertation**

Presented to the Faculty of the Graduate School of

The University of Texas at Austin

in Partial Fulfillment

of the Requirements

for the Degree of

**Doctor of Philosophy**

**The University of Texas at Austin**

**December, 2003**

## **Dedication**

To my family who have endlessly supported and encouraged me: my precious daughter, Seung Hye Choi, my loving wife, Hee Sun Yang, my esteemed parents and parents-in-law, Myung Hwan Choi, Se Ja Moon, Jae Cheon Yang, and Kil Soon Cho.

## **Acknowledgements**

The author would like to acknowledge Professor Allen J. Bard in gratitude for his guidance and support of author's research. The author would like to thank Dr. Wujian Miao for his helpful discussion on the ECL mechanism of amine coreactants, Dr. Don O'Connor for fluorescence lifetime measurements, Dr. Ken-Tsung Wong for providing ter(9,9-diarylfurorene)s. The author would also like to thank Drs. Fu-Ren F. Fan, Katherine Holt, Bob LeSure, and Donald Pile for their revision of this dissertation.

**ELECTROGENERATED CHEMILUMINESCENCE WITH  
AMINE AND BENZOYL PEROXIDE COREACTANTS:  
REACTIVITY AND REACTION MECHANISM STUDIES**

Publication No. \_\_\_\_\_

Jai-Pil Choi, Ph.D.

The University of Texas at Austin, 2003

Supervisor: Allen J. Bard

The electrogenerated chemiluminescence (ECL) of tris(2,2'-bipyridine)ruthenium(II),  $\text{Ru}(\text{bpy})_3^{2+}$ , was investigated using amine coreactants. When amine coreactants were oxidized, they produced both sufficiently strong reducing ( $\text{R}_2\text{NC}^\bullet\text{HR}'$ ) and oxidizing ( $\text{R}_2\text{N}^{\bullet+}\text{CH}_2\text{R}'$ ) agents and these agents were relatively stable to diffuse and react with  $\text{Ru}(\text{bpy})_3^{2+}$  or electrochemically generated  $\text{Ru}(\text{bpy})_3^{3+}$  to generate  $\text{Ru}(\text{bpy})_3^{2+*}$ . Most amine coreactants produced two ECL waves in a plot of ECL vs electrode potentials: the first occurred before the oxidation of  $\text{Ru}(\text{bpy})_3^{2+}$  and the second occurred immediately after the oxidation of  $\text{Ru}(\text{bpy})_3^{2+}$ , implying two different ECL mechanisms participate in the first and second ECL, except for *N, N, N', N'*-tetra-*n*-propylmethane diamine

and *N, N, N', N'*-tetra-*n*-propylethylene diamine. ECL produced by monoamine coreactants gave stronger emissions than diamines, and acyclic amines produced stronger ECL than heteroalicyclic amines. The ECL intensity increased as the number of carbon atoms increased in the same group of amines except for those with the piperazine group. Tri-*n*-propylamine produced the most intense first and second ECL.

Benzoyl peroxide (BPO) was studied as a new coreactant for neutral red (NR), ter(9,9-diarylfuorene)s (TDAFs) and Ru(bpy)<sub>3</sub><sup>2+</sup>. When BPO was reduced, it produced the strong oxidizing agent, C<sub>6</sub>H<sub>5</sub>CO<sub>2</sub><sup>•</sup> via an ECE process. Then electrochemically reduced NR<sup>•-</sup>, TDAF<sup>•-</sup>, or Ru(bpy)<sub>3</sub><sup>+</sup> reacted with C<sub>6</sub>H<sub>5</sub>CO<sub>2</sub><sup>•</sup> to produce ECL. At a high concentration of BPO (e.g. > 10 mM compared to 0.5 mM NR), ECL quenching by BPO was significant, as confirmed by fluorescence quenching experiments. NR could be used as both a pH indicator and ECL emitter in acetonitrile. A yellow-to-red color change was observed when a NR solution was titrated with acids. The protonated form of NR (NRH<sup>+</sup>) did not produce ECL due to two-electron reduction of NRH<sup>+</sup> and lack of sufficient energy for the ECL reaction. However, NR generated ECL emission of 610 nm. TDAFs emitted at ~ 400 nm (blue ECL). In annihilation ECL, significant emission of TDAF excimers, mainly formed by coulombic interactions when radical cations were annihilated by radical anions, interfered with their blue emission ( $\phi_{\text{ECL}} \leq 0.05 \%$ ) Excimers

were not observed in fluorescence. No significant excimer emission was found when BPO coreactant was used.

## Table of Contents

List of Tables.....	xiii
List of Figures .....	xiv
List of Schemes .....	xxiii
Chapter 1 Fundamentals of Electrogenerated Chemiluminescence (ECL).....	1
1.1 Introduction .....	1
1.2 Ion Annihilation .....	2
1.3 Coreactants .....	5
1.4 Formation of Excimers or Exciplexes.....	6
1.5 Preannihilation ECL.....	9
1.6 Concluding Remark.....	10
References .....	11
Chapter 2 Electrogenerated Chemiluminescence of Tris(2,2'-bipyridine)ruthenium(II), Ru(bpy) <sub>3</sub> <sup>2+</sup> /Tri- <i>n</i> -propylamine (TPrA) System – A New Route Involving TPrA <sup>*+</sup> Cation Radicals.....	14
2.1 Introduction.....	14
2.2 Experimental Section .....	18
Chemicals .....	18
Immobilization of Ru(bpy) <sub>2</sub> [bpy(COOH) <sub>2</sub> ] <sup>2+</sup> on an ITO Electrode.....	18
Electrochemical and ECL measurements.....	19
ESR Experiments .....	20
2.3 Results and Discussion.....	22
Electrochemical and ECL behavior of the Ru(bpy) <sub>3</sub> <sup>2+</sup> /TPrA system.....	22
SECM – ECL Experiments .....	30
Fast scan CV and digital simulations .....	38

ESR of TPrA <sup>•+</sup> in aqueous solution.....	42
2.4 Conclusions .....	46
References .....	48
Chapter 3 Structure and Reactivity Aspects of Various Amine Coreactants and Coreactive Buffers on the Electrogenerated Chemiluminescence of Tris(2,2'-bipyridine)ruthenium(II) Complex, Ru(bpy) <sub>3</sub> <sup>2+</sup> , in Aqueous Media .....	50
3.1 Introduction .....	50
3.2 Experimental Section .....	54
Chemicals and Solutions .....	54
Syntheses of TPDAM, TPDAE, TPDAP, PP, DEPz, and DPPz .....	59
<i>N,N,N',N'</i> -Tetra- <i>n</i> -propylmethanediamine (TPDAM) .....	59
<i>N,N,N',N'</i> -Tetra- <i>n</i> -propylethylenediamine (TPDAE) .....	60
<i>N,N,N',N'</i> -Tetra- <i>n</i> -propylpropane-1,3-diamine (TPDAP) .....	60
1-Propylpiperidine (PP).....	60
1,4-Diethylpiperazine (DEPz).....	61
1,4-Dipropylpiperazine (DPPz) .....	61
Instruments and Procedures .....	61
3.3 Results and Discussion.....	62
Electrochemistry of Ru(bpy) <sub>3</sub> <sup>2+</sup> and 14 Different Amine Coreactants .....	62
ECL of Ru(bpy) <sub>3</sub> <sup>2+</sup> by amine coreactants.....	66
<i>The first ECL</i> .....	72
<i>The second ECL</i> .....	74
ECL of Ru(bpy) <sub>3</sub> <sup>2+</sup> in Coreactive Buffers .....	83
3.4 Conclusions .....	87
References .....	89
Chapter 4 Acid-Base Properties, Electrochemistry, and Electrogenerated Chemiluminescence of Neutral Red in Acetonitrile .....	92
4.1 Introduction .....	92

4.2 Experimental Section .....	95
Materials.....	95
Spectroscopy .....	96
Electrochemistry.....	96
Electrogenerated Chemiluminescence (ECL) .....	97
4.3 Results and Discussion.....	98
Acid-Base Properties of NR in MeCN .....	98
Electrochemistry of NR and NRH <sup>+</sup> .....	101
Electrogenerated Chemiluminescence (ECL) of NR .....	114
Concentration effects on the ECL of NR .....	121
ECL of Ru(bpy) <sub>3</sub> <sup>2+</sup> with BPO and ECL Efficiency.....	127
4.4 Conclusions .....	131
Supporting Information .....	132
References .....	135
Chapter 5 Electrogenerated Chemiluminescence of	
Ter(9,9-diarylfuorene)s: Excited Singlet State Emission vs. Excimer	
Emission .....	138
5.1 Introduction .....	138
5.2 Experimental Section .....	141
Chemicals .....	141
Apparatus and Instrumentation .....	143
Calculations .....	144
5.3 Results and Discussion.....	144
Absorbance, Fluorescence, and Phosphorescence .....	144
Electrochemistry.....	148
Electrogenerated Chemiluminescence (ECL) – Ion annihilation.....	154
Electrogenerated Chemiluminescence (ECL) – Coreactant.....	160
Modeling the Excimer .....	165
Triplet ECL Emission.....	166

ECL Efficiency.....	168
5.4 Conclusions .....	169
Supporting Information .....	170
References .....	174
Chapter 6 Concluding Remarks .....	177
References .....	181
Appendix A List of Symbols.....	182
Roman Symbols .....	182
Greek Symbols .....	184
Glossary.....	186
References .....	190
Vita .....	202

## List of Tables

Table 3.1:	Summary of Electrochemical Data for the Oxidation of Amines .....	68
Table 3.2:	List of $pK_a$ Values of Coreactants, Optimum pH for the Second ECL and Its ECL intensities .....	82
Table 3.3:	$pK_a$ , Anodic Peak Potential ( $E_p$ ), the First and Second ECL wave Intensities, and the Relative second ECL wave Intensity ( $I_{CB}/I_{TPrA}$ ) of Coreactant Buffers .....	86
Table 4.1:	Summary of $E_{1/2}$ , $n$ , and $D$ for the Reductions of NR and $NRH^+$ .....	112
Table 5.1:	Summary of Spectroscopic Data .....	149
Table 5.2:	Summary of Electrochemical Data .....	153
Table 5.3.:	Physical Data of Ion annihilation Reaction and Coreactant Reaction for ECL .....	155

## List of Figures

Figure 2.1: Setup for SECM – ECL .....	21
Figure 2.2: (a) ECL and (b) cyclic voltammogram of 1.0 nM Ru(bpy) <sub>3</sub> <sup>2+</sup> in the presence of 0.10 M TPrA with 0.1 M Tris/0.10 M LiClO <sub>4</sub> buffer (pH = 8) at a 3 mm diameter glassy carbon electrode at scan rate 50 mV/s. (c) As (a) but with 1.0 μM Ru(bpy) <sub>3</sub> <sup>2+</sup> . The ECL intensity scale is given for (c) and should be multiplied by 100 for (a).....	24
Figure 2.3: Linear sweep voltammograms (LSV) and their corresponding ECL signals for 1 μM Ru(bpy) <sub>3</sub> <sup>2+</sup> and 50 mM TPrA in pH 8.5 PBS at a 3 mm diameter glassy carbon electrode at different scan rates. Inset, plot of the first and the second ECL signals versus $v^{1/2}$ .....	25
Figure 2.4: (a) The first ECL peak intensity as a function of TPrA concentration with 1 μM Ru(bpy) <sub>3</sub> <sup>2+</sup> (0.20 M PBS, pH 7.5). A 3 mm diameter glassy carbon electrode was used at a scan rate of 100 mV/s.....	27
(b) The first ECL peak intensity as a function of Ru(bpy) <sub>3</sub> <sup>2+</sup> concentration with 100 mM TPrA (0.20 M PBS, pH 8.5). A 3 mm diameter glassy carbon electrode was used at a scan rate of 100 mV/s.....	28
(c) The first and the second ECL responses in 100 mM TPrA (0.20 M PBS, pH 8.5) with different Ru(bpy) <sub>3</sub> <sup>2+</sup> concentrations: 1 mM (solid line), 0.50 mM (dashed line), 0.10 mM (dotted line) and 0.05 mM (dash-dotted line). A 3 mm diameter glassy carbon electrode was used at a scan rate of 100 mV/s.....	29

Figure 2.5: An approach curve obtained for the oxidation of 10.0 mM TPrA (0.10 M Tris/0.10 M LiClO <sub>4</sub> buffer, pH = 8) at a 1.5 mm diameter hemispherical Au electrode held at 0.85 V vs. Ag/AgCl. An ITO/OSiRu <sup>II</sup> electrode at open circuit served as the substrate .....	31
Figure 2.6: Cyclic voltammogram and ECL signal obtained in 10.0 mM TPrA (0.10 M Tris/0.10 M LiClO <sub>4</sub> buffer, pH = 8) at a 1.5 mm diameter hemispherical Au electrode when the tip/substrate separation distance, <i>d</i> , was 1.92 μm. A scan rate of 50 mV/s was used, and the substrate was an ITO/OSiRu <sup>II</sup> electrode at open circuit .....	33
Figure 2.7: ECL peak intensity as a function of tip distance .....	34
Figure 2.8: (a) A simulated CV of TPrA oxidation in pH 8 solution at a scan rate of 900 V/s. Parameters used in the simulation were (see Scheme 2.4 for further information): $E^{\circ}_{\text{TPrA}^{*+}/\text{TPrA}} = 0.88$ V vs. Ag/AgCl, $k_s$ (for eqs. 4.2 & 4.4) = 0.01 cm/s, $E^{\circ}_{\text{PI}/\text{TPrA}^{\bullet}} = -1.7$ V vs. Ag/AgCl, for eq. 4.3 $k_f = 3500 \text{ s}^{-1}$ & $k_b = 7 \times 10^6 \text{ s}^{-1}$ , $c_{(\text{TPrA} + \text{TPrAH}^+)} = 10 \text{ mM}$ . All species were assumed to have a diffusion coefficient of $5 \times 10^{-6} \text{ cm}^2/\text{s}$ except for H <sup>+</sup> ( $D_{\text{H}^+} = 5 \times 10^{-5} \text{ cm}^2/\text{s}$ ) .....	40
(b) to (e) the concentration profiles for TPrA <sup>*+</sup> (solid line) and TPrA <sup>•</sup> (dotted line) at a specific points, A, B, C, and D, shown in (a). Parameters used in the simulation were (see Scheme 2.4 for further information): $E^{\circ}_{\text{TPrA}^{*+}/\text{TPrA}} = 0.88$ V vs. Ag/AgCl, $k_s$ (for eqs. 4.2 & 4.4) = 0.01 cm/s, $E^{\circ}_{\text{PI}/\text{TPrA}^{\bullet}} = -1.7$ V vs. Ag/AgCl, for eq. 4.3 $k_f = 3500 \text{ s}^{-1}$ & $k_b = 7 \times 10^6 \text{ s}^{-1}$ , $c_{(\text{TPrA} + \text{TPrAH}^+)} = 10 \text{ mM}$ . All species were assumed to have a	

diffusion coefficient of $5 \times 10^{-6} \text{ cm}^2/\text{s}$ except for $\text{H}^+$ ( $D_{\text{H}^+} = 5 \times 10^{-5} \text{ cm}^2/\text{s}$ ) .....	41
Figure 2.9: A simulated concentration profile for $\text{TPrA}^{++}$ formed at a 1.5 mm diameter hemispherical tip. This curve corresponds to potential A on the cyclic voltammogram (inset) for 10.0 mM TPrA (0.10 M Tris/0.10 M $\text{LiClO}_4$ , pH 8) with a scan rate of 50 mV/s. Other parameters required for the simulation are as in Figure 2.8 .....	43
Figure 2.10: Experimentally measured (dotted line) and simulated (solid line) ESR spectra of $\text{TPrA}^{++}$ generated by the oxidation of TPrA by $\text{Ru}(\text{bpy})_3^{3+}$ in an aqueous pH 7 solution at $20^\circ\text{C}$ .....	45
Figure 3.1: Molecular structures of amine coreactants. Acronyms are defined in the text .....	55
Figure 3.2: Molecular structures of coreactant buffers (CB). Acronyms are defined in the text .....	56
Figure 3.3: Cyclic voltammograms (CV) of 1 mM $\text{Ru}(\text{bpy})_3^{2+}$ in (a) pH 2.5, (b) pH 6.5, (c) pH 9.5, (d) pH 10.5, (e) pH 11.5, and (f) pH 12.5 of 0.2 M PBS at 0.1 V/s using a glassy carbon electrode (area = $0.07 \text{ cm}^2$ ). The dotted lines are background CVs .....	63
Figure 3.4: (a) Cyclic voltammograms of 10 mM TEtA in pH 12.5 PBS measured at various scan rates ( $v$ ). (b) Dependence of peak potentials for TEtA oxidation on $\log v$ . A GCE (area = $0.07 \text{ cm}^2$ ) was used as a working electrode .....	67
Figure 3.5: Simultaneous CV and ECL of $1 \mu\text{M Ru}(\text{bpy})_3^{2+}$ with 10 mM $N,N,N',N'$ -tetraethyl-1,3-propanediamine (TEDAP) in pH 7.5 PBS. Scan rate. = 0.1 V/s. A GCE (area = $0.07 \text{ cm}^2$ ) was used .....	70

Figure 3.6: Simultaneous CV and ECL of 1 $\mu\text{M}$ $\text{Ru}(\text{bpy})_3^{2+}$ with 10 mM $N,N,N',N'$ -tetra- <i>n</i> -propylethylenediamine (TPDAE) in pH 7.5 PBS. Scan rate. = 0.1 V/s. A GCE (area = 0.07 $\text{cm}^2$ ) was used.....	71
Figure 3.7: Comparison of the first ECL wave intensities of 1 $\mu\text{M}$ $\text{Ru}(\text{bpy})_3^{2+}$ generated with various amine coreactants (10 mM) in pH 7.5 PBS. Scan rate = 0.1 V/s. A GCE (area = 0.07 $\text{cm}^2$ ) was used.....	73
Figure 3.8: Dependence of the second ECL produced in a solution of 1 $\mu\text{M}$ $\text{Ru}(\text{bpy})_3^{2+}$ and 10 mM acyclic monoamine group coreactant (TEtA or TPrA) on the pH of PBS. Each data point is the average value of three measurements and contains less than 10 % deviation. A GCE (area = 0.07 $\text{cm}^2$ ) was used. ....	75
Figure 3.9: Dependence of the second ECL produced in a solution of 1 $\mu\text{M}$ $\text{Ru}(\text{bpy})_3^{2+}$ and 10 mM acyclic $N,N,N',N'$ -tetraethyldiamine group coreactant (TEDAM, TEDAE, or TEDAP) on the pH of PBS. Each data point is the average value of three measurements and contains less than 10 % deviation. A GCE (area = 0.07 $\text{cm}^2$ ) was used.....	76
Figure 3.10: Dependence of the second ECL produced in a solution of 1 $\mu\text{M}$ $\text{Ru}(\text{bpy})_3^{2+}$ and 10 mM acyclic $N,N,N',N'$ -tetra- <i>n</i> -propyldiamine group coreactant (TPDAM, TPDAE, or TPDAP) on the pH of PBS. Each data point is the average value of three measurements and contains less than 10 % deviation. A GCE (area = 0.07 $\text{cm}^2$ ) was used.....	77

Figure 3.11: Dependence of the second ECL produced in a solution of 1 $\mu\text{M}$ $\text{Ru}(\text{bpy})_3^{2+}$ and 10 mM heteroalicyclic monoamine group coreactant (MP, EP, or PP) on the pH of PBS. Each data point is the average value of three measurements and contains less than 10 % deviation. A GCE (area = $0.07 \text{ cm}^2$ ) was used .....	78
Figure 3.12: Dependence of the second ECL produced in a solution of 1 $\mu\text{M}$ $\text{Ru}(\text{bpy})_3^{2+}$ and 10 mM heteroalicyclic diamine group coreactant (DMPz, DEPz, or DPPz) on the pH of PBS. Each data point is the average value of three measurements and contains less than 10 % deviation. A GCE (area = $0.07 \text{ cm}^2$ ) was used. ....	79
Figure 3.13: Dependence of the anodic current for the oxidation of 10 mM TPDAP on pH of PBS. Scan Rate = 0.1 V/s. A GCE (area = $0.07 \text{ cm}^2$ ) was used.....	81
Figure 3.14: Simultaneous CV and ECL 1 $\mu\text{M}$ $\text{Ru}(\text{bpy})_3^{2+}$ in pH 7.5 of DIPSO buffer (0.2 M) solution containing 0.1 M NaCl as a supporting electrolyte. Scan rate = 0.1 V/s. A GCE (area = $0.07 \text{ cm}^2$ ) was used.....	84
Figure 4.1: Electronic absorption spectra of 10 $\mu\text{M}$ NR titrated with (a) 0 $\mu\text{M}$ (b) 2 $\mu\text{M}$ (c) 3 $\mu\text{M}$ (d) 4 $\mu\text{M}$ (e) 5 $\mu\text{M}$ (f) 6 $\mu\text{M}$ (g) 7 $\mu\text{M}$ (h) 10 $\mu\text{M}$ of anhydrous $\text{HClO}_4$ in MeCN. Inset is a plot of $\log \{[\text{ClO}_4^-] - [\text{NRH}^+]\}$ vs. $\log \{[\text{NRH}^+]/[\text{NR}]\}$ .....	99
Figure 4.2: Cyclic voltammograms of 1 mM neutral red (NR) in 0.1 M TBAP/MeCN. Scan rate = 0.1 V/s. A Pt electrode was used (area = $0.03 \text{ cm}^2$ ) .....	102

Figure 4.3: Dependence of peak potentials ( $E_p$ ) and peak currents ( $i_{pc}$ and $i_{pa}$ ) for the NR reduction on the scan rate ( $v$ ). $i_{pc}$ represents the reduction peak current of NR and $i_{pa}$ denotes the corresponding oxidation current of reduced NR. 1mM NR in 0.1 M TBAP/MeCN and a Pt electrode (area = $7.9 \times 10^{-3}$ cm <sup>2</sup> ) were used .....	103
Figure 4.4: Cyclic voltammograms of 1 mM neutral red (NR) with (a) 0.00 mM, (b) 0.26 mM, (c) 0.52 mM, (d) 0.78 mM, (e) 1.04 mM, (f) 1.30 mM, (g) 1.56 mM, and (h) 1.82 mM trifluoroacetic acid (TFA) in 0.1 M TBAP/MeCN. Scan Rate = 0.1 V/s. The same Pt electrode was used for each measurement (area = 0.03 cm <sup>2</sup> ).....	105
Figure 4.5: Dependence of reduction peak currents ( $i_p$ ) NR and NRH <sup>+</sup> on the concentration of TFA in 0.1 M TBAP/MeCN. 1 mM NR was titrated with 0.13 M TFA/0.1 M TBAP /MeCN stock solution. Scan rate = 0.1 V/s. A same Pt electrode was used for each measurement (area = 0.03 cm <sup>2</sup> ).....	106
Figure 4.6: Cyclic voltammograms of 1 mM NR and NRH <sup>+</sup> produced by adding 2 mM TFA in 0.1 M TBAP/MeCN. A Pt-UME of 25 $\mu$ m ( $a = 12.5 \mu$ m) was used. Scan rate = 10 mV/s.....	109
Figure 4.7: Plots of the normalized current ratio, $i_d(t)/i_{ss}$ , against the inverse square root of time for the reductions of (a) 1 mM NR and (b) 1 mM NRH <sup>+</sup> in 0.1 M TBAP/MeCN. The sampling rate is 100 $\mu$ sec per point. 12.5 $\mu$ m radius Pt-UME employed .....	110
Figure 4.8: Simultaneous (a) ECL and (b) CV of 1 mM NR and 5 mM BPO in 0.1 M TBAP/MeCN at 0.1 V/s. A Pt electrode was used (area = 0.03 cm <sup>2</sup> ).....	115

Figure 4.9: ECL (solid line) spectrum of 1 mM NR and fluorescence spectra of 5 $\mu$ M NR (dotted line) and 5 $\mu$ M NRH <sup>+</sup> (dashed line). ECL was generated with 10 mM BPO by pulsing the electrode potential between 0 V and – 1.6 V vs. Ag QRE (0.1 sec pulse-width and 5 min integration). $\lambda_{\text{ex}}$ for NR and NRH <sup>+</sup> were 440 nm and 530 nm, respectively.....	118
Figure 4.10: ECL spectra of 1 mM NR with 10 mM BPO in MeCN (dotted line) and CH <sub>2</sub> Cl <sub>2</sub> (solid line). ECL was generated by pulsing the potential between 0 V and – 1.6 V vs. Ag QRE with 5 min integration time. The same Pt electrode was used for each measurement (area =0.03 cm <sup>2</sup> ).....	120
Figure 4.11: Effect of NR concentrations on its ECL produced with a fixed 5 mM BPO. ECL was measured with a PMT and by sweeping an electrode potential at 0.1 V/s. The same Pt electrode was used for each measurement (area =0.03 cm <sup>2</sup> ).....	122
Figure 4.12: Effect of TFA concentrations on the ECL of 1 mM NR produced with 5 mM BPO. ECL was measured with a PMT and by sweeping an electrode potential at 0.1 V/s. The same Pt electrode was used for each measurement (area =0.03 cm <sup>2</sup> ).....	123
Figure 4.13: Effect of BPO concentrations on the ECL of 0.5 mM NR. ECL was measured with a PMT and by sweeping the electrode potential at 0.1 V/s. Inset represents the low concentration region (0 mM to 2.5 mM BPO). The same Pt electrode was used for each measurement (area =0.03 cm <sup>2</sup> ).....	125
Figure 4.14: Stern-Volmer plot of the NR fluorescence quenching by BPO in the absence of molecular oxygen. $C_{\text{NR}} = 1 \mu\text{M}$ . $\lambda_{\text{ex}} = 440 \text{ nm}$ .....	128

Figure 4.15: Simultaneous (a) cyclic voltammogram and (b) ECL wave of 1 mM Ru(bpy) <sub>3</sub> <sup>2+</sup> and 5 mM BPO in 0.1 M TBAP/MeCN at 0.1 V/s. Inset of (b) represents the ECL spectra measured under the same condition.....	129
Supporting Information Figure 4.1.....	132
Supporting Information Figure 4.2.....	133
Supporting Information Figure 4.3.....	134
Figure 5.1: Molecular structures of TDAF-1, TDAF-2 and BPO .....	142
Figure 5.2: Absorption and fluorescence ( $\lambda_{\text{ex}} = 350$ nm) spectra of (a) TDAF-1 and (b) TDAF-2 in MeCN:Bz (1:1,v:v) at room temperature under atmospheric conditions. Absorbance: 10 $\mu\text{M}$ of TDAF; fluorescence: 1 $\mu\text{M}$ of TDAF. (c) Phosphorescence ( $\lambda_{\text{ex}} = 355$ nm) spectra of 10.1 $\mu\text{M}$ TDAF-1 (I) and 9.8 $\mu\text{M}$ TDAF-2 (II) obtained at 77 K in deoxygenated methylcyclohexane. The spectra were taken at a delay time of 5 ms .....	145
Figure 5.3: Cyclic voltammograms of (a) 0.5 mM TDAF-1 and (b) 0.5 mM TDAF-2 in MeCN:Bz (1:1,v:v)/0.1 M TBAP at 0.1 V/s. Inset: differential pulse voltammogram (DPV) with increment potential, 4 mV, amplitude, 0.05 V, pulse width, 0.05 s .....	151
Figure 5.4: ECL spectra of (a) 0.5 mM TDAF-1 and (b) 0.5 mM TDAF-2 in MeCN:Bz (1:1,v:v)/0.1 M TBAP. 0.1 s pulses by alternating between + 1.58 V and – 1.95 V vs. Ag QRE for (a) and + 1.54 V and – 1.97 V vs. Ag QRE for (b). All spectra were obtained with an integration time of 5 min .....	156

Figure 5.5: Schematic diagram of ECL and excimer formation mechanism.....	159
Figure 5.6: ECL (solid line) spectra of (a) 0.5 mM TDAF-1 and (b) 0.5 mM TDAF-2 with 5 mM BPO in MeCN:Bz (1:1,v:v)/ 0.1 M TBAP. 0.1 s pulses alternating 0 V and – 1.96 V vs. Ag QRE for (a) and + 0 V and – 1.98 V vs. Ag QRE for (b). All ECL spectra were obtained with an integration time of 5 min. Fluorescence spectra (dotted line) were obtained with (a) 1 $\mu$ M TDAF-1 and (b) 1 $\mu$ M TDAF-2 without BPO. $\lambda_{\text{ex}} = 350$ nm for both (a) and (b).....	162
Figure 5.7: Model of a dimer of TDAF-1 from radical ions.....	167
Supporting Information Figure 5.1.....	170
Supporting Information Figure 5.2.....	172
Supporting Information Figure 5.3.....	173
Figure 6.1: Structures of (a) PIPES, (b) PIPPS, and (c) PIPBS.....	179

## List of Schemes

Scheme 1.1	.....	2
Scheme 1.2	.....	6
Scheme 1.3	.....	8
Scheme 1.4	.....	9
Scheme 2.1	.....	15
Scheme 2.2	.....	15
Scheme 2.3	.....	16
Scheme 2.4	.....	35
Scheme 2.5	.....	37
Scheme 2.6	.....	37
Scheme 3.1	.....	52
Scheme 3.2	.....	53
Scheme 3.3	.....	53
Scheme 3.4	.....	65
Scheme 4.1	.....	113
Scheme 4.2	.....	116
Scheme 4.3	.....	130
Scheme 5.1	.....	139
Scheme 5.2	.....	140
Scheme 5.3	.....	141
Scheme 5.4	.....	161
Scheme 5.5	.....	164

# **Chapter 1: Fundamentals of Electrogenerated Chemiluminescence (ECL)**

## **1.1 Introduction**

Electrogenerated chemiluminescence (ECL) is a phenomenon where light emission arises from a high energy electron transfer reaction between electrogenerated species, which is usually accompanied with the regeneration of the emitting species. Although luminescence during electrolysis was already observed<sup>1,2</sup> in the 1920's, the first detailed ECL<sup>3</sup> study was reported by Hercules in 1964. Since 1964, ECL has been extensively investigated to elucidate the mechanism and the origin of ECL, and many reviews<sup>4-9</sup> are available in the literature.

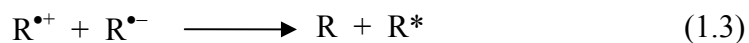
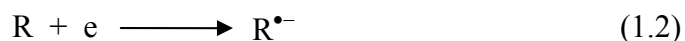
ECL is a kind of chemiluminescence (CL), in that light emission is produced by an energetic electron transfer reaction. However, the difference between CL and ECL is how the light emission is controlled. In CL, luminescence is governed by merely mixing or flowing an emitter with necessary reagents in a reaction vessel. In contrast, in ECL, light emission is controlled by turning on/off the electrode potential. As an analytical technique, ECL has some advantages over CL: (1) ECL has more spatial freedom than CL, in that the emission spot can be controlled and manipulated by moving an electrode or varying the size/number

of electrodes because the ECL reaction occurs only in the diffusion layer of an electrode, (2) ECL can be more selective than CL, in that the generation of excited states can be selectively controlled by varying the electrode potentials, (3) ECL is usually a non-destructive technique because ECL emitters are regenerated after the ECL emission. In this chapter, the fundamental principles of ECL will be reviewed before the main topics are discussed.

## 1.2 Ion Annihilation

ECL can be generated by ion annihilation when the ECL emitters (R) are electrochemically oxidized and reduced to sufficiently stable radical cations ( $R^{\bullet+}$ ) and anions ( $R^{\bullet-}$ ), respectively. The produced radical ions are annihilated by the oppositely charged radical ions to generate the excited state species ( $R^*$ ), as shown in Scheme 1.1.

### Scheme 1.1

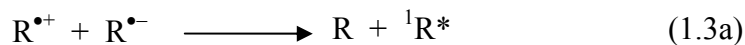


Depending on the energy available in the ion annihilation, eq. (1.3), the produced  $R^*$  could be either the lowest excited singlet state species ( $^1R^*$ ) or the triplet state species ( $^3R^*$ ). The energy available in eq. (1.3) can be calculated from the electrode potentials for eq. (1.1) and eq. (1.2) as defined in eq. (1.5)<sup>4</sup>.

$$-\Delta H_{\text{ann}} = E_p(R/R^{\bullet+}) - E_p(R/R^{\bullet-}) - 0.1 \text{ eV} \quad (1.5)$$

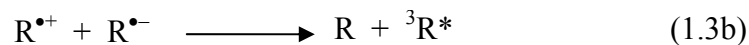
where  $-\Delta H_{\text{ann}}$  is the enthalpy for the ion annihilation of eq. (1.3),  $E_p$  is the peak potential for the electrochemical oxidation or reduction of R, and 0.1 eV is an estimate of the temperature-entropy approximation term ( $T\Delta S$ ) at 25 °C. If the energy ( $-\Delta H_{\text{ann}}$ ) estimated from eq. (1.5) is larger than the energy ( $E_s$ ) required to produce the lowest excited singlet state ( $^1R^*$ ) from the ground state of R, it is possible to directly generate  $^1R^*$  from eq. (1.3), and this system is called *an energy-sufficient system* or *the S-route*. A typical example of an energy-sufficient system is the  $\text{DPA}^{\bullet+}/\text{DPA}^{\bullet-}$  (DPA = 9,10-diphenylanthracene) system.<sup>10,11</sup>

### S-route



In contrast, if  $-\Delta H_{\text{ann}}$  is smaller than  $E_s$  but larger than the triplet state energy ( $E_t$ ), the triplet state ( $^3R^*$ ) is initially formed, and then  $^1R^*$  can be formed by triplet-triplet annihilation (TTA) as shown in eq. (1.6). This is called *an energy-deficient system* or *the T-route*. Typical examples of energy deficient systems are the  $\text{TMPD}^{\bullet+}/\text{DPA}^{\bullet-}$  and the  $\text{TMPD}^{\bullet+}/\text{AN}^{\bullet-}$  systems (TMPD = *N,N,N',N'*-tetramethyl-*p*-phenylenediamine and AN = anthracene).<sup>10,12</sup> The efficiency of the direct emission from  $^3R^*$  is usually low in a solution phase because of the long radiative lifetime of  $^3R^*$  and its quenching by radical ions or other species, such as molecular oxygen ( $\text{O}_2$ ).

### T-route



If  $-\Delta H_{\text{ann}}$  is nearly marginal to  $E_s$ , the T-route can contribute to the formation of  $^1R^*$  in addition to the S-route, and it is called *the ST-route*. Although the T-route is inefficient in the presence of considerable S-route,<sup>11,13-15</sup> it is still possible for the ST-route to exist. A typical example is the rubrene anion-cation annihilation in benzonitrile.<sup>16-18</sup>

### 1.3 Coreactants

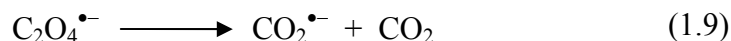
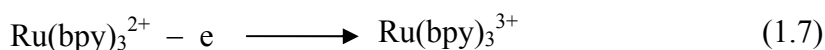
A coreactant is a compound that can produce a reactive intermediate (a strong reducing or oxidizing agent) by a reaction following the electrochemical or chemical electron transfer reaction. Employing a coreactant is useful especially when either  $R^{\bullet+}$  or  $R^{\bullet-}$  is not stable enough for ECL reaction, or when the ECL solvent has a narrow potential window so that  $R^{\bullet+}$  or  $R^{\bullet-}$  cannot be formed. In an aqueous solvent, the use of a coreactant is very important because water has a narrow potential window, many organic compounds have a low solubility, and many radical ions of organic emitters are unstable in an aqueous solvent.

The first coreactant used for ECL was oxalate ion ( $C_2O_4^{2-}$ ).<sup>19,20</sup> When  $C_2O_4^{2-}$  is oxidized, it produces the sufficiently strong reducing agent,  $CO_2^{\bullet-}$  ( $E^\circ = -1.9$  V vs. NHE<sup>21</sup>), and  $CO_2$ . For example,  $Ru(bpy)_3^{2+}$  dissolved in an aqueous solution can produce ECL in the presence of  $C_2O_4^{2-}$  via Scheme 1.2. In addition, various amines<sup>22-25</sup> and peroxydisulfate ( $S_2O_8^{2-}$ )<sup>26-28</sup> have been used as coreactants.

The following conditions are suggested for an efficient coreactant candidate: (1) the coreactant should be reasonably soluble in a solvent because the ECL intensity is generally proportional to its concentration, (2) the reactive intermediate species generated electrochemically and/or chemically should be stable enough to undergo the ECL reaction with an emitting species, (3) the rate of reaction between the intermediate and the radical ion of an ECL emitter must

be rapid, (4) the coreactant and its intermediate should have inert or weak quenching effect on ECL, and (5) the coreactant itself should not produce any light emission.

### Scheme 1.2



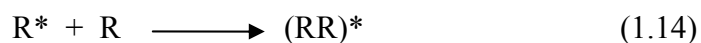
or



## 1.4 Formation of Excimers or Exciplexes

The term, excimer, introduced by Stevens and Hutton<sup>29</sup> represents an electronically excited dimeric species, which is immediately dissociated after its emission. The usual characteristics of excimer emission are the broad structureless emission band appearing at the longer wavelength side of the monomeric fluorescence and its increasing emission intensity with increasing concentration. In addition, the absorption spectra of the sample show the only monomeric characters. In fluorescence, the excimer [(RR)\*] is usually formed by

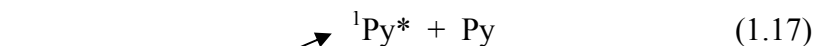
the association of an excited state ( $R^*$ ) species with the corresponding ground state species ( $R$ ) [eq. (1.14)]. Depending on the spin multiplicity of  $R^*$ , the excimers may be singlet or triplet. In ECL, on the other hand, the excimers can be formed not only by the direct generation during the ion annihilation [eq. (1.15)], but also by the association of  $R^*$  with  $R$  [eq. (1.14)]. However, depending on the molecular structure of  $R$  and the lifetime of  $R^*$ , eq. (1.14) may be negligible in ECL.



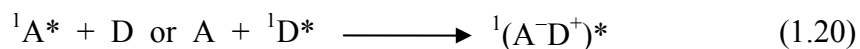
Chandross, *et. al.*<sup>30</sup> first reported the excimer emissions in ECL with anthracene, 9,10-dimethylantracene, phenanthrene, perylene, and 3,4-benzpyrene and they suggested that the excimer might be mainly formed by eq. (1.15), because the fluorescence spectra of anthracene, 9,10-dimethylantracene, and phenanthrene did not show any excimer emission.

The excimer can also be formed via the triplet-triplet annihilation (TTA). Maloy and Bard<sup>31</sup> demonstrated that the TTA of triplet state pyrene ( ${}^3\text{Py}^*$ ) contributed to the formation of excimer when the radical anion of pyrene (Py) was annihilated by the radical cation of TMPD (T-route) at the rotating ring-disk electrode (RRDE) as shown in Scheme 1.3.

**Scheme 1.3**



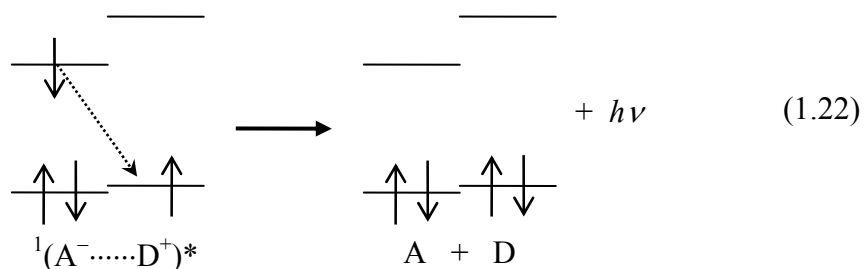
Similar to the formation of excimers, the exciplex (excited complex or hetero-excimer) can be formed by the annihilation of radical ions [eq. (1.19)], the association of  ${}^1\text{A}^*$  with D (or *vice versa*) [eq. (1.20)], and the TTA of  ${}^3\text{A}^*$  and  ${}^3\text{D}^*$  [eq. (1.21)]. In ECL, exciplex emission arises mainly through eq. (1.19)<sup>32</sup>, although the mode of exciplex formation depends primarily on the energy available in ion annihilation. The singlet quenching path, eq. (1.20), is inefficient in ECL unless the excited singlet state ( ${}^1\text{A}^*$ ) is directly produced by the S-route in the proximity of the ground state (D).



where A represents an electron acceptor molecule and D denotes an electron donor molecule. The emission from formed exciplexes may be rationalized by the

following scheme 1.4.

**Scheme 1.4**



A typical example of an exciplex observed in ECL is the  $\text{PTP}^{\bullet-}/\text{TPTA}^{\bullet+}$  (PTP = *p*-terphenyl and TPTA = tri-*p*-tolylamine) system in acetonitrile.<sup>33</sup>

### 1.5 Preannihilation ECL

It was reported that weak ECL was produced when only  $\text{R}^{\bullet+}$  or  $\text{R}^{\bullet-}$  was generated in a solvent without any coreactants,<sup>34-37</sup> and the ECL spectrum was identical to the fluorescence spectrum in all cases. Such luminescence is called the preannihilation ECL and it is usually thought that the light emission may be generated by a reacting species produced from solvents, electrolytes, or impurities. For example, when rubrene was electrochemically reduced at  $-1.6$  V in DMF and then the electrode potential was scanned back to  $-0.2$  V where rubrene was not oxidized yet, light emission was observed.<sup>35</sup>

## 1.6 Concluding Remark

Recently, ECL is of great interest for analytical applications as a result of its high sensitivity and selectivity. ECL produced by a coreactant has been employed in a variety of areas: fiber optic ECL sensor,<sup>38-40</sup> detection method for HPLC,<sup>41-43</sup> ECL biosensing,<sup>44-46</sup> immunoassay and DNA-probe assay analyses,<sup>47-49</sup> etc. Therefore, it is important to understand ECL reaction mechanisms and reactivities of coreactants. In this dissertation, the reaction mechanisms and reactivities of amine (Chapters 2 and 3) and benzoyl peroxide (Chapters 4 and 5) coreactants are described for the ECL of  $\text{Ru}(\text{bpy})_3^{2+}$ , neutral red, and ter(9,9-diarylfluorene)s.

## References

- (1) Dufford, R. T.; Nightingale, D.; Gaddum, L. W. *J. Am. Chem. Soc.* **1927**, *49*, 1858.
- (2) Harvey, N. *J. Phys. Chem.* **1929**, *33*, 1456.
- (3) Hercules, D. M. *Science* **1964**, *145*, 808.
- (4) Faulkner, L. R.; Bard, A. J. In *Electroanalytical Chemistry*; Bard, A. J., Ed., Marcel Dekker: New York, 1977; Vol. 10, p1.
- (5) Faulkner, L. R. *Methods Enzymol.* **1978**, *57*, 494.
- (6) Glass, R. S.; Faulkner, L. R. In *Chemical and Biological Generation of Excited States*; Adam, W.; Cilento, G., Eds., Academic Press, New York, 1982, Chapter 6.
- (7) Knight, A. W.; Greenway, G. M. *Analyst* **1994**, *119*, 879.
- (8) Lee, W. Y. *Mikrochim. Acta* **1997**, *127*, 19.
- (9) Bard, A. J.; Debad, J. D.; Leland, J. K.; Sigal, G. B.; Wilbur, J. L.; Wohlstadter, J. N. In *Encyclopedia of Analytical Chemistry: Applications, Theory, and Instrumentation*, Meyer, R. A. Ed.; John Wiley & Sons: New York, 2000, p. 9842.
- (10) Faulkner, L. R.; Tachikawa, H.; Bard, A. J. *J. Am. Chem. Soc.* **1972**, *94*, 691.
- (11) Bezman, R.; Faulkner, L. R. *J. Am. Chem. Soc.* **1972**, *94*, 6317.
- (12) Faulkner, L. R.; Bard, A. J. *J. Am. Chem. Soc.* **1969**, *91*, 209.
- (13) Bezman, R.; Faulkner, L. R. *J. Am. Chem. Soc.* **1973**, *95*, 3083
- (14) Bezman, R.; Faulkner, L. R. *J. Am. Chem. Soc.* **1972**, *94*, 6324.
- (15) Bezman, R.; Faulkner, L. R. *J. Am. Chem. Soc.* **1972**, *94*, 6331.
- (16) Tachikawa, H.; Bard, A. J. *Chem. Phys. Letters* **1974**, *26*, 246.
- (17) Periasamy, N.; Santhanam, K. S. V. *Proc. Ind. Acad. Sci.* **1974**, *80A*, 821.
- (18) Pighin, A.; Conway, B. E. *J. Electrochem. Soc.* **1975**, *122*, 619.
- (19) Chang, M. -M.; Saji, T.; Bard, A. J. *J. Am. Chem. Soc.* **1977**, *99*, 5399.

- (20) Rubinstein, I.; Bard, A. J. *J. Am. Chem. Soc.* **1981**, *103*, 512.
- (21) Butler, J.; Hengline, A. *Radiat. Phys. Chem.* **1980**, *15*, 603.
- (22) Noffsinger, J. B.; Danielson, N. D. *Anal. Chem.* **1987**, *59*, 865.
- (23) Leland, J. K.; Powell, M. J. *J. Electrochem. Soc.* **1990**, *137*, 3127.
- (24) Zu, Y.; Bard, A. J. *Anal. Chem.* **2000**, *72*, 3223.
- (25) Kanoufi, F.; Zu, Y.; Bard, A. J. *J. Phys. Chem. B* **2001**, *105*, 210.
- (26) White, H. S.; Bard, A. J. *J. Am. Chem. Soc.* **1982**, *104*, 6891.
- (27) Becker, W. G.; Seung, H. S.; Bard, A. J. *J. Electroanal. Chem.* **1984**, *167*, 127.
- (28) Fabrizio, E. F.; Prieto, I.; Bard, A. J. *J. Am. Chem. Soc.* **2000**, *122*, 4996.
- (29) Stevens, B.; Hutton, E. *Nature*, **1960**, *186*, 1045.
- (30) Chandross, E. A.; Longworth, J. W.; Visco, R.E. *J. Am. Chem. Soc.* **1965**, *87*, 3259.
- (31) Maloy, J. T.; Bard, A. J. *J. Am. Chem. Soc.* **1971**, *93*, 5968.
- (32) Bard, A. J.; Park, S. M. In *The Exciplex*; Gordon, M.; Ware, W. R., Eds.; Academic Press: New York, 1975, p. 305.
- (33) Keszthelyi, C. P.; Bard, A. J. *Chem. Phys. Letters* **1974**, *24*, 300.
- (34) Hercules, D. M.; Lansbury, R. C.; Roe, D. K. *J. Am. Chem. Soc.* **1966**, *88*, 4578.
- (35) Maricle, D. L.; Maurer, A. *J. Am. Chem. Soc.* **1967**, *89*, 188.
- (36) Zweig, A.; Hoffman, A. K.; Maricle, D. L.; Maurer, A. H. *Chem. Commun.* **1967**, 106.
- (37) Zweig, A.; Maricle, D. L.; Brinen, J. S.; Maurer, A. H. *J. Am. Chem. Soc.* **1967**, *89*, 473.
- (38) Egashira, N.; Kumasako, H.; Ohga, K. *Anal. Sci.* **1990**, *6*, 903.
- (39) Kuhn, L. S.; Weber, A.; Weber, S. G. *Anal. Chem.* **1990**, *62*, 1613.
- (40) Preston, J.; Nieman, T. A. *Anal. Chem.* **1996**, *68*, 966.
- (41) Noffsinger, J. B.; Danielson, N. D. *J. Chromatogr.* **1987**, *387*, 520.

- (42) Uchikura, K.; Kirisawa, M. *Anal.Sci.* **1991**, 7, 971.
- (43) Skotty, D. R.; Lee, W. Y.; Nieman, T. A. *Anal. Chem.* **1996**, 68, 1530.
- (44) Martin, A. F.; Nieman, T. A. *Anal. Chim. Acta* **1993**, 281, 475.
- (45) Yokoyama, K.; Sasaki, S.; Ikebukuro, K.; Takeuchi, T.; Karube, I.; Tokitsu, Y.; Masuda, Y. *Talanta* **1994**, 31, 1035.
- (46) Jameison, F.; Sanchez, R. I.; Dong, L.; Leland J. K.; Yost, D.; Martin, M. T. *Anal. Chem.* **1996**, 68, 1298.
- (47) Blackburn, G. F.; Shah, H. P.; Kenten, J. H.; Leland, J.; Kamin, R. A.; Link, J.; Peterman, J.; Powell, M. J.; Shah, A.; Talley, D. B.; Tyagi, S. K.; Wilkins, E.; Wu, T. G.; Massey, R. J. *Clin. Chem.* **1991**, 37, 1534.
- (48) Kenten, J. H.; Casadei, J.; Link, J.; Lupold, S.; Willey, J.; Powell, M. J.; Rees, A.; Massey, R. J. *Clin. Chem.* **1991**, 37, 1626.
- (49) DiCesare, J.; Grossman, B.; Katz, E.; Picozza, E.; Ragusa, R.; Woundenberg, T. *Biotechniques* **1993**, 15, 152.

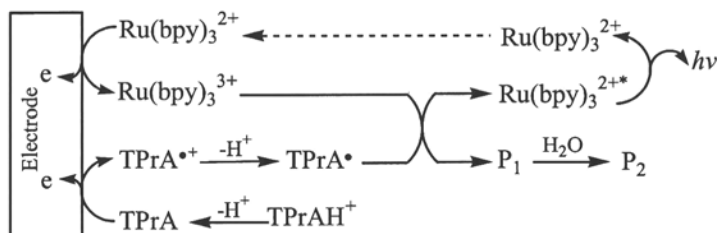
## **Chapter 2: Electrogenenerated Chemiluminescence of Tris(2,2'-bipyridine)ruthenium(II), Ru(bpy)<sub>3</sub><sup>2+</sup>/Tri-*n*-propylamine (TPrA) System – A New Route Involving TPrA<sup>•+</sup> Cation Radicals**

### **2.1 Introduction**

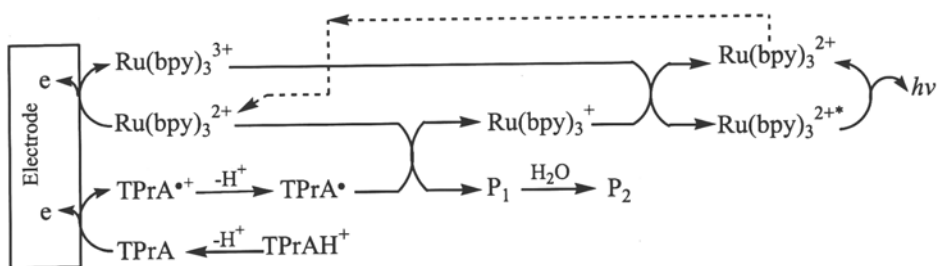
Noffsinger and Danielson<sup>1</sup> first reported the chemiluminescence of tris(2,2'-bipyridine)ruthenium(III), Ru(bpy)<sub>3</sub><sup>3+</sup> (bpy = 2,2'-bipyridine), with aliphatic amines. Following this study, Leland and Powell<sup>2</sup> reported the electrogenerated chemiluminescence (ECL) of the Ru(bpy)<sub>3</sub><sup>2+</sup> with tri-*n*-propylamine (TPrA) as a coreactant. Since then, a wide range of ECL analytical applications involving Ru(bpy)<sub>3</sub><sup>2+</sup> or its derivatives as labels have been reported.<sup>3</sup> The Ru(bpy)<sub>3</sub><sup>2+</sup> (or its derivatives) with TPrA exhibit the highest ECL efficiency and this system forms the basis of commercial systems for immunoassay and DNA analysis.<sup>2-4</sup> The ECL intensity for this system is proportional to the concentration of both Ru(bpy)<sub>3</sub><sup>2+</sup> and TPrA species,<sup>2,4-6</sup> and also depends on the solution pH and the electrode material.<sup>1,2,5</sup> The ECL mechanism of this reaction has been investigated by many workers,<sup>1,2,4,5,7</sup> and follows the now familiar coreactant mechanism<sup>8</sup> where the oxidation of TPrA generates a strongly reducing species. This oxidation can be via a catalytic route where electrogenerated

$\text{Ru}(\text{bpy})_3^{3+}$  reacts with TPrA as well as by the direct reaction of TPrA at the electrode described by both Scheme 2.1 and Scheme 2.2:

**Scheme 2.1**



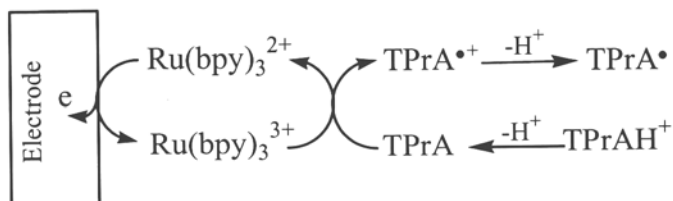
**Scheme 2.2**



where  $\text{TPrA}^{\bullet+} = (\text{CH}_3\text{CH}_2\text{CH}_2)_3\text{N}^{\bullet+}$ ,  $\text{TPrAH}^+ = \text{Pr}_3\text{NH}^+$ ,  $\text{TPrA}^{\bullet} = \text{Pr}_2\text{NC}^{\bullet}\text{HCH}_2\text{CH}_3$ ,  $\text{P}_1 = \text{Pr}_2\text{N}^+\text{C}=\text{HCH}_2\text{CH}_3$ , and  $\text{P}_2 = \text{Pr}_2\text{NH} + \text{CH}_3\text{CH}_2\text{CHO}$ . The “catalytic” route involving homogeneous oxidation of TPrA with  $\text{Ru}(\text{bpy})_3^{3+}$  is shown in Scheme 2.3. The contribution of this process to the overall ECL intensity, depends upon the  $\text{Ru}(\text{bpy})_3^{2+}$  concentration, and is small when relatively

low concentrations of  $\text{Ru}(\text{bpy})_3^{2+}$  are used.<sup>5</sup>

**Scheme 2.3**



The mechanisms proposed above, however, do not account for a number of observations made for this ECL system. The strong dependence of ECL efficiency on electrode material<sup>5</sup> and surfactants<sup>9</sup> strongly supports the importance of the direct oxidation of TPrA. However, two ECL waves occur at a glassy carbon and a gold electrode, with the first ECL wave in a potential range less positive than that for the oxidation of  $\text{Ru}(\text{bpy})_3^{2+}$  (while the second wave occurs at potentials for  $\text{Ru}(\text{bpy})_3^{2+}$  oxidation). Both waves were associated with the emission of  $\text{Ru}(\text{bpy})_3^{2+*}$  to  $\text{Ru}(\text{bpy})_3^{2+}$ . The necessary oxidant to produce ECL at this first wave is not apparent. Moreover, in the commercial Origen analyzer (IGEN International, Inc., Gaithersburg, MD), the  $\text{Ru}(\text{bpy})_3^{2+}$ -tagged species in immunoassay are immobilized on 2.8  $\mu\text{m}$  diameter magnetic beads that are brought to an electrode by a magnetic field. Direct oxidation of  $\text{Ru}(\text{bpy})_3^{2+}$  on the beads would only occur for those within electron tunneling distance from the electrode,  $\sim 1$  to 2 nm, so most of the labels on the bead would not contribute to

the ECL response. However, the high sensitivity of the technique indicates that most of the labels on the beads participate in the reaction, so that some other reactions involving the TPrA coreactant must generate precursors that can form  $\text{Ru}(\text{bpy})_3^{2+*}$ . Clearly, the present ECL mechanisms proposed above (Schemes 2.1 – 2.3) cannot explain these results. Moreover, there has been no convincing explanation of the relative efficiencies of related coreactants, e.g.,  $\text{Et}_3\text{N}$  vs. TPrA, based on the mechanism that only involves the free radical reductant as an intermediate (e.g., correlating the reducing power of the radical with observed ECL emission efficiency).

An understanding of the mechanism of the  $\text{Ru}(\text{bpy})_3^{2+}/\text{TPrA}$  system is important in designing and selecting new coreactants and in improving the sensitivity and reproducibility of the ECL system. In this chapter, a new route involving  $\text{TPrA}^{\bullet+}$  cation radical reduction for the generation of the excited state  $\text{Ru}(\text{bpy})_3^{2+*}$  is presented. This mechanism is supported by a scanning electrochemical microscopy (SECM) – ECL experiment, cyclic voltammetry (CV) and CV digital simulations, and the direct detection by electron spin resonance (ESR) showing that the  $\text{TPrA}^{\bullet+}$  cation radical is relatively stable under conditions similar to those used in the ECL experiments, i.e., in aqueous solutions at neutral pH.

## 2.2 Experimental Section

**Chemicals.** Tris(2,2'-bipyridyl)ruthenium(II) dichloride hexahydrate ( $\text{Ru}(\text{bpy})_3\text{Cl}_2 \cdot 6\text{H}_2\text{O}$ ), tri-*n*-propylamine (TPrA, 99+ %), and Fremy's salt [ $(\text{KSO}_3)_2\text{NO}$ ] from Aldrich (Milwaukee, WI), (3-aminopropyl)-trimethoxysilane [ $(\text{CH}_3\text{O})_3\text{Si}(\text{CH}_2)_3\text{NH}_2$ ,  $\geq 97$  %] and lithium perchlorate ( $\text{LiClO}_4$ ,  $> 99$  %) from Fluka (Milwaukee, WI), potassium permanganate ( $\text{KMnO}_4$ ), sodium phosphate dibasic heptahydrate ( $\text{Na}_2\text{HPO}_4 \cdot 7\text{H}_2\text{O}$ , 98.0 %), and phosphoric acid ( $\text{H}_3\text{PO}_4$ , 85 %) from Fisher (Fairlawn, NJ), potassium phosphate monobasic ( $\text{KH}_2\text{PO}_4$ , 99.6 %) from J. T. Baker (Phillipsburg, NJ), tris(hydroxymethyl)aminomethane (Tris, ultrapure) from Life Technologies (Rockville, MD), 1-ethyl-3-(3-dimethylaminopropyl) carbodiimide hydrochloride (EDAC, SigmaUltra) and 1-methylimidazole from Sigma (Louis, MO), hydrochloric acid ( $\text{HCl}$ , GR) from EM (Gibbstown, NJ), toluene (A.R.) from Mallinckrodt (Hazelwood, MO), and EtOH (200-proof) from Aaper Alcohol (Shelbyville, KY) were used without further purification. Bis(2,2'-bipyridine)-4,4'-dicarboxy-2,2'-bipyridineruthenium(II) hexafluorophosphates,  $\text{Ru}(\text{bpy})_2[\text{bpy}(\text{COOH})_2](\text{PF}_6)_2$ , was prepared by following a procedure in the literature.<sup>10</sup> Unless otherwise stated, all solutions were freshly prepared with deionized water (Milli Q, Millipore).

**Immobilization of  $\text{Ru}(\text{bpy})_2[\text{bpy}(\text{COOH})_2]^{2+}$  on an ITO Electrode.** A clean and dried indium tin oxide (ITO) electrode (resistance, 30-60 ohm/square; Delta Technologies, Stillwater, MN) with dimensions of  $\sim 1 \times 1 \text{ cm}^2$  was immersed

in a 5 % of  $(\text{CH}_3\text{O})_3\text{Si}(\text{CH}_2)_3\text{NH}_2$  toluene solution and kept in a desiccator for 24 hrs. During this process,  $(\text{CH}_3\text{O})_3\text{Si}(\text{CH}_2)_3\text{NH}_2$  becomes immobilized by formation of ITO/O-Si(CH<sub>2</sub>)<sub>3</sub>NH<sub>2</sub> bonds.<sup>11</sup> The electrode was then washed with EtOH and transferred into a 0.10 M 1-methylimidazole/HCl buffer solution (pH = 7) containing ~ 10 mM Ru(bpy)<sub>2</sub>[bpy(COOH)<sub>2</sub>]<sup>2+</sup> and 10 mM EDAC. After a 45 min incubation at 70 °C, the ITO electrode was washed thoroughly with EtOH and then water. By this treatment, a monolayer of Ru(bpy)<sub>2</sub>[bpy(COOH)<sub>2</sub>]<sup>2+</sup> was covalently attached to the aminosilane formed previously on the ITO, to produce ITO/O-Si(CH<sub>2</sub>)<sub>3</sub>NH-[CO(bpy)(COOH)](bpy)<sub>2</sub>Ru(II) (designated as ITO/OSiRu<sup>II</sup>). The ITO/OSiRu<sup>II</sup> electrode was subsequently immersed in a 0.10 M Tris/HCl buffer (pH = 8) and maintained in the dark until further use.

**Electrochemical and ECL measurements.** Fast scan CV was performed with the model 660 electrochemical workstation (CH Instruments, Austin, TX). A conventional three-electrode cell was used, with a Pt wire as the counter electrode and an Ag/AgCl/KCl(sat.) as the reference electrode. The working electrodes used for the examination of TPrA redox behavior at fast scan rates were of different materials [Pt, Au, carbon fiber, and glassy carbon (GC)] and different dimensions (3 mm, 100 μm, 25 μm, 5 μm diameter Pt; 2 mm diameter Au; 3 mm diameter GC and 10 μm diameter carbon fiber). The ECL along with the CV signals were measured simultaneously with a home-built potentiostat combined with a photomultiplier tube (PMT, Hamamatsu R4220p, Japan) installed under the

electrochemical cell. A voltage of  $-750$  V was supplied to the PMT with a high-voltage power supply series 225 (Bertan High Voltage Corp., Hicksville, NY). A 3 mm diameter GC working electrode, and the counter and reference electrodes the same as those used for fast scan CV were used.

The SECM-ECL experiments were taken with a CHI 900 SECM system (CH Instruments, Austin, TX) combined with the ECL instrument described. Figure 2.1 shows a schematic diagram of the setup. The working electrode (tip), was a 1.5 mm diameter hemispherical Au, and the ITO/OSiRu<sup>II</sup> (“modified ITO”) served as the substrate. The direct oxidation of covalently attached Ru(bpy)<sub>2</sub>[bpy(COOH)<sub>2</sub>]<sup>2+</sup> species at the ITO electrode was avoided by holding the electrode at an open circuit. A Pt wire and an Ag/AgCl/KCl (sat.) electrode were also used as the counter and reference electrodes, respectively.

The simulation of the cyclic voltammogram of TPrA oxidation in aqueous solution was carried out by using the simulation package DigiSim<sup>®</sup> V 3.03 (Bioanalytical System Inc., West Lafayette, IN).

**ESR Experiments.** The cation radical of TPrA, TPrA<sup>•+</sup>, was generated by flowing 0.10 M TPrA (pH 7, adjusted by HNO<sub>3</sub>) and  $\sim 0.030$  M Ru(bpy)<sub>3</sub><sup>3+</sup> solutions through a quartz flat cell<sup>12</sup> via a two-jet mixing chamber (Wilmad, Prod. No. WG-801-Q, Buena, NJ). The Ru(bpy)<sub>3</sub><sup>3+</sup> solution was freshly prepared by bubbling Cl<sub>2</sub> gas generated via the reaction of solid KMnO<sub>4</sub> and concentrated HCl directly into a 0.030 M Ru(bpy)<sub>3</sub>Cl<sub>2</sub> solution. A clear color change from reddish

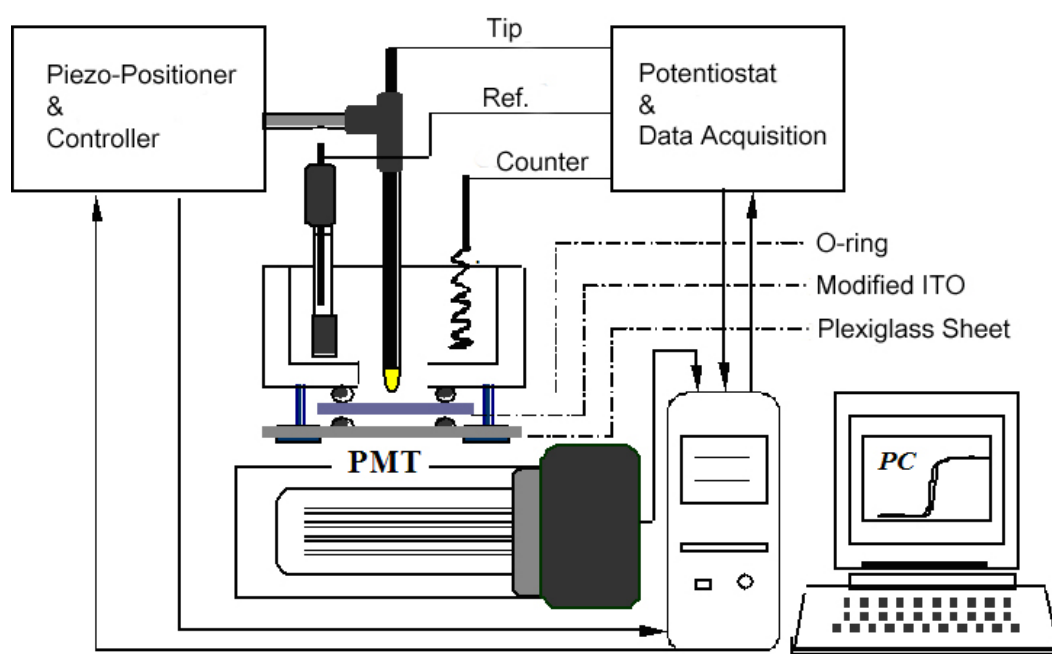


**Figure 2.1.** Setup for SECM – ECL.

orange to dark greenish blue was observed upon the complete oxidation of  $\text{Ru}(\text{bpy})_3^{2+}$  to  $\text{Ru}(\text{bpy})_3^{3+}$ .

X-band ESR spectra were recorded on an ER-300 ESR spectrometer (IBM Instruments Inc.) with a modulation frequency of 100 kHz and microwave power at 12.6 mW. The swept field and the  $g$  value were calibrated externally using a 5.0 mM aqueous Fremy's salt solution.<sup>13,14</sup> The quartz flat cell was installed in a  $\text{TE}_{102}$  rectangular cavity. Overall, solution flow rates of 2 to 5 mL/s were employed and the relative flow rates for the TPrA and  $\text{Ru}(\text{bpy})_3^{3+}$  solutions were adjusted so that an orange color appeared at the outlet of the flow cell.

The spectra were simulated using PEST Winsim Software<sup>15</sup> (National Institute of Environmental Health Sciences, National Institute of Health, Research Triangle Park, NC).

All experiments were conducted at a temperature of  $20 \pm 2$  °C, unless otherwise stated.

## 2.3 Results and Discussion

### **Electrochemical and ECL behavior of the $\text{Ru}(\text{bpy})_3^{2+}$ /TPrA system.**

An earlier report<sup>5</sup> showed that at low concentrations of  $\text{Ru}(\text{bpy})_3^{2+}$  ( $\sim \mu\text{M}$ ) and 10 to 100 mM TPrA in aqueous 0.15 M phosphate buffer, pH 7.5, the ECL emission vs. potential curves displayed two broad waves. Similar behavior was also observed when a much lower concentration of  $\text{Ru}(\text{bpy})_3^{2+}$ , 1.0 nM,

[Figure 2.2 (a)] and a different buffer solution, 0.10 M Tris/0.10 M LiClO<sub>4</sub>, pH = 8, were used [Figure 2.2]. The initial ECL signal started at potentials where the direct oxidation of TPrA at the GC electrode occurs [Figure. 2.2 (a) and (b)], and reached a first maximum at a potential of about 0.90 V vs. Ag/AgCl, about 50 mV less positive than the peak potential for TPrA oxidation, and well before Ru(bpy)<sub>3</sub><sup>2+</sup> oxidation. The second ECL signal has a peak potential value of 1.14 V vs. Ag/AgCl, in the potential region of the direct oxidation of Ru(bpy)<sub>3</sub><sup>2+</sup> at a GC electrode.<sup>5</sup> For comparison, Figure 2.2 also includes the ECL signal profile obtained with the Ru(bpy)<sub>3</sub><sup>2+</sup> concentration of 1.0 μM [Figure. 2.2 (c)]. The corresponding TPrA oxidation CV is not included, since it is essentially the same as that in Figure 2.2 (b). The relative ECL intensity from the first wave is significant, particularly in the 1.0 nM Ru(bpy)<sub>3</sub><sup>2+</sup> solution, and thus the bulk of the ECL signal obtained in this system with low concentrations of analytes, as in immunoassays and DNA probes with Ru(bpy)<sub>3</sub><sup>2+</sup> as an ECL label, probably originates from the first ECL wave. Note that even with a high concentration of Ru(bpy)<sub>3</sub><sup>2+</sup> (~ mM), the ECL signal first appeared in a potential range less positive than that for the oxidation of Ru(bpy)<sub>3</sub><sup>2+</sup>. However, the initial ECL signal is relatively small compared to the large ECL signal generated via Schemes 2.1 and 2.2.

Figure 2.3 shows linear sweep voltammograms (LSV) and the corresponding ECL signals obtained from 1 μM Ru(bpy)<sub>3</sub><sup>2+</sup> and 50 mM TPrA in

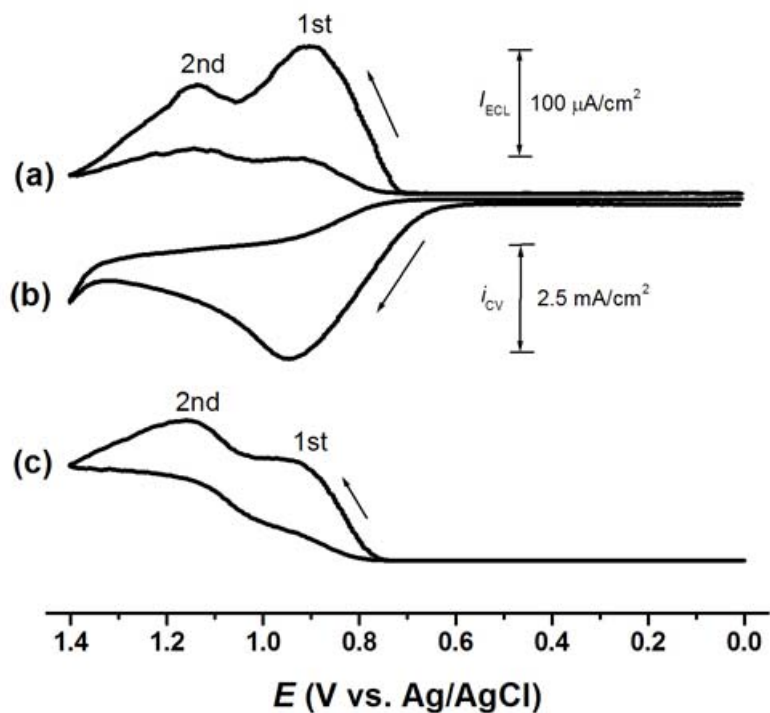


**Figure 2.2.** (a) ECL and (b) cyclic voltammogram of 1.0 nM  $\text{Ru}(\text{bpy})_3^{2+}$  in the presence of 0.10 M TPrA with 0.1 M Tris/0.10 M  $\text{LiClO}_4$  buffer (pH = 8) at a 3 mm diameter glassy carbon electrode at scan rate 50 mV/s. (c) As (a) but with 1.0  $\mu\text{M}$   $\text{Ru}(\text{bpy})_3^{2+}$ . The ECL intensity scale is given for (c) and should be multiplied by 100 for (a).

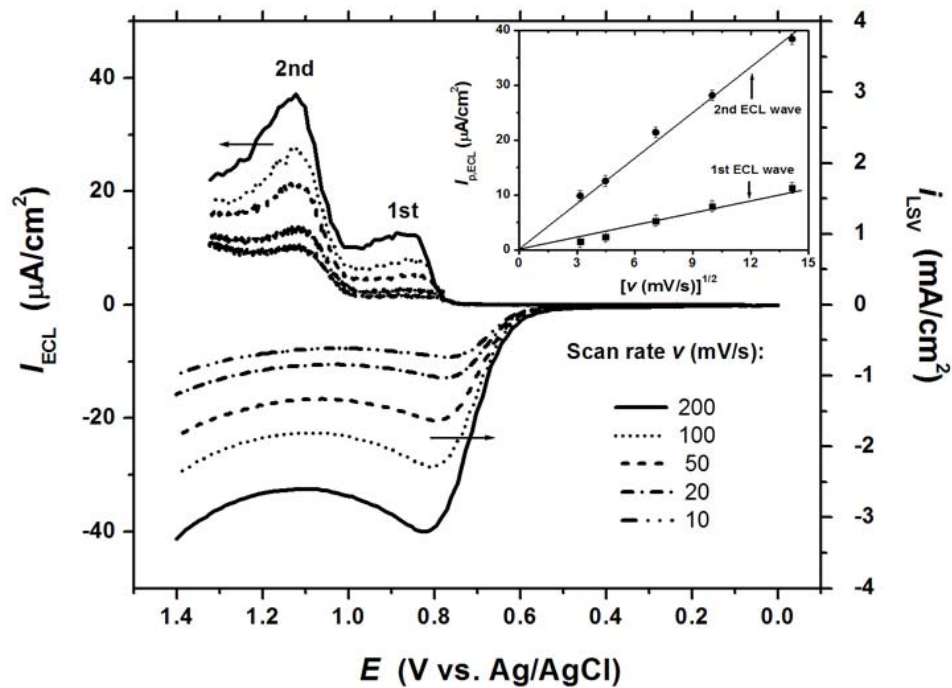


**Figure 2.3.** Linear sweep voltammograms (LSV) and their corresponding ECL signals for  $1 \mu\text{M Ru}(\text{bpy})_3^{2+}$  and  $50 \text{ mM TPrA}$  in  $\text{pH } 8.5 \text{ PBS}$  at a  $3 \text{ mm}$  diameter glassy carbon electrode at different scan rates. Inset, plot of the first and the second ECL signals versus  $v^{1/2}$ .

0.20 M phosphate buffer solution (PBS, pH 8.5) at a GC electrode at different potential scan rates ( $\nu$ ). A linear relationship between the ECL peak intensity ( $I_{p,ECL}$ ) for both the first and the second ECL waves and  $\nu^{1/2}$  was observed [Figure 2.3, inset], consistent with the linear relationship between the peak current for the oxidation of TPrA and  $\nu^{1/2}$ . These results suggest that the first ECL signal is directly related to the oxidation of TPrA.

The effect of both TPrA and  $\text{Ru}(\text{bpy})_3^{2+}$  concentrations on the first ECL peak intensity ( $I_{p1,ECL}$ ) was also investigated. As shown in Figure 2.4 (a), in 1  $\mu\text{M}$   $\text{Ru}(\text{bpy})_3^{2+}$  (0.20 M PBS, pH 7.5), the  $I_{p1,ECL}$  is linearly proportional to the concentration of TPrA. No ECL signal was detected in the absence of either TPrA or  $\text{Ru}(\text{bpy})_3^{2+}$ , so the first ECL signal must be associated with a reaction between the species generated from TPrA and  $\text{Ru}(\text{bpy})_3^{2+}$ . Figure 2.4 (b) shows the  $I_{p1,ECL}$  changes as a function of  $\text{Ru}(\text{bpy})_3^{2+}$  concentration when TPrA concentration kept at a constant value of 100 mM (0.20 M PBS, pH 8.5). In the range of 10 pM to 50  $\mu\text{M}$  of  $\text{Ru}(\text{bpy})_3^{2+}$ ,  $I_{p1,ECL}$  steadily rises with an increase of  $\text{Ru}(\text{bpy})_3^{2+}$  concentration. Beyond 50  $\mu\text{M}$ ,  $I_{p1,ECL}$  reaches a plateau. In contrast, the ECL intensity of the second wave was always proportional to the concentration of  $\text{Ru}(\text{bpy})_3^{2+}$ , for concentrations up to at least 1 mM. Figure 2.4 (c) shows both the first and the second ECL responses when the  $\text{Ru}(\text{bpy})_3^{2+}$  concentration was in the “plateau” range of 50  $\mu\text{M}$  to 1.0 mM. These results clearly indicate that the mechanism for the first ECL signal is different from the second one.

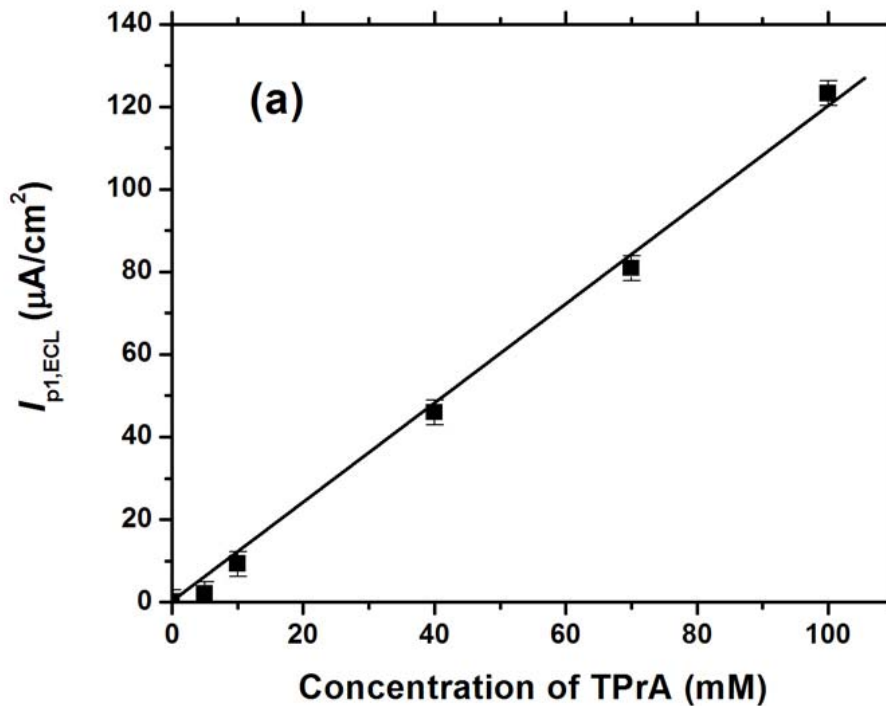


**Figure 2.4.** (a) The first ECL peak intensity as a function of TPrA concentration with  $1 \mu\text{M Ru}(\text{bpy})_3^{2+}$  (0.20 M PBS, pH 7.5). A 3 mm diameter glassy carbon electrode was used at a scan rate of 100 mV/s.

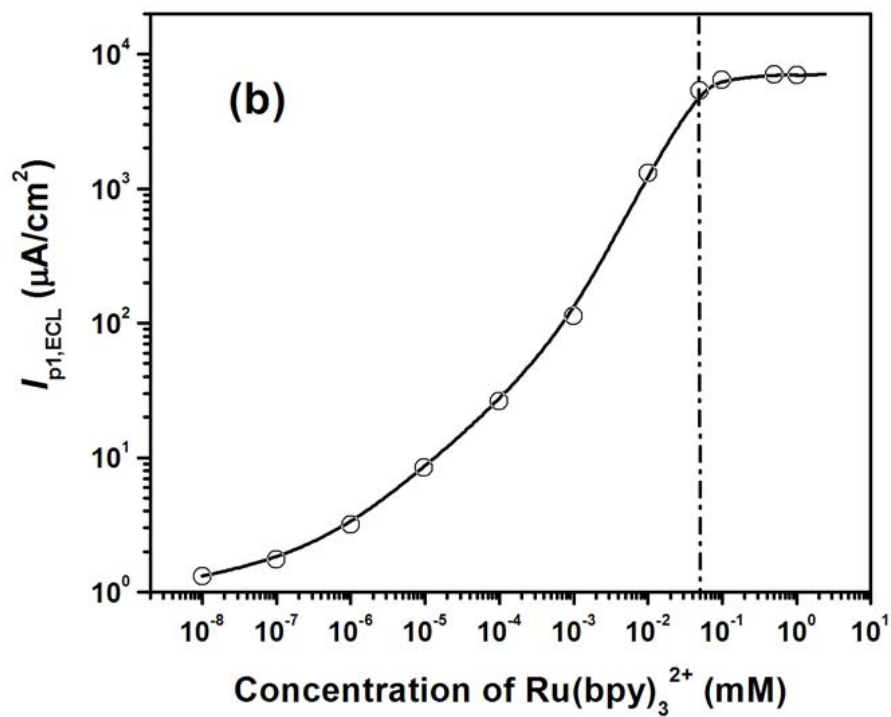


**Figure 2.4.** (b) The first ECL peak intensity as a function of Ru(bpy)<sub>3</sub><sup>2+</sup> concentration with 100 mM TPrA (0.20 M PBS, pH 8.5). A 3 mm diameter glassy carbon electrode was used at a scan rate of 100 mV/s.

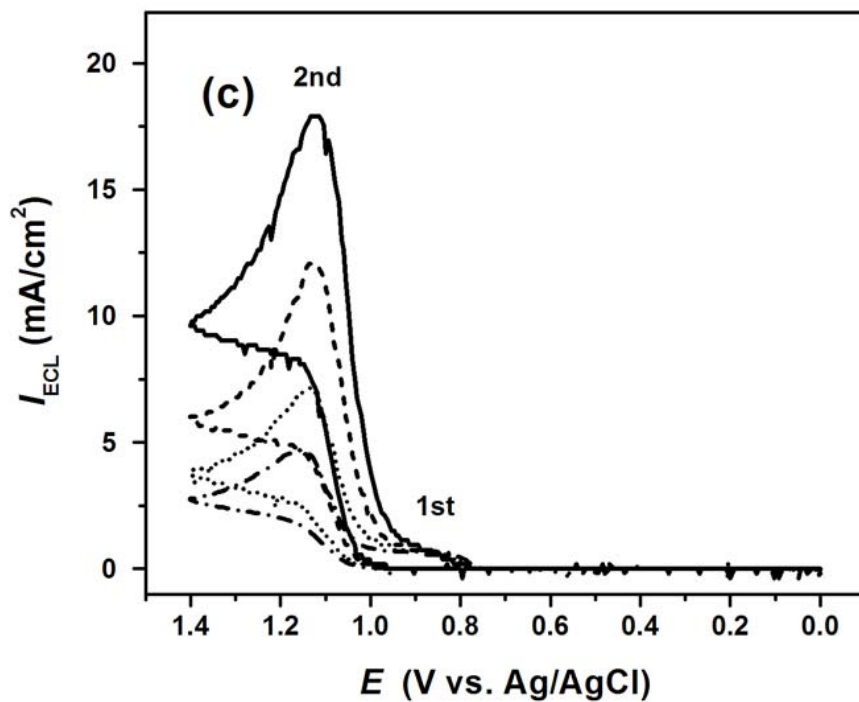


**Figure 2.4.** (c) The first and the second ECL responses in 100 mM TPrA (0.20 M PBS, pH 8.5) with different  $\text{Ru}(\text{bpy})_3^{2+}$  concentrations: 1 mM (solid line), 0.50 mM (dashed line), 0.10 mM (dotted line) and 0.05 mM (dash-dotted line). A 3 mm diameter glassy carbon electrode was used at a scan rate of 100 mV/s.

As demonstrated later, the intensity of the first ECL signal is determined by the quantity of TPrA derived radicals (cation and free) generated from the oxidation of TPrA at the electrode. In a relative excess of  $\text{Ru}(\text{bpy})_3^{2+}$  solution, the  $I_{1\text{st,ECL}}$  is governed by the concentration of TPrA [Figure 2.4 (a)]. On the other hand, when the reaction produces excess TPrA radicals relative to the concentration of  $\text{Ru}(\text{bpy})_3^{2+}$ , the  $I_{1\text{st,ECL}}$  will be controlled by the concentration of  $\text{Ru}(\text{bpy})_3^{2+}$ . When the  $\text{Ru}(\text{bpy})_3^{2+}$  concentration is equivalent to or greater than the concentration of radicals formed from TPrA oxidation, the  $I_{1\text{st,ECL}}$  will be independent of the concentration of  $\text{Ru}(\text{bpy})_3^{2+}$ . Figure 2.4 (c) exhibits these two features simultaneously.

**SECM – ECL Experiments.** To prove that oxidation of TPrA generates an ECL signal without direct oxidation of  $\text{Ru}(\text{bpy})_3^{2+}$ , experiments with the instrumental setup shown in Figure 2.1 were carried out. In this experiment,  $\{\text{Ru}(\text{bpy})_2[\text{bpy}(\text{COOH})_2]\}^{2+}$  was covalently immobilized on an ITO electrode. During the course of the SECM – ECL experiment, this modified ITO electrode was at an open circuit potential and served as the substrate. The reaction medium used was 10.0 mM TPrA solution in 0.10 M Tris/0.10 M  $\text{LiClO}_4$  buffer (pH = 8). Note that the tip in this experiment was considerably larger than those usually employed in SECM<sup>16</sup> to generate a sufficient flux of TPrA radicals to obtain an observable emission signal. However, this electrode still showed a decreasing SECM current response on approach to a substrate that blocked diffusion of

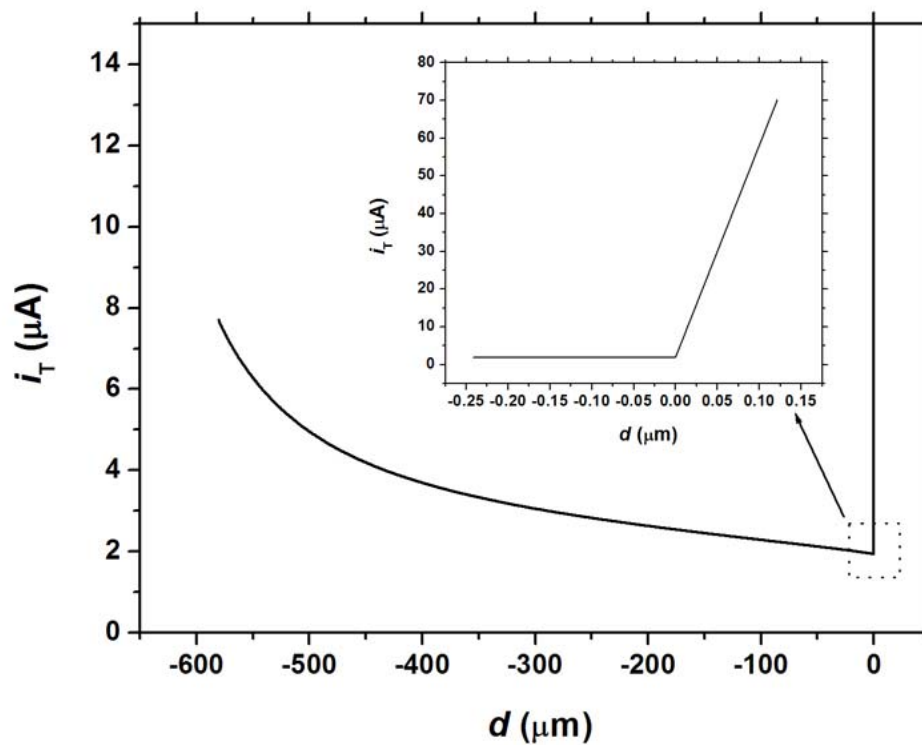


**Figure 2.5.** An approach curve obtained for the oxidation of 10.0 mM TPrA (0.10 M Tris/0.10 M LiClO<sub>4</sub> buffer, pH = 8) at a 1.5 mm diameter hemispherical Au electrode held at 0.85 V vs. Ag/AgCl. An ITO/OSiRu<sup>II</sup> electrode at open circuit served as the substrate.

reactant to the tip [Figure 2.5]. The distance between the tip and the substrate ( $d$ ) was estimated from this approach curve. By holding the tip potential at 0.85 V vs. Ag/AgCl, where TPrA oxidation occurs, a gradual decrease in tip current was initially observed as the tip slowly approached the substrate ( $\sim 0.05 \mu\text{m/s}$  at the last stage). The zero distance was indicated by a sudden increase in the tip current when contact is made between the tip and ITO. The tip was withdrawn from the substrate a given distance and cycled between 0 and 1.0 V vs. Ag/AgCl at  $\nu = 50 \text{ mV/s}$ , and the current and any ECL signal generated in the electrochemical cell were monitored. A typical experimental result for  $d = 1.92 \mu\text{m}$  is given in Figure 2.6. Upon oxidation of TPrA at  $\sim 0.80 \text{ V vs. Ag/AgCl}$ , an ECL signal appears and tracks the tip current during potential cycling. A pair of pre-waves located at  $\sim 0.5 \text{ V vs. Ag/AgCl}$  on the CV was frequently observed during the oxidation of TPrA, and may be attributed to the gold surface oxide formation and reduction.<sup>5</sup> The ECL signal could be detected only within a very small  $d$  ( $< \sim 5$  to  $6 \mu\text{m}$ ); the maximum intensity as a function of the tip distance is shown in Figure 2.7. At short distance, the ECL intensity decreased almost exponentially with the tip distance, indicating that the amount of dissolved  $\text{Ru}(\text{bpy})_2[(\text{bpy}(\text{COOH})_2)]^{2+}$  species from the substrate in the solution phase (if any) is negligible under the experimental conditions. This experiment clearly demonstrates that by simply oxidizing TPrA intermediates are formed that can

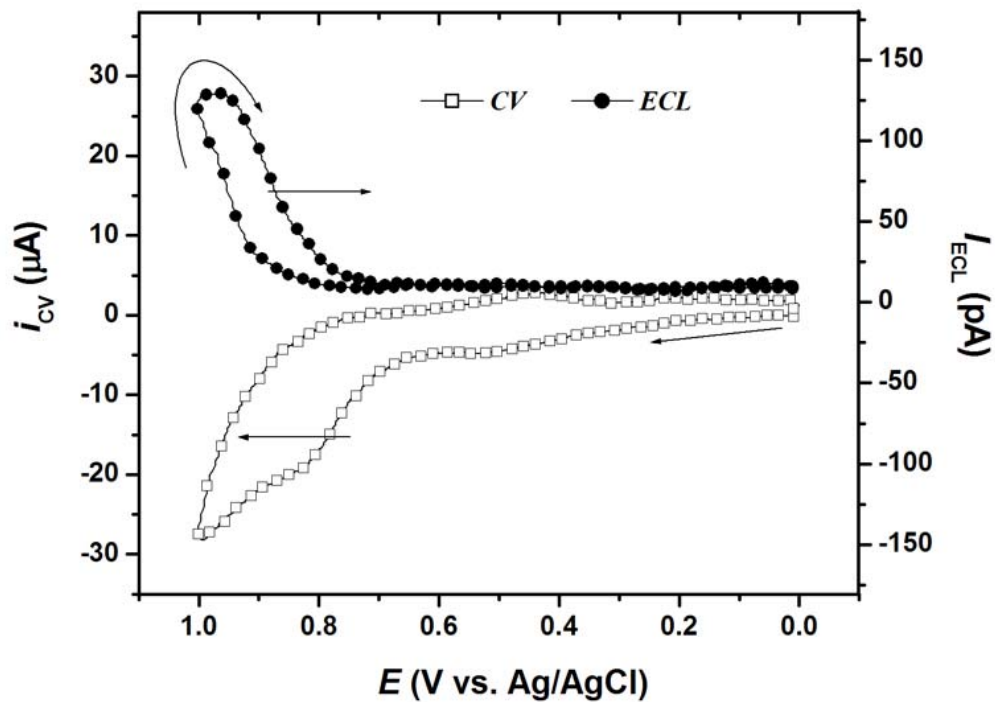


**Figure 2.6.** Cyclic voltammogram and ECL signal obtained in 10.0 mM TPrA (0.10 M Tris/0.10 M LiClO<sub>4</sub> buffer, pH = 8) at a 1.5 mm diameter hemispherical Au electrode when the tip/substrate separation distance,  $d$ , was 1.92  $\mu\text{m}$ . A scan rate of 50 mV/s was used, and the substrate was an ITO/OSiRu<sup>II</sup> electrode at open circuit.

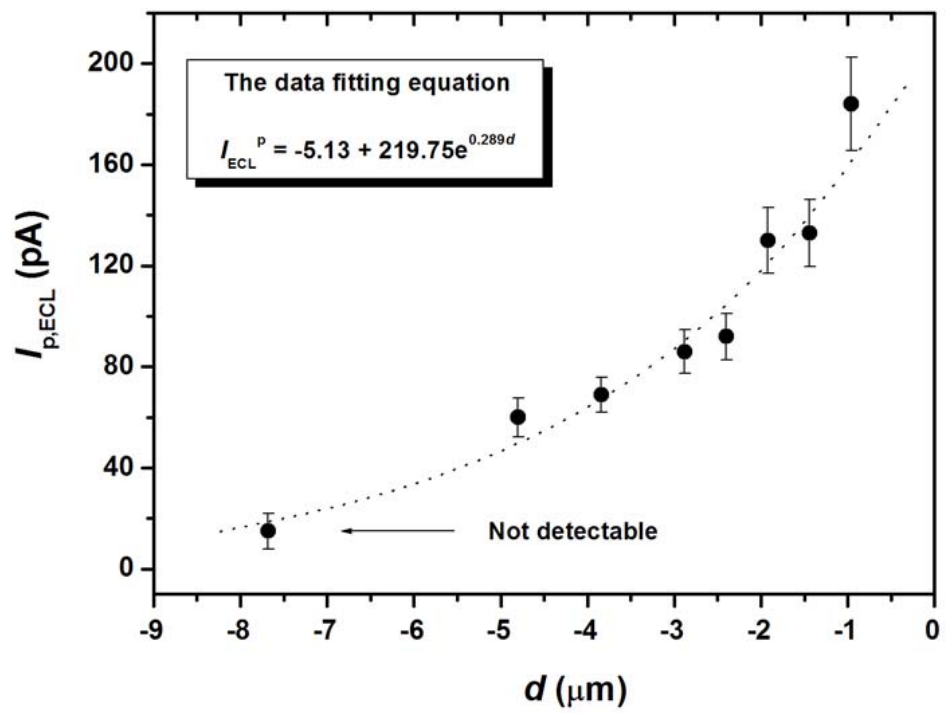
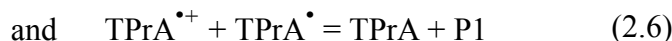
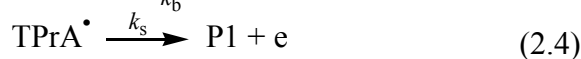
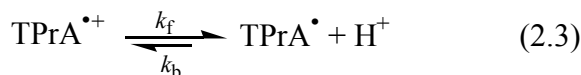
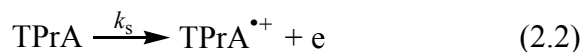


Figure 2.7. ECL peak intensity as a function of tip distance.

cause excitation of  $\text{Ru}(\text{bpy})_3^{2+}$  and is a direct confirmation of the ability to form excited states at all positions of a 2.8  $\mu\text{m}$  bead on an electrode surface.

The electrochemical oxidation of TPrA under various conditions has been extensively studied and the following mechanism for reactions occurring in aqueous solution is generally accepted (Scheme 2.4):<sup>4,17-21</sup>

**Scheme 2.4**



where  $\text{TPrA}^{\bullet+}$ ,  $\text{TPrA}^\bullet$ , P1 and P2 species have the same significance as in Scheme 2.2.

Deprotonated TPrA molecules first undergo one-electron oxidation to form TPrA cation radicals ( $\text{TPrA}^{\bullet+}$ ), which rapidly deprotonate to form TPrA free radicals ( $\text{TPrA}^\bullet$ ). These oxidize further by losing one electron to produce the iminium ion (P1), which subsequently hydrolyzes to products, P2.

On the basis of previous study,<sup>5</sup> we believe that the ECL signal generated under the present conditions is the emission of immobilized  $\text{Ru}(\text{bpy})_2[(\text{bpy}(\text{COOH})_2)]^{2+*}$ , simplified as  $\text{Ru}(\text{bpy})_3^{2+*}$  in the following discussions, since  $\text{Ru}(\text{bpy})_2[(\text{bpy}(\text{COOH})_2)]^{2+}$  and  $\text{Ru}(\text{bpy})_3^{2+}$  species exhibit very similar electrochemical behavior.<sup>22</sup> According to Scheme 2.4, the direct oxidation of TPrA at the tip of SECM - ECL experiments leads to the formation of reducing radicals ( $\text{TPrA}^\bullet$ ,  $E^\circ = \sim -1.7$  V vs.  $\text{Ag}/\text{AgCl}$ <sup>23</sup>) that can diffuse away from the tip and reach the substrate and react with immobilized  $\text{Ru}(\text{bpy})_3^{2+}$  to generate  $\text{Ru}(\text{bpy})_3^+$ . To produce  $\text{Ru}(\text{bpy})_3^{2+*}$ , some oxidant is required to remove an electron from  $\text{Ru}(\text{bpy})_3^+$ . The most likely oxidant candidate in this system is the cation radical  $\text{TPrA}^{\bullet+}$ ,  $E^\circ = \sim 0.83$  to  $0.95$  V vs.  $\text{Ag}/\text{AgCl}$ . However the deprotonation process of  $\text{TPrA}^{\bullet+}$  to  $\text{TPrA}^\bullet$  has usually been taken to be an extremely rapid process, resulting in an insufficient flux of  $\text{TPrA}^{\bullet+}$  from the tip to produce measurable ECL. We considered the possible production of  $\text{Ru}(\text{bpy})_3^{3+}$  from reaction of  $\text{Ru}(\text{bpy})_3^{2+}$  with  $\text{TPrA}^{\bullet+}$ , but the redox potential of the  $\text{TPrA}^{\bullet+}/\text{TPrA}$  couple is not sufficient for this reaction (see Scheme 2.5,<sup>24</sup> where the potentials have been converted to  $\text{Ag}/\text{AgCl}$  by taking  $E^\circ_{\text{Ag}/\text{AgCl}} = 0.20$  V vs.  $\text{NHE}$ <sup>25</sup>).



coefficient of  $4 \times 10^{-6}$  cm<sup>2</sup>/s, the lifetime,  $\tau$ , of the cation radical would be  $\sim 0.1$  ms.

**Fast scan CV and digital simulations.** With  $\tau \sim 0.1$  ms, one would estimate that TPrA<sup>•+</sup> could be detected by CV, if  $v > \sim 260$  V/s ( $\sim RT/F\tau$ ).<sup>25</sup> Fast scan CV experiments were thus carried out to detect TPrA<sup>•+</sup> species after TPrA oxidation at the electrode by scan reversal. A wide range of TPrA aqueous solutions ( $\sim 0.010$  to  $0.10$  M) with different supporting electrolytes and different pHs (from  $0.2$  M H<sub>2</sub>SO<sub>4</sub> to pH  $\sim 10$ ), different materials of the working electrode (GC, carbon fiber, Au, Pt) with different dimensions (from  $5$   $\mu$ m to  $3$  mm diameters), and different scan rates between  $20$  mV/s to  $1000$  V/s were used. However no wave associated with the reduction of TPrA<sup>•+</sup> on the reverse scan of the CVs was ever found. Scan rates faster than  $1000$  V/s and CV with background subtraction were also tried without success, since in these cases, significant charging currents and probably limitations from the rate of the heterogeneous electron transfer from TPrA interfered.

The failure to detect the cation radical can be ascribed to the fact that the oxidation of TPrA is an ECE process<sup>25</sup> and that at potentials where TPrA<sup>•+</sup> is reduced, the radical TPrA<sup>•</sup> is oxidized, so that a cathodic current is at least partially compensated by an anodic one. To investigate this effect, CV digital simulations following Scheme 2.4 were carried out assuming different values for

the heterogeneous electron transfer rate constants [ $k_s$  in eqs. 2.1 and 2.4], and the  $k_f$  and  $k_b$  values of eq. 2.3. Other parameters were either adopted from the literature or assigned to reasonable values. Figure 2.8 (a) shows a simulated CV of TPrA oxidation in pH 8 solution at a scan rate of 900 V/s, with the parameters shown in the figure caption. The cross over on the reverse scan, where the anodic current is larger on the reverse scan than it is on the forward scan current (at  $\sim 0.96$  V vs. Ag/AgCl), can be attributed to the greater contribution of TPrA $^{\bullet}$  to the measured current. The concentration profiles ( $c$  vs.  $x$ ) for both TPrA $^{\bullet+}$  and TPrA $^{\bullet}$  at specific potential values are shown in Figures 2.8 (b) to (e). Upon the oxidation of TPrA, a significant amount of TPrA $^{\bullet+}$  cation radical is formed at the electrode surface [Figure 2.8 (b)], which further dissociated to TPrA $^{\bullet}$ . Since the free radical is a very strong reducing agent and can be oxidized immediately at the electrode, its surface concentration equaling zero is expected. During the potential scan period of A to B [Figures. 2.8 (b) and (c)], due to the continuous conversion of TPrA $^{\bullet+}$  to TPrA $^{\bullet}$ , as well as diffusion to the bulk solution, the surface concentration of TPrA $^{\bullet+}$  starts to decrease, while the overall amount of TPrA $^{\bullet}$  in the electrode surface region increases. After potential B, substantial reduction of TPrA $^{\bullet+}$  to TPrA is expected, which results in a cathodic current and the surface concentration of TPrA $^{\bullet+}$  species decreases dramatically [Figure 2.8 (d)]. Note that even in this potential region, the overall current at the electrode is always anodic,

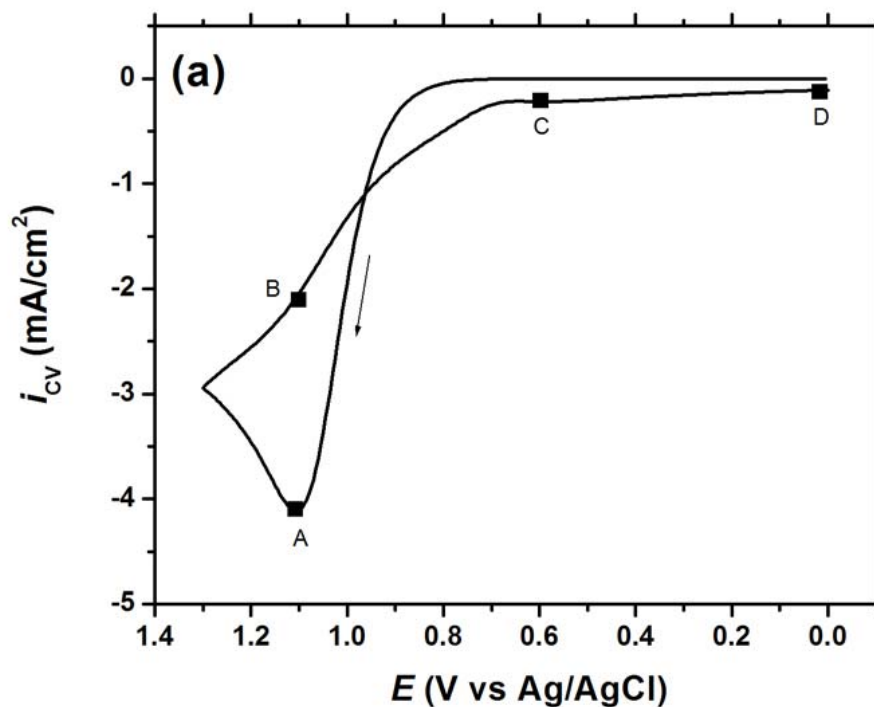


**Figure 2.8.** (a) A simulated CV of TPrA oxidation in pH 8 solution at a scan rate of 900 V/s. Parameters used in the simulation were (see Scheme 2.4 for further information):  $E^{\circ}_{\text{TPrA}^{*+}/\text{TPrA}} = 0.88$  V vs. Ag/AgCl,  $k_s$  (for eqs. 4.2 & 4.4) = 0.01 cm/s,  $E^{\circ}_{\text{P1}/\text{TPrA}^{\bullet}} = -1.7$  V vs. Ag/AgCl, for eq. 4.3  $k_f = 3500$  s<sup>-1</sup> &  $k_b = 7 \times 10^6$  s<sup>-1</sup>,  $c_{(\text{TPrA} + \text{TPrAH}^+)} = 10$  mM. All species were assumed to have a diffusion coefficient of  $5 \times 10^{-6}$  cm<sup>2</sup>/s except for H<sup>+</sup> ( $D_{\text{H}^+} = 5 \times 10^{-5}$  cm<sup>2</sup>/s).

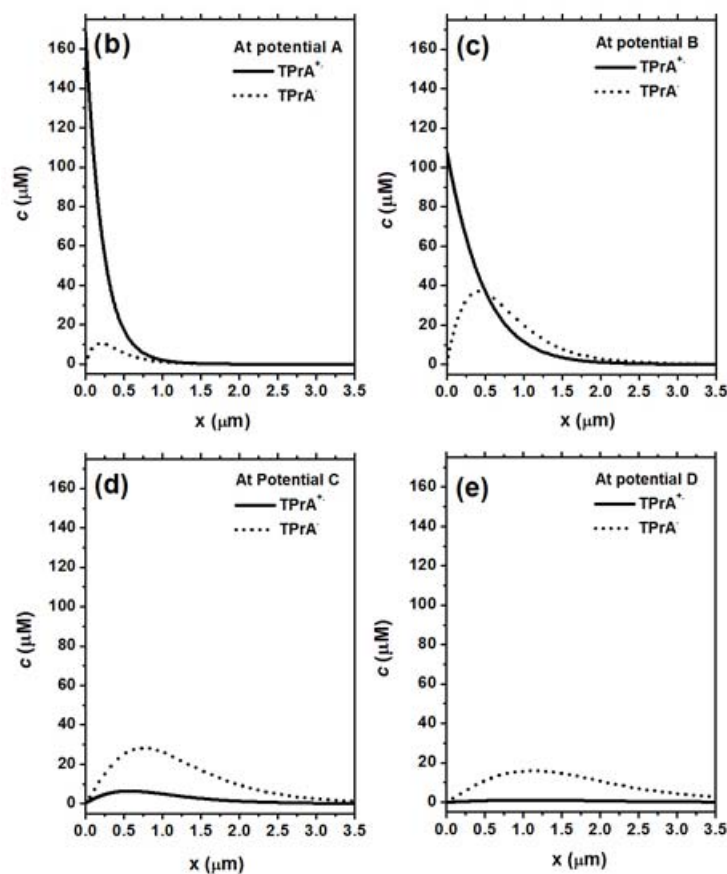


**Figure 2.8.** (b) to (e) the concentration profiles for TPrA<sup>+</sup> (solid line) and TPrA<sup>•</sup> (dotted line) at a specific points, A, B, C, and D, shown in (a). Parameters used in the simulation were (see Scheme 2.4 for further information):  $E^{\circ}_{\text{TPrA}^{+}/\text{TPrA}^{\bullet}} = 0.88$  V vs. Ag/AgCl,  $k_s$  (for eqs. 4.2 & 4.4) = 0.01 cm/s,  $E^{\circ}_{\text{P1}/\text{TPrA}^{\bullet}} = -1.7$  V vs. Ag/AgCl, for eq. 4.3  $k_f = 3500$  s<sup>-1</sup> &  $k_b = 7 \times 10^6$  s<sup>-1</sup>,  $c_{(\text{TPrA} + \text{TPrAH}^+)} = 10$  mM. All species were assumed to have a diffusion coefficient of  $5 \times 10^{-6}$  cm<sup>2</sup>/s except for H<sup>+</sup> ( $D_{\text{H}^+} = 5 \times 10^{-5}$  cm<sup>2</sup>/s).

because the current contribution from the oxidation of TPrA<sup>•</sup> is larger. Therefore, the absence of a reduction wave following the oxidation of TPrA with fast scan CV does not indicate that TPrA<sup>•+</sup> is so unstable that it cannot participate in the ECL reaction.

These digital simulations were carried out using the lifetime of TPrA<sup>•+</sup> obtained from the previous SECM – ECL experiment in 10 mM TPrA (pH 8). Figure 2.9 shows the simulated concentration distribution for TPrA<sup>•+</sup> formed at the tip as a function of distance from the tip. This curve was recorded at the potential A on the CV [inset of Figure 2.9], at which a maximum surface concentration and a maximum diffusion distance of TPrA<sup>•+</sup> was observed. By comparing the data shown in Figure 2.9 with those in Figure 2.7, about 3.6 % of the initial TPrA<sup>•+</sup> (or 71 nM, at  $x = 6 \mu\text{m}$ , Figure 2.9) are needed to diffuse to the substrate and react with immobilized Ru(bpy)<sub>3</sub><sup>2+</sup> to generate an ECL signal.

With the assumption that the TPrA<sup>•+</sup> deprotonation reaction (eq. 2.3) is a first-order process, the half-life ( $\tau_{1/2}$ ) of TPrA<sup>•+</sup> is  $\tau_{1/2} = 0.693/k_f$ , where  $k_f$  is the forward rate constant of eq. 2.3,  $\sim 3500 \text{ s}^{-1}$  based on the digital simulation.

**ESR of TPrA<sup>•+</sup> in aqueous solution.** With the above estimated life time, it should be possible to detect TPrA<sup>•+</sup> by ESR. Tertiary amine radical cations are generally believed to be short-lived intermediates in amine oxidation because of rapid deprotonation at the  $\alpha$ -carbon to produce  $\alpha$ -aminoalkyl free radicals.<sup>17</sup>

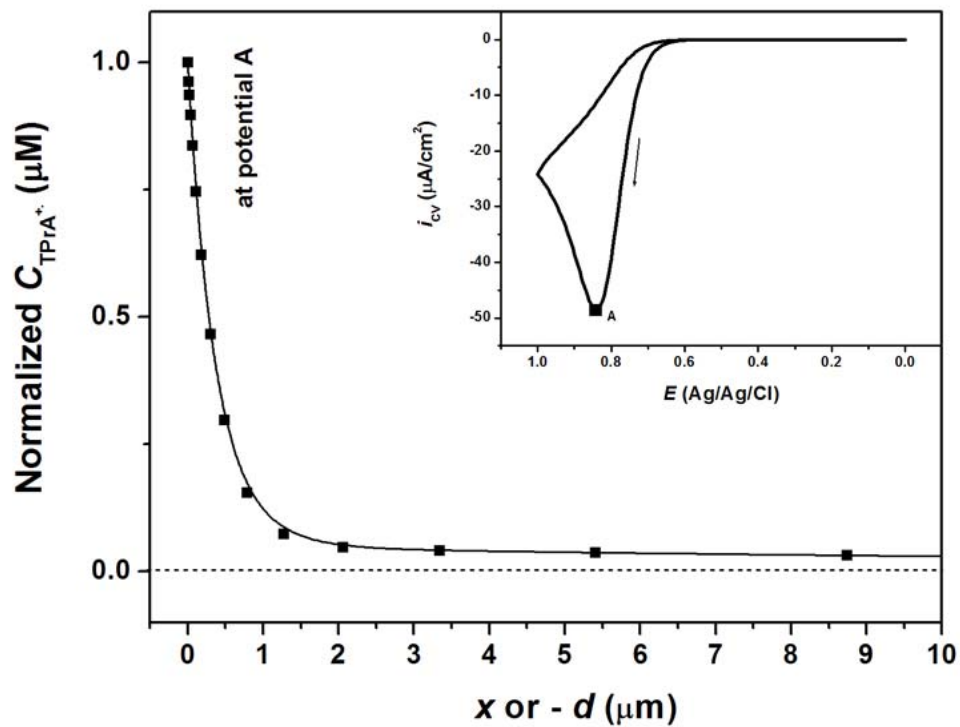


**Figure 2.9.** A simulated concentration profile for TPrA<sup>+</sup> formed at a 1.5 mm diameter hemispherical tip. This curve corresponds to potential A on the cyclic voltammogram (inset) for 10.0 mM TPrA (0.10 M Tris/0.10 M LiClO<sub>4</sub>, pH 8) with a scan rate of 50 mV/s. Other parameters required for the simulation are as in Figure 2.8.

Under some experimental conditions, such as strongly acidic solution and formation by ionizing radiation, the ESR of several small aliphatic amines cation radicals has been reported.<sup>17,26,27</sup>

To detect the TPrA<sup>•+</sup> cation radicals, an ESR quartz flat flow cell was used. Such cells have proven effective in producing a steady-state concentration of many reactive intermediates within the microwave cavity of the ESR instrument. Freshly prepared ~ 0.03 M Ru(bpy)<sub>3</sub><sup>3+</sup> and 0.10 M TPrA (pH 7) aqueous solutions were flowed into the mixing chamber at a rate of 2 to 5 mL/s and the ESR spectrum of the product in the quartz cell obtained. The major advantages of using Ru(bpy)<sub>3</sub><sup>3+</sup> as the oxidant are that the reaction between Ru(bpy)<sub>3</sub><sup>3+</sup> and TPrA is rapid at neutral pH<sup>4</sup> and it is a one-electron transfer process. Many other oxidants, such as Ce<sup>4+</sup>, KMnO<sub>4</sub>, KBrO<sub>3</sub> and Cl<sub>2</sub>, were found to be unsuitable for TPrA oxidation, because either they required the use of strongly acidic solutions, where TPrA oxidation was slow, the oxidant itself or its reduction products gave strong ESR background, or the redox reaction was not fast enough. Figure 2.10 shows the experimentally measured (dotted line) as well as the simulated (solid line) ESR spectra of TPrA<sup>•+</sup> generated in the flow cell at 20 °C. The spectrum consists of a relatively intense and sharp septet with a splitting of ~ 20 G due to the six equivalent  $\alpha$ -hydrogens. On the basis of the simulation, hyperfine coupling constants of 19.87 G and 20.05 G for <sup>14</sup>N (1N,  $I = 1$ ) and  $\alpha$ -<sup>1</sup>H (6H,  $I = 1/2$ ) were evaluated. The experimental ESR spectrum had a

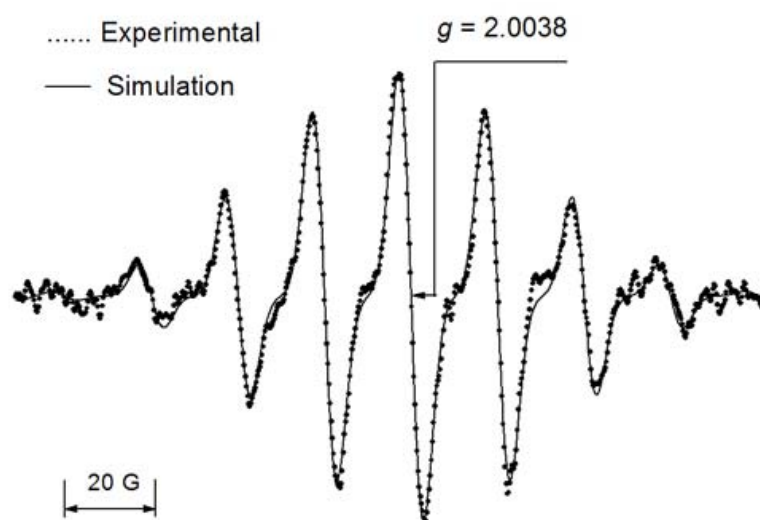


**Figure 2.10.** Experimentally measured (dotted line) and simulated (solid line) ESR spectra of  $\text{TPrA}^{\bullet+}$  generated by the oxidation of TPrA by  $\text{Ru}(\text{bpy})_3^{3+}$  in an aqueous pH 7 solution at 20 °C.

$g$ -value of 2.0038. Recently, Liu *et. al.*<sup>27</sup> have reported the structure and dynamics of TPrA<sup>•+</sup> cation radicals generated in solid AlPO<sub>4-5</sub> by ionizing radiation. Our solution-phase ESR spectrum is consistent with their solid-state ESR spectrum at 300 K.

During the ESR experiments, Ru(bpy)<sub>3</sub><sup>3+</sup> and Ru(bpy)<sub>3</sub><sup>+</sup> species can also produce signals. However, they have no effect on the ESR spectrum of TPrA<sup>•+</sup>, since the  $g$ -values of these two species are very different than that of TPrA<sup>•+</sup>.<sup>28-31</sup> No ESR signal associated with TPrA<sup>•</sup> was observed, probably because they were oxidized by excess oxidant in the solution. Note that the expected ESR spectrum of the carbon-centered TPrA<sup>•</sup> would be very different than the one observed.

## 2.4 Conclusions

The ECL emission as a function of potential for the Ru(bpy)<sub>3</sub><sup>2+</sup>/TPrA system consists of two waves. The first occurs with the direct oxidation of TPrA at the electrode, and the second where Ru(bpy)<sub>3</sub><sup>2+</sup> is oxidized. In dilute Ru(bpy)<sub>3</sub><sup>2+</sup> solutions ( $< \sim \mu\text{M}$ ) containing mM TPrA, the intensity of the first ECL wave is significant and can be larger than that for the second ECL wave. A new route for the generation of Ru(bpy)<sub>3</sub><sup>2+\*</sup> at potentials of the first wave is proposed, where TPrA<sup>•+</sup> formed during TPrA oxidation is a sufficiently stable intermediate that can oxidize Ru(bpy)<sub>3</sub><sup>+</sup> (formed from the reduction of Ru(bpy)<sub>3</sub><sup>2+</sup> by TPrA<sup>•</sup> free radical) to give Ru(bpy)<sub>3</sub><sup>2+\*</sup>. Based on SECM – ECL experiments and digital

simulation, a half-life of  $\sim 0.2$  ms was estimated for  $\text{TPrA}^{\bullet+}$  in aqueous solution. An ESR spectrum of  $\text{TPrA}^{\bullet+}$  in aqueous solution was obtained via flow mixing experiments. Fast scan CV experiments and simulations revealed that the absence of reduction wave for  $\text{TPrA}^{\bullet+}$  on the reverse scan can be attributed to the cancellation of the component of current from the reduction of  $\text{TPrA}^{\bullet+}$  by the anodic current contribution from the oxidation of  $\text{TPrA}^{\bullet}$ . These results also explain why selection of highly efficient coreactants is difficult for determination of low concentrations of Ru-label. The coreactant must form both oxidant (e.g.  $\text{TPrA}^{\bullet+}$ ) and reductant (e.g.  $\text{TPrA}^{\bullet}$ ) with appropriate redox potentials and lifetimes. Thus, the deprotonation rate of  $\text{TPrA}^{\bullet+}$  must be just right to build up the needed concentrations of both species.

## References

- (1) Noffsinger, J. B.; Danielson, N. D. *Anal. Chem.* **1987**, *59*, 865.
- (2) Leland, J. K.; Powell, M. J. *J. Electrochem. Soc.* **1990**, *137*, 3127.
- (3) Bard, A. J.; Debad, J. D.; Leland, J. K.; Sigal, G. B.; Wilbur, J. L.; Wohlstadter, J. N., "Chemiluminescence, Electrogenerated," in *Encyclopedia of Analytical Chemistry: Applications, Theory and Instrumentation*, R. A. Meyers, Ed., John Wiley & Sons: New York, 2000, Vol. 11, p. 9842 and references therein.
- (4) Kanoufi, F.; Zu, Y.; Bard, A. J. *J. Phys. Chem. B* **2001**, *105*, 210.
- (5) Zu, Y.; Bard, A. J. *Anal. Chem.* **2000**, *72*, 3223.
- (6) Gross, E. M.; Pastore, P.; Wightman, R. M. *J. Phys. Chem. B* **2001**, *105*, 8732.
- (7) He, L.; Cox, K. A.; Danielson, N. D. *Anal. Lett.* **1990**, *23*, 195.
- (8) Rubinstein, I.; Bard, A. J. *J. Am. Chem. Soc.* **1981**, *103*, 512.
- (9) Zu, Y.; Bard, A. J. *Anal. Chem.* **2001**, *73*, 3960.
- (10) Sprintschnik, G.; Sprintschnik, H. W.; Kirsch, P. P.; Whitten, D. G. *J. Am. Chem. Soc.* **1977**, *99*, 4947.
- (11) Murray, R. W. In *Electroanalytical Chemistry*; Bard, A. J., Ed.; Marcel Dekker, Inc.: New York, 1984; Vol. 13, p 191.
- (12) Charkoudian, J. C. *J. Magn. Reson.* **1984**, *57*, 287.
- (13) Windle, J. J.; Wiersema, A. K. *J. Chem. Phys.* **1963**, *39*, 1139.
- (14) Pake, G. E.; Townsend, J.; Weissman, S. I. *Phys. Rev.* **1952**, *85*, 682.
- (15) Duling, D. R. *J. Magn. Reson., Ser. B* **1994**, *104*, 105.
- (16) Bard, A. J.; Mirkin, M. V., Eds., *Scanning Electrochemical Microscopy*, Marcel Dekker, New York, 2001.
- (17) Chow, Y. L.; Danen, W. C.; Nelsen, S. F.; Rosenblatt, D. H. *Chem. Rev.* **1978**, *78*, 243.
- (18) Mann, C. K. *Anal. Chem.* **1964**, *36*, 2424.

- \
- (19) Masui, M.; Sayo, H.; Tsuda, Y. *J. Chem. Soc., B* **1968**, 973.
  - (20) Portis, L. C.; Bhat, V. V.; Mann, C. K. *J. Org. Chem.* **1970**, *35*, 2175.
  - (21) Ross, S. D. *Tetrahedron Lett.* **1973**, 1237.
  - (22) Elliott, C. M.; Hershenhart, E. J. *J. Am. Chem. Soc.* **1982**, *104*, 7519.
  - (23) Lai, R., Bard, A. J., *unpublished experiments*.
  - (24) Roundhill, D. M. In *Photochemistry and Photophysics of Metal Complexes*; Fackler, J. J. P., Ed.; Plenum Press: New York, 1994, p 165.
  - (25) Bard, A. J.; Faulkner, L. R. *Electrochemical Methods*; 2nd ed.; John Wiley & Sons, Inc.: New York, 2000.
  - (26) Eastland, G. W.; Rao, D. N. R.; Symons, M. C. R. *J. Chem. Soc., Perkin Trans. 2* **1984**, 1551.
  - (27) Liu, W.; Yamanaka, S.; Shiotani, M.; Michalik, J.; Lund, A. *Phys. Chem. Chem. Phys.* **2001**, *3*, 1611.
  - (28) Ledney, M.; Dutta, P. K. *J. Am. Chem. Soc.* **1995**, *117*, 7687.
  - (29) Quayle, W. H.; Lunsford, J. H. *Inorg. Chem.* **1982**, *21*, 97.
  - (30) Matsuura, K.; Kevan, L. *J. Phys. Chem.* **1996**, *100*, 10652.
  - (31) Matsuura, K.; Kevan, L. *Radiat. Phys. Chem.* **2001**, *62*, 399.

**Chapter 3: Structure and Reactivity Aspects of Various Amine  
Coreactants and Coreactant Buffers on the Electrogenerated  
Chemiluminescence of Tris(2,2'-bipyridine)ruthenium(II)  
Complex, Ru(bpy)<sub>3</sub><sup>2+</sup>, in Aqueous Media**

**3.1 Introduction**

Generally, electrogenerated chemiluminescence (ECL)<sup>1-3</sup> can be achieved either by ion annihilation or by use of coreactants. In the ion annihilation mode, the excited state (R\*) of an emitter (R) is produced by an energetic electron transfer reaction between electrochemically generated R<sup>•+</sup> and R<sup>•-</sup>.



However, this mode requires that both R<sup>•+</sup> and R<sup>•-</sup> are accessible and fairly stable with a sufficiently long lifetime in the diffusion layer of the electrode to obtain the ECL reaction.

If these conditions cannot be obtained, coreactants can be employed. A coreactant is an electrochemically active reagent that can produce a reactive species, which can reduce R<sup>•+</sup> or oxidize R<sup>•-</sup> to generate R\*. Therefore, ECL can

be achieved by sweeping or pulsing the electrode potential in only one direction, either cathodic or anodic. Using a coreactant for ECL has some advantages over the ion annihilation mode; (a) it is not necessary to generate both  $R^{\bullet+}$  and  $R^{\bullet-}$  at the electrode, (b) it is useful when an emitter has an unstable  $R^{\bullet+}$  or  $R^{\bullet-}$  form, and (c) it is useful for solvents having a narrow potential window, such as water, so that either  $R^{\bullet+}$  or  $R^{\bullet-}$  cannot be formed.

Amines are good candidates as coreactants in aqueous media, and tri-*n*-propylamine (TPrA) among them has been studied intensively<sup>4-8</sup>. In chapter 1 and previous studies,<sup>9,10</sup> tris(2,2'-bipyridine)ruthenium(II),  $Ru(bpy)_3^{2+}$  ( $bpy = 2,2'$ -bipyridine), was shown to generate two ECL waves in a plot of the ECL intensity vs. potential when TPrA was used as a coreactant. The first ECL wave began at the same potential where TPrA was oxidized, but before  $Ru(bpy)_3^{2+}$  was oxidized. This ECL continued until  $Ru(bpy)_3^{2+}$  was oxidized. According to the proposed mechanism of the first ECL wave, TPrA produces a radical cation ( $Pr_3N^{\bullet+}$ ) [eq. (3.2)] and a free radical ( $Pr_2NC^{\bullet}HEt$ ) [eq. (3.3)] both having a sufficiently long lifetime,<sup>10</sup> when TPrA is oxidized at an electrode. The produced  $Pr_2NC^{\bullet}HEt$  reduces  $Ru(bpy)_3^{2+}$  to  $Ru(bpy)_3^+$ , which will be oxidized to the excited state of  $Ru(bpy)_3^{2+}$  by  $Pr_3N^{\bullet+}$  later. The mechanism of this first ECL wave is shown in Scheme 3.1.

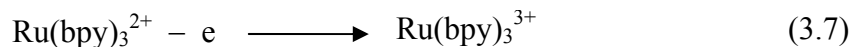
### Scheme 3.1



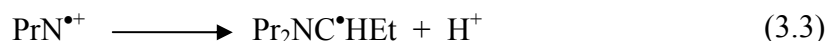
where Pr is  $\text{CH}_3\text{CH}_2\text{CH}_2-$  and Et is  $\text{CH}_3\text{CH}_2-$ .

The second ECL wave arises at potentials where both  $\text{Ru}(\text{bpy})_3^{2+}$  and TPrA are oxidized. Two routes<sup>6,7</sup>, direct oxidation (Scheme 3.2) and catalytic (Scheme 3.3) routes, contribute to the second ECL wave. The excited state of  $\text{Ru}(\text{bpy})_3^{2+}$  is formed by an electron transfer reaction between  $\text{Ru}(\text{bpy})_3^{3+}$  and  $\text{Pr}_2\text{NC}^{\bullet}\text{HEt}$  in both routes [eq. (3.8)]. In the direct oxidation route (Scheme 3.2), the generation of  $\text{Pr}_2\text{NC}^{\bullet}\text{HEt}$  is initiated by a heterogeneous electrode reaction, while this radical ion ( $\text{Pr}_2\text{NC}^{\bullet}\text{HEt}$ ) is produced by a homogeneous oxidation by electrochemically generated  $\text{Ru}(\text{bpy})_3^{3+}$  in the catalytic route (Scheme 3.3). The relative contribution of these different routes to the second ECL wave depends on the experimental conditions, such as electrode potential and relative concentration of  $\text{Ru}(\text{bpy})_3^{2+}$  and TPrA.<sup>7</sup>

### Scheme 3.2 (*Direct Oxidation Route*)



### Scheme 3.3 (*Catalytic Route*)



In both routes, the generation of  $\text{Ru}(\text{bpy})_3^+$  by  $\text{PrNC}^{\bullet}\text{HEt}$  [eq. (3.4)] is also possible, so an annihilation reaction between  $\text{Ru}(\text{bpy})_3^+$  and  $\text{Ru}(\text{bpy})_3^{3+}$  may also occur.

ECL by amine coreactants is strongly dependent on the stability and reactivity of amine radicals produced on oxidation, which depends on the molecular structures of amines. Therefore, it is important to correlate the stability and reactivity of amines to their molecular structures. Noffsinger, *et. al.*<sup>11</sup> reported that the chemiluminescence (CL) intensity of  $\text{Ru}(\text{bpy})_3^{3+}$  in aqueous media

increased in order of primary < secondary < tertiary amine, and Nieman<sup>12</sup>, *et. al.* demonstrated that the ECL intensity of Ru(bpy)<sub>3</sub><sup>2+</sup> increased in order of mono-*n*-propylamine < di-*n*-propylamine < tri-*n*-propylamine. However, there has been no report concerning on the relative stability and reactivity of cationic and free radicals of amine coreactants for the first and second ECL waves.

In this chapter, the structure and reactivity aspects of 14 different amine coreactants toward the ECL of Ru(bpy)<sub>3</sub><sup>2+</sup> in phosphate buffer solutions (PBS) at different pH are discussed. The use of coreactant buffers, which function as both coreactant and buffer is also studied. The molecular structures of amine coreactants and coreactant buffers are shown in Figure 3.1 and Figure 3.2, respectively.

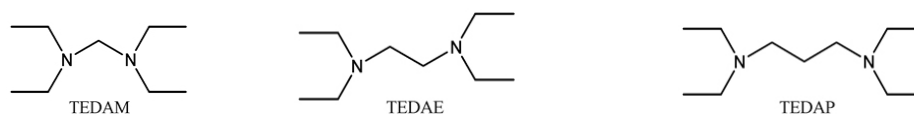
## 3.2 Experimental Section

**Chemicals and Solutions.** Tris(2,2'-bipyridyl)dichlororuthenium(II) hexahydrate, Ru(bpy)<sub>3</sub>Cl<sub>2</sub>·6H<sub>2</sub>O (99.99 %), dibromomethane (99 %), 1,2-dibromoethane (99+ %), 1,3-dibromopropane (99 %), di-*n*-propylamine (99+ %), 1-bromopropane (99 %), piperidine (99.5+ %), bromoethane (99+ %), piperazine (99 %) were obtained from Aldrich (Milwaukee, WI) and used as received. Triethylamine (TEtA, 99.5 %), tri-*n*-propylamine (TPrA, 99+ %), *N,N,N',N'*-tetraethylmethanediamine (TEDAM, 97 %), *N,N,N',N'*-tetraethylethylenediamine

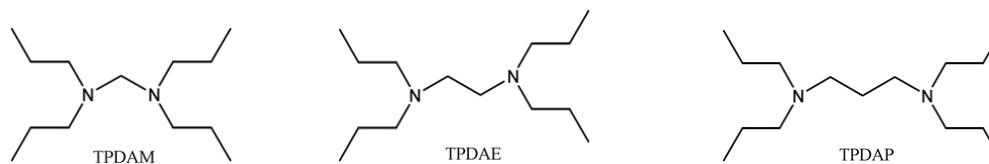
(a) Acyclic monoamine group



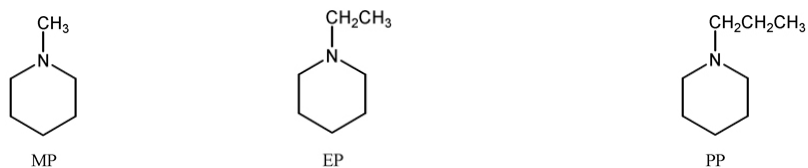
(b) Acyclic *N,N,N',N'*-tetraethyl diamine group



(c) Acyclic *N,N,N',N'*-tetra-*n*-propyl diamine group



(d) Heteroalicyclic monoamine group



(e) Heteroalicyclic diamine group

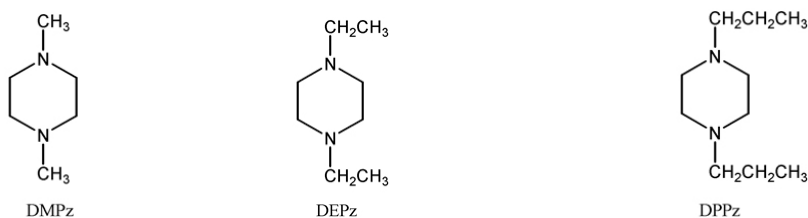
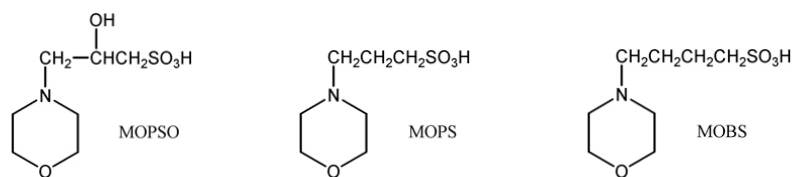
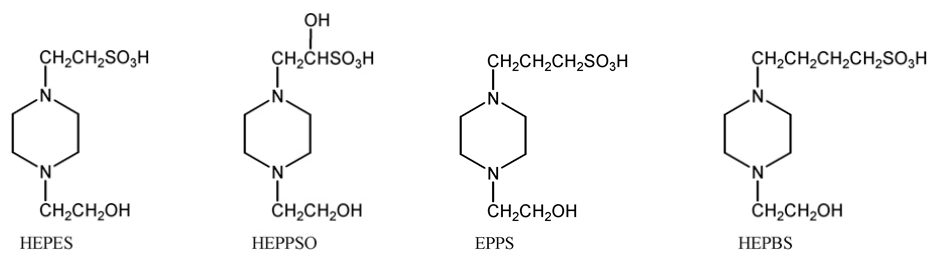


**Figure 3.1.** Molecular structures of amine coreactants. Acronyms are defined in the text.

(a) Morpholine group



(b) Piperazine group



(c) Acyclic tertiary amine group

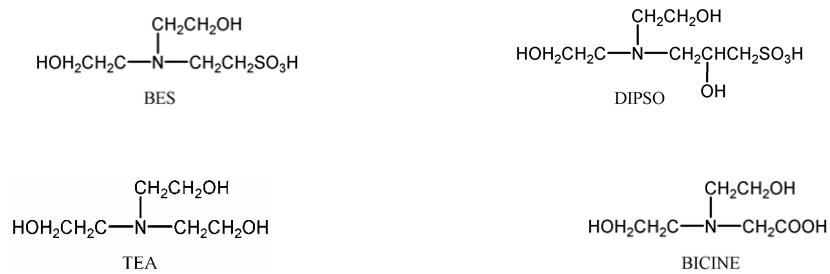
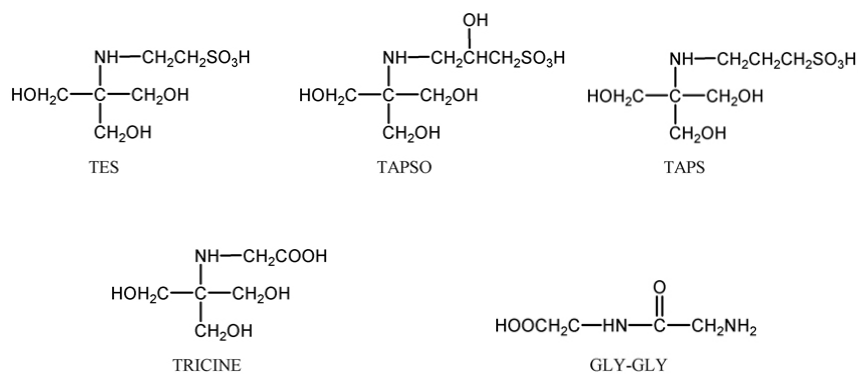


**Figure 3.2** *Continued on the next page.*

(d) Acyclic secondary amine group



(e) Acyclic secondary diamine group

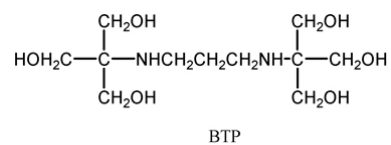


**Figure 3.2. (Cont.)** Molecular structures of coreactant buffers (CB). Acronyms are defined in the text.

(TEDAE, 98 %), *N,N,N',N'*-tetraethyl-1,3-propanediamine (TEDAP, 97%), 1-methylpiperidine (MP, 98+ %), 1-ethylpiperidine (EP, 99 %), and 1,4-dimethylpiperazine (DMPz, 98 %) were purchased from Aldrich (Milwaukee, WI) and vacuum distilled before use. *N,N,N',N'*-Tetra-*n*-propylmethanediamine (TPDAM), *N,N,N',N'*-tetra-*n*-propylethylenediamine (TPDAE), *N,N,N',N'*-tetra-*n*-propyl-1,3-propanediamine (TPDAP), 1-*n*-propylpiperidine (PP), 1,4-diethylpiperazine (DEPz), and 1,4-di-*n*-propylpiperazine (DPPz) were synthesized by direct alkylations from the appropriate starting materials (see Syntheses section). Molecular weights and structures of synthesized amines were confirmed by their mass spectra and nuclear magnetic resonance (NMR) spectra. Phosphoric acid (H<sub>3</sub>PO<sub>4</sub>, 85 %), monobasic- (NaH<sub>2</sub>PO<sub>4</sub>·H<sub>2</sub>O), dibasic- (Na<sub>2</sub>HPO<sub>4</sub>·12H<sub>2</sub>O), and tribasic sodium phosphate (Na<sub>3</sub>PO<sub>4</sub>·7H<sub>2</sub>O) from Fisher Scientific Co. (Fair Lawn, NJ) were used without further purification. 3-[*N*-Morpholino]-2-hydroxypropanesulfonic acid (MOPSO), 1,3-bis[tris(hydroxymethyl)methylamino]propane (BTP), *N,N*-bis[2-hydroxyethyl]-2-aminoethanesulfonic acid (BES), 3-[*N*-morpholino]propanesulfonic acid (MOPS), *N*-tris[hydroxymethyl]methyl-2-aminoethanesulfonic acid (TES), *N*-[2-hydroxyethyl]piperazine-*N'*-[2-ethanesulfonic acid] (HEPES), 3-[*N,N*-bis(2-hydroxyethyl)amino]-2-hydroxypropanesulfonic acid (DIPSO), 4-[*N*-morpholino]butanesulfonic acid (MOBS), 3-[*N*-tris(hydroxymethyl)methylamino]-2-hydroxypropanesulfonic acid (TAPSO),

*N*-[2-hydroxyethyl]piperazine-*N'*-[2-hydroxypropanesulfonic acid] (HEPPSO), triethanolamine (TEA), *N*-[2-hydroxyethyl]piperazine-*N'*-[3-propanesulfonic acid] (EPPS), *N*-tris[hydroxymethyl]methylglycine (TRICINE), *N*-glycylglycine (GLY-GLY), *N,N*-bis[2-hydroxyethyl]glycine (BICINE), *N*-[2-hydroxyethyl]piperazine-*N'*-[4-butanesulfonic acid] (HEPBS), and *N*-tris[hydroxymethyl]methyl-3-aminopropanesulfonic acid (TAPS) were obtained from Sigma (St. Louis, MO) and used without further purification. 0.2 M phosphate buffer solutions with various pH values were prepared by a literature method.<sup>13</sup> 0.2 M coreactant buffer solutions were prepared by dissolving coreactant buffers in deionized water containing 0.1 M NaCl. The pH values of all buffer solutions were adjusted with either ~6 M sodium hydroxide (NaOH) or ~6 M hydrochloric acid (HCl) solution. Deionized water (Milli-Q, Millipore) was used to prepare all buffer solutions.

#### **Syntheses of TPDAM, TPDAE, TPDAP, PP, DEPz, and DPPz.**

*N,N,N',N'*-Tetra-*n*-propylmethanediamine (TPDAM). TPDAM was synthesized by refluxing neat dibromomethane (10 ml) and excess di-*n*-propylamine (60 ml) at 120 °C without any solvent for 12 hrs. Once a reaction was done, white precipitates were formed. These precipitates were filtered and lightly washed with ether. Then they were dissolved in deionized water (50 ml) and this solution was saturated with sodium hydroxide (NaOH). Using ether, TPDAM was extracted from the NaOH saturated solution, and then vacuum distilled. [48 % of yield. <sup>1</sup>H

NMR (CDCl<sub>3</sub>)  $\delta$  0.84 (*t*, 12H,  $J = 7.3$  Hz, terminal CH<sub>3</sub>-), 1.37 – 1.49 (*m*, at  $\beta$ -position of propyl branch), 3.14 (*s*, 2H, -CH<sub>2</sub>- backbone). CI-MS (CH<sub>4</sub>)  $m/z$  calculated for C<sub>13</sub>H<sub>30</sub>N<sub>2</sub> 214.37, found 215 (M+1)<sup>+</sup>.]

*N,N,N',N'*-Tetra-*n*-propylethylenediamine (TPDAE). TPDAE was synthesized by the same procedure as TPDAM synthesis. 12 ml of 1,2-dibromoethane and excess di-*n*-propylamine (60 ml) were used as starting materials. [64 % of yield. <sup>1</sup>H NMR (CDCl<sub>3</sub>)  $\delta$  0.84 (*t*, 12H,  $J = 7.3$  Hz, terminal CH<sub>3</sub>-), 1.36 – 1.49 (*m*, 8H, -CH<sub>2</sub>- at  $\beta$ -position of propyl branch), 2.33 – 2.38 (*m*, 8H, -CH<sub>2</sub>- at  $\alpha$ -position of propyl branch), 2.49 (*s*, 4H, -CH<sub>2</sub>- in ethylene backbone). CI-MS (CH<sub>4</sub>)  $m/z$  calculated for C<sub>14</sub>H<sub>32</sub>N<sub>2</sub> 228.39, found 229 (M+1)<sup>+</sup>.]

*N,N,N',N'*-Tetra-*n*-propylpropane-1,3-diamine (TPDAP). TPDAP was synthesized by the same procedure as TPDAM synthesis. 14 ml of 1,3-dibromopropane and excess di-*n*-propylamine (60 ml) were used as starting materials. [62 % of yield. <sup>1</sup>H NMR (CDCl<sub>3</sub>)  $\delta$  0.84 (*t*, 12H,  $J = 7.3$  Hz, terminal CH<sub>3</sub>-), 1.36 – 1.48 (*m*, 8H, -CH<sub>2</sub>-  $\beta$ -position in propyl branch), 1.50 – 1.60 (*m*, 2H, -CH<sub>2</sub>-  $\beta$ -position in propylene backbone), 2.31 – 2.41 (*m*, 12H, -CH<sub>2</sub>- at  $\alpha$ -position). CI-MS (CH<sub>4</sub>)  $m/z$  calculated for C<sub>15</sub>H<sub>34</sub>N<sub>2</sub> 242.41, found 243 (M+1)<sup>+</sup>.]

*1*-Propylpiperidine (PP). PP was synthesized by the same procedure as TPDAM synthesis. 13 ml of 1-bromopropane and excess piperidine (45 ml) were used as starting materials. The temperature of reflux was 110 °C. [56 % of yield.

$^1\text{H}$  NMR ( $\text{CDCl}_3$ )  $\delta$  0.86 (*t*, 3H,  $J = 7.4$  Hz, terminal  $-\text{CH}_3$ ), 1.10 – 1.80 (*m*, 8H,  $-\text{CH}_2-$  at  $\beta$ - and  $\gamma$ -position), 2.29 – 2.31 (*m*, 6H,  $-\text{CH}_2-$  at  $\alpha$ -position). CI-MS ( $\text{CH}_4$ )  $m/z$  calculated for  $\text{C}_8\text{H}_{17}\text{N}$  127.21, found 128 ( $\text{M}+1$ ) $^+$ .]

*1,4-Diethylpiperazine (DEPz)*. DEPz was synthesized with 12 g of piperazine and 35 ml of 1-bromoethane. Both of them were dissolved in 50 ml ethanol and then refluxed at 100 °C for 12 hrs. Once white precipitates were formed, they were filtered and gently washed with ethanol and then dried. These precipitates were dissolved in deionized water (50 ml) and then saturated with NaOH. After crude DEPz was extracted with ether, it was purified by vacuum distillation. [24 % of yield.  $^1\text{H}$  NMR ( $\text{CDCl}_3$ )  $\delta$  0.99 (*t*, 6H,  $J = 7.4$  Hz, terminal  $-\text{CH}_3$ ), 2.00 – 2.30 (*m*, 4H at  $\alpha$ -position of ethyl group), 2.53 (*s*, 8H,  $-\text{CH}_2-$  at the ring). CI-MS ( $\text{CH}_4$ )  $m/z$  calculated for  $\text{C}_8\text{H}_{18}\text{N}_2$  142. 24, found 143 ( $\text{M}+1$ ) $^+$ .]

*1,4-Dipropylpiperazine (DPPz)*. DPPz was synthesized by the same procedure as DEPz synthesis. Pure solid of piperazine and 1-bromopropane were used as starting materials. [22 % of yield.  $^1\text{H}$  NMR ( $\text{CDCl}_3$ )  $\delta$  0.86 (*t*, 6H,  $J = 7.3$  Hz, terminal  $-\text{CH}_3$ ), 1.30 – 1.80 (*m*, 4H,  $-\text{CH}_2-$  at  $\beta$ -position of propyl group), 1.90 – 2.20 (*t*, 4H, at  $\alpha$ -position of propyl group), 2.48 (*s*, 8H,  $-\text{CH}_2-$  at the ring). CI-MS ( $\text{CH}_4$ )  $m/z$  calculated for  $\text{C}_{10}\text{H}_{22}\text{N}_2$  170.30, found 171 ( $\text{M}+1$ ) $^+$ .]

**Instrumentation and Procedures.** A glassy carbon electrode (GCE, area = 0.07  $\text{cm}^2$ ) was polished prior to experiments, using 1 micron diamond

suspension on a nylon cloth and then 0.25 micron diamond suspension on a microcloth (Buehler, Lake Bluff, IL). In addition, the GCE was lightly polished with deionized water on a microcloth immediately before each measurement. For electrochemical and ECL measurements, a conventional three-electrode electrochemical cell was employed. A GCE (3 mm diameter) served as a working electrode, a Pt wire as a counter, and Ag/AgCl as a reference electrode. Cyclic voltammograms (CV) were measured with either the model 660 electrochemical workstation (CH Instruments, Austin, TX), or a home-built potentiostat. Simultaneous ECL signals with CV were recorded using a Hamamatsu R4220p photomultiplier tube (PMT) placed just beneath the electrochemical cell. A high-voltage power supply series 225 (Bertan High Voltage Co., Hicksville, NY) was used to provide – 750 V to a PMT for the appropriate sensitivity. All solutions were deaerated by bubbling N<sub>2</sub> gas before each measurement.

### 3.3 Results and Discussion

#### **Electrochemistry of Ru(bpy)<sub>3</sub><sup>2+</sup> and 14 Different Amine Coreactants.**

In an organic solvent, such as acetonitrile (MeCN), Ru(bpy)<sub>3</sub><sup>2+</sup> usually displays a one-electron reversible oxidation and its oxidized form, Ru(bpy)<sub>3</sub><sup>3+</sup>, can remain in contact with air for overnight.<sup>14</sup> On the other hand, the reversibility of electrochemical oxidation of Ru(bpy)<sub>3</sub><sup>2+</sup> in aqueous media depends on the pH of the solution. Figure 3.3 shows the cyclic voltammograms (CV) for

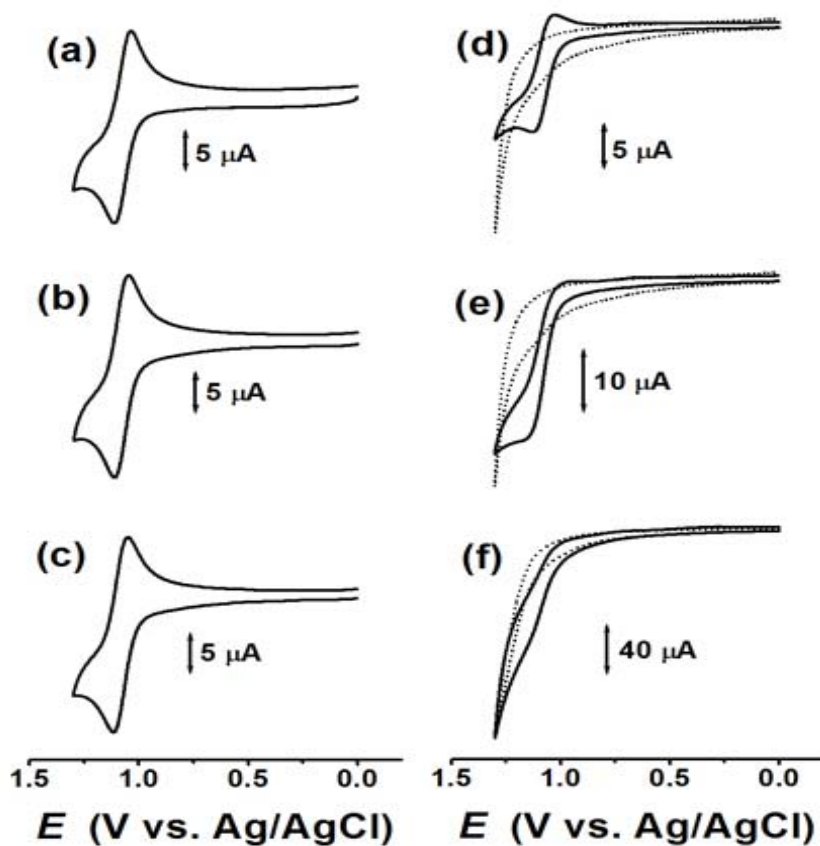


**Figure 3.3.** Cyclic voltammograms (CV) of 1 mM  $\text{Ru}(\text{bpy})_3^{2+}$  in (a) pH 2.5, (b) pH 6.5, (c) pH 9.5, (d) pH 10.5, (e) pH 11.5, and (f) pH 12.5 of 0.2 M PBS at 0.1 V/s using a glassy carbon electrode (area = 0.07 cm<sup>2</sup>). The dotted lines are background CVs.

the electrochemical oxidation of  $\text{Ru}(\text{bpy})_3^{2+}$  in phosphate buffer solutions (PBS) of different pH values, measured at 0.1 V/s. In the range of pH 2.5 to pH 9.5, the peak potential separation ( $\Delta E_p$ ) of the  $\text{Ru}(\text{bpy})_3^{2+/3+}$  couple was  $\sim 63$  mV, which was close to 59 mV for an one-electron reversible redox reaction, and the ratio of peak currents ( $i_c/i_a$ ) for the  $\text{Ru}(\text{bpy})_3^{2+/3+}$  couple was  $\sim 1$  ( $i_c/i_a = 0.91$ ). The half-wave potential ( $E_{1/2}$ ) was + 1.1 V vs. Ag/AgCl. Therefore, the electrochemical oxidation of  $\text{Ru}(\text{bpy})_3^{2+}$  was reversible in this pH range. However, the electrochemical oxidation of  $\text{Ru}(\text{bpy})_3^{2+}$  became more and more irreversible as the pH value of the solution increased. No reversible wave was shown even if the background current of the solvent was subtracted (pH 10.5 – pH 12.5). At pH 10.5, the electrochemical oxidation of  $\text{Ru}(\text{bpy})_3^{2+}$  was considered to be quasi-reversible, because its  $\Delta E_p$  was 100 mV and  $i_c/i_a$  was  $\sim 0.6$ . At pHs 11.5 and 12.5, the electrochemical oxidation of  $\text{Ru}(\text{bpy})_3^{2+}$  might be irreversible probably due to oxidation of the solvent. Although there have been many arguments<sup>15–21</sup> on the stability and reactivity of both  $\text{Ru}(\text{bpy})_3^{2+}$  and  $\text{Ru}(\text{bpy})_3^{3+}$  with base, such as  $\text{OH}^-$ , its stability and reaction mechanism is still uncertain.

Electrochemical oxidations of most tertiary amines are well known<sup>22–26</sup> and follow the ECE process as shown in Scheme 3.4. Their CVs show one or two oxidation waves depending on the pH of the solution and the reactivity of free radicals of tertiary amines for hydrolysis. The second oxidation wave in the CV is

usually considered to be the oxidation of dialkylamine which is the hydrolysis product of an oxidized tertiary amine [the product ( $R_2NH$ ) of eq. (3.13)].<sup>24,25</sup>

**Scheme 3.4**



With 10 mM concentrations of 14 different amines, cyclic voltammetry was carried out using a glassy carbon electrode (GCE) in the PBS of pH 12.5, where all amines existed as deprotonated forms. Each CV showed irreversible electrochemical oxidations. For a totally irreversible wave in CV where the first electron transfer is the rate determining step, the peak potential ( $E_p$ ) is the function of scan rate as defined in eq. (3.14)<sup>27</sup>:

$$E_p = E^\circ + (RT/\alpha F)[0.780 + \ln(D^{1/2}/k^\circ) + \ln(\alpha F/RT)^{1/2}] + (2.303RT/2\alpha F)\log \nu \quad (3.14)$$

where  $E^\circ$  is the standard potential,  $R$  is the gas constant,  $T$  is temperature,  $\alpha$  is the

transfer coefficient,  $F$  is the faraday constant,  $D$  is the diffusion coefficient,  $k^\circ$  is the standard heterogeneous rate constant, and  $\nu$  is the scan rate. In CV experiments, the anodic peak potentials ( $E_{p,a}$ ) of amines used in this work were linearly shifted to more positive potentials as the scan rate logarithmically increased. For example, Figure 3.4 shows CVs of 10 mM TEtA in pH 12.5 PBS at various scan rates (10 mV/s – 200 mV/s) and dependence of  $E_{p,a}$  on  $\log \nu$ .  $E_{p,a}$  of the TEtA oxidation was linearly dependent on  $\log \nu$ . The transfer coefficients ( $\alpha$ ) of 14 amines could be calculated from the slope ( $\partial E_{p,a} / \partial \log \nu$ ) of a plot of  $E_{p,a}$  vs.  $\log \nu$ , and are summarized in Table 3.1. The  $\alpha$  values of 14 amines were close to 0.5 ( $\alpha = 0.42 \sim 0.56$ ), indicating that a slow heterogeneous electron transfer reaction [eq. (3.10)] intervened in the overall chemical kinetic control [eq. (3.11)].<sup>6</sup>

Because of the compensation of the TPrA<sup>•</sup> (free radical) oxidation current from the TPrA<sup>•+</sup> (radical cation) reduction current, it is difficult to obtain a reversible oxidation wave of TPrA even from the fast scan CV to measure  $E_{1/2}$  for eq. (3.2).<sup>10</sup> Analogously, the CVs of the other amines did not show reversible oxidation waves due to the same reason. From eq. (3.14), however, unknown  $E^\circ$  value for eq. (3.10) can be approximated from the  $y$ -intercept ( $C$ ) of a plot of  $E_{p,a}$  vs.  $\log \nu$ . Assuming that  $\alpha$  is 0.5,  $D$  is  $5 \times 10^{-6}$  cm<sup>2</sup>/s, and  $0.001$  cm/s  $\leq k^\circ \leq 1$  cm/s, the  $y$ -intercept ( $C$ ) term of eq. (3.14) can be shorten to eq. (3.15):

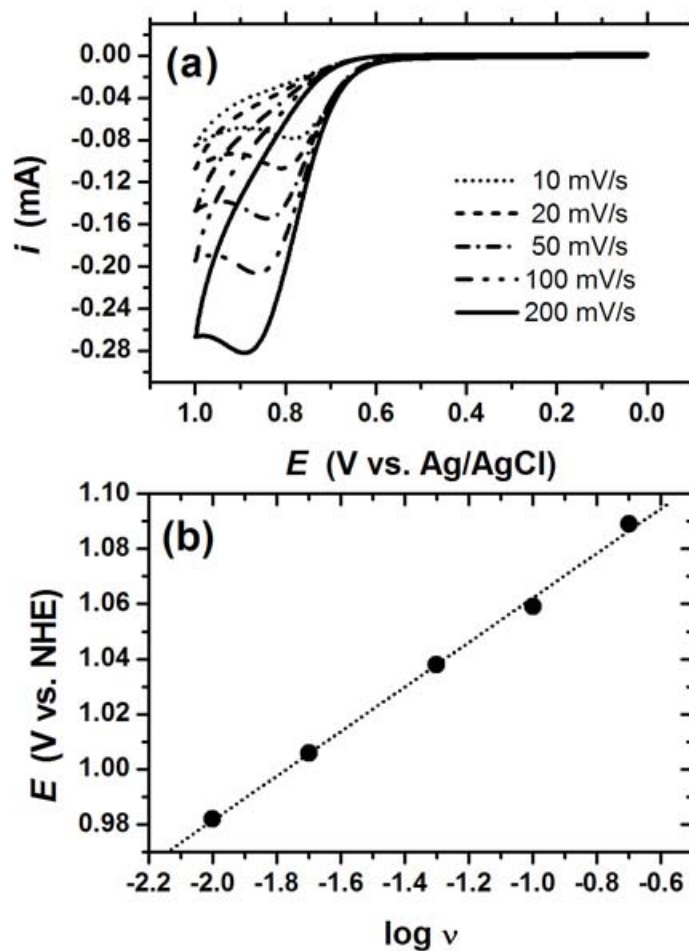


**Figure 3.4.** (a) Cyclic voltammograms of 10 mM TEtA in pH 12.5 PBS measured at various scan rates ( $v$ ). (b) Dependence of peak potentials for TEtA oxidation on  $\log v$ . A GCE (area = 0.07 cm<sup>2</sup>) was used as a working electrode.

**Table 3.1. Summary of Electrochemical Data for the Oxidation of Amines.**

Amine	$\partial E_{p,a}/\partial \log \nu$ (mV/decade)	$\alpha$	$C$ (V) <sup>a</sup>	$E_p$ (V) <sup>b</sup>
TEtA	69.8 ± 0.1	0.42	1.13	1.06
TPrA	52.8 ± 0.5	0.56	0.96	0.91
TEDAM	69.8 ± 0.1	0.42	1.50	1.43
TEDAE	69.8 ± 0.3	0.42	1.05	0.98
TEDAP	66.3 ± 0.5	0.45	1.18	1.11
TPDAM	54.9 ± 0.6	0.54	0.78	0.73
TPDAE	63.7 ± 0.4	0.46	0.79	0.75
TPDAP	69.6 ± 0.6	0.43	0.95	0.87
MP	69.4 ± 0.4	0.43	1.26	1.19
EP	69.4 ± 0.3	0.43	1.20	1.13
PP	69.8 ± 0.1	0.42	1.18	1.11
DMPz	54.4 ± 0.4	0.54	1.46	1.41
DEPz	69.8 ± 0.1	0.42	1.45	1.38
DPPz	60.4 ± 0.2	0.49	1.39	1.33

*All Potentials were measured at a GCE (area = 0.07 cm<sup>2</sup>) with an Ag/AgCl reference electrode and then converted to the potentials vs. NHE. Scan rate ( $\nu$ ) range : 10 mV/s – 200 mV/s.*

*a.* The y-intercept of the plot of  $E_p$  vs.  $\log \nu$ .

*b.* Measured at the scan rate of 0.1 V/s.

$$E^\circ - 0.20 \leq C \leq E^\circ + 0.16 \quad (3.15)$$

$$C - 0.16 \leq E^\circ \leq C + 0.20 \quad (3.16)$$

Therefore, the  $C$  values summarized in Table 3.1 can be useful information to get a rough estimate of the  $E^\circ$  values of radical cations of amines.

**ECL of Ru(bpy)<sub>3</sub><sup>2+</sup> by amine coreactants.** ECL of Ru(bpy)<sub>3</sub><sup>2+</sup> was observed when the electrode potential was anodically swept in a solution containing Ru(bpy)<sub>3</sub><sup>2+</sup> and an amine coreactant and followed the parallel process to Schemes 3.1, 3.2, and 3.3. Figure 3.5 shows simultaneous CV and ECL measured under the condition of 1 μM Ru(bpy)<sub>3</sub><sup>2+</sup> and 10 mM TEDAP in pH 7.5 PBS with the scan rate of 0.1 V/s. From the CV, TEDAP began to be oxidized at + 0.55 V vs. Ag/AgCl and it might generate both TEDAP<sup>•+</sup> (radical cation) and TEDAP<sup>•</sup> (free radical) that participated in the ECL reaction later. Similar to ECL by TPrA<sup>10</sup>, TEDAP produced the first ECL wave before Ru(bpy)<sub>3</sub><sup>2+</sup> was oxidized ( $E_{1/2} = + 1.1$  V vs. Ag/AgCl). Then, the second ECL wave occurred at around + 1.1 V vs. Ag/AgCl, where Ru(bpy)<sub>3</sub><sup>2+</sup> was oxidized. The presence of the first ECL wave indicates that the radical cation of TEDAP is also produced and has a sufficient lifetime to reduce Ru(bpy)<sub>3</sub><sup>+</sup> to Ru(bpy)<sub>3</sub><sup>2+\*</sup> in the solution. On the other hand, Figure 3.6 is the simultaneous CV and ECL of 1 μM Ru(bpy)<sub>3</sub><sup>2+</sup> and 10 mM

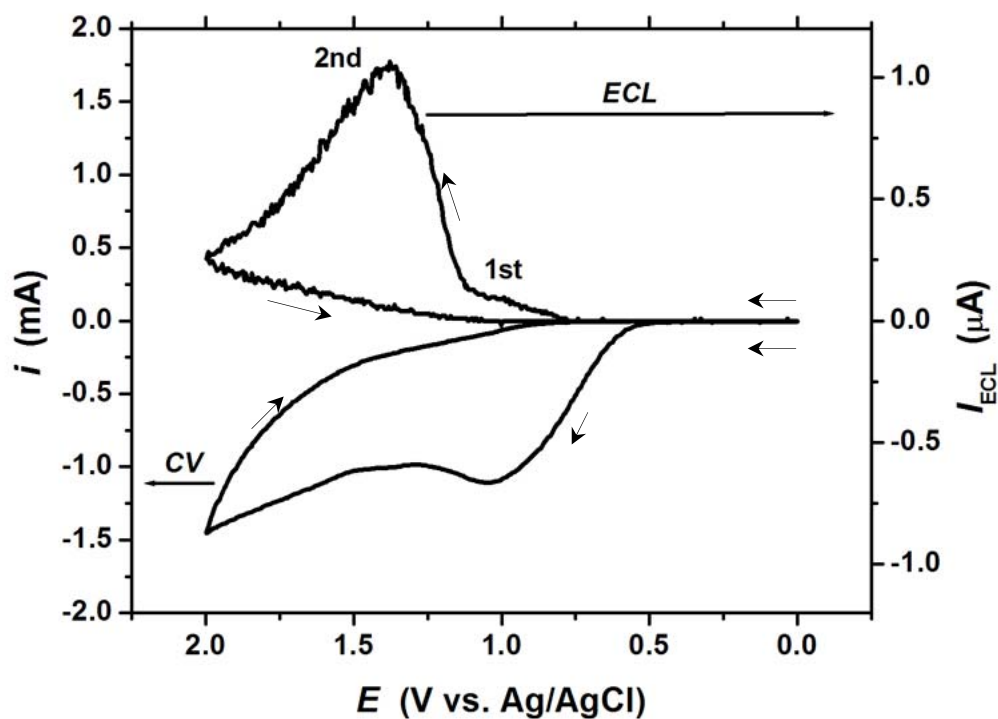


**Figure 3.5.** Simultaneous CV and ECL of 1  $\mu\text{M}$   $\text{Ru}(\text{bpy})_3^{2+}$  with 10 mM  $N,N,N',N'$ -tetraethyl-1,3-propanediamine (TEDAP) in pH 7.5 PBS. Scan rate. = 0.1 V/s. A GCE (area = 0.07  $\text{cm}^2$ ) was used.

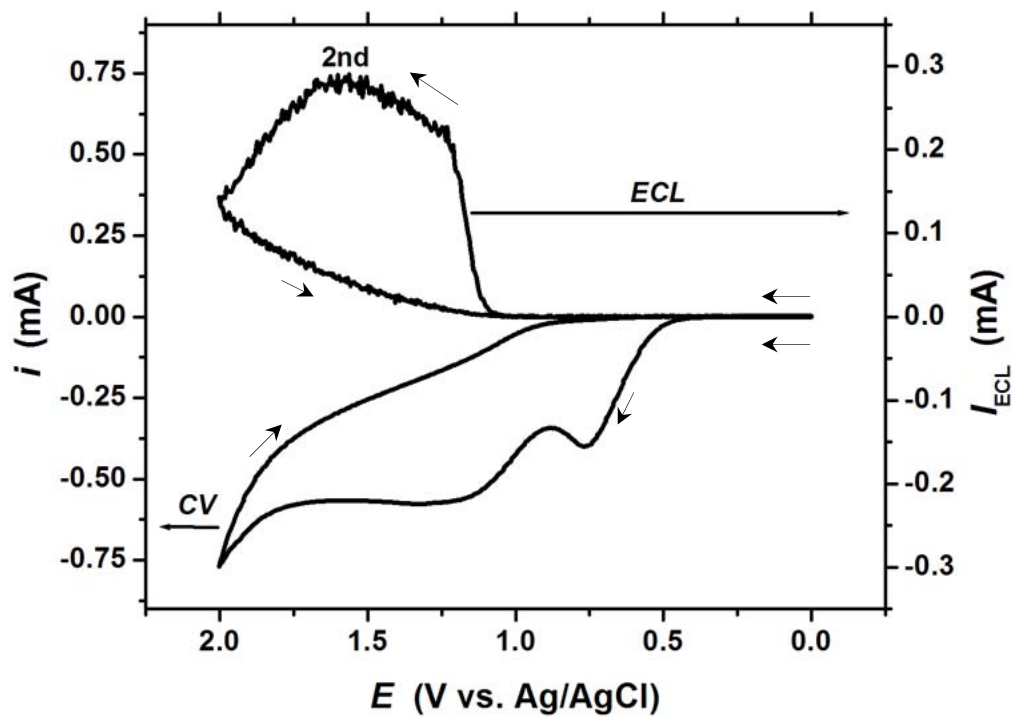


**Figure 3.6.** Simultaneous CV and ECL of 1  $\mu\text{M}$   $\text{Ru}(\text{bpy})_3^{2+}$  with 10 mM  $N,N,N',N'$ -tetra- $n$ -propylethylenediamine (TPDAE) in pH 7.5 PBS. Scan rate. = 0.1 V/s. A GCE (area = 0.07  $\text{cm}^2$ ) was used.

TPDAE in pH 7.5 PBS with the scan rate of 0.1 V/s. Although TPDAE also produced both TPDAE<sup>•+</sup> (radical cation) and TPDAE<sup>•</sup> (free radical) during its oxidation, TPDAE displayed only the second ECL wave.

*The first ECL.* The maximum intensities of the first ECL waves obtained with Ru(bpy)<sub>3</sub><sup>2+</sup> (1 μM) and each different amine coreactant (10 mM) in pH 7.5 PBS are shown in Figure 3.7. Like TPDAE shown in Figure 3.6, TPDAM also did not show the first ECL wave, because the radical cations of TPDAM and TPDAE, probably, were either extremely short-lived transients or not sufficiently energetic to produce Ru(bpy)<sub>3</sub><sup>2+\*</sup>. Based on the fact that TPDAP produced the first ECL, it could be speculated that the radical cations of TPDAM and TPDAE were not extremely short-lived. In general, the radical cation of an amine coreactant must have an  $E^\circ$  value that is more positive than at least + 0.94 V<sup>28</sup> vs. NHE in order to generate Ru(bpy)<sub>3</sub><sup>2+\*</sup> (2.12 eV)<sup>29</sup> from Ru(bpy)<sub>3</sub><sup>+</sup> ( $E^\circ$  of Ru(bpy)<sub>3</sub><sup>2+/+</sup> in water = - 1.28 V vs. NHE<sup>29</sup>). As shown in Table 3.1, the  $C$  values of TPDAM (+ 0.78 V) and TPDAE (+ 0.79 V), which are close to their real  $E^\circ$  values were much lower than the required value, + 0.94 V. As a result, radical cations of TPDAM and TPDAE were not strong enough to generate Ru(bpy)<sub>3</sub><sup>2+\*</sup>. In contrast, the  $C$  values of other amine coreactants were quite higher than + 0.94 V, so that the first ECL wave was observed.

In view of the first ECL wave, monoamine coreactant (TEtA, TPrA, MP, EP, and PP) gave much stronger emissions than did diamine coreactants

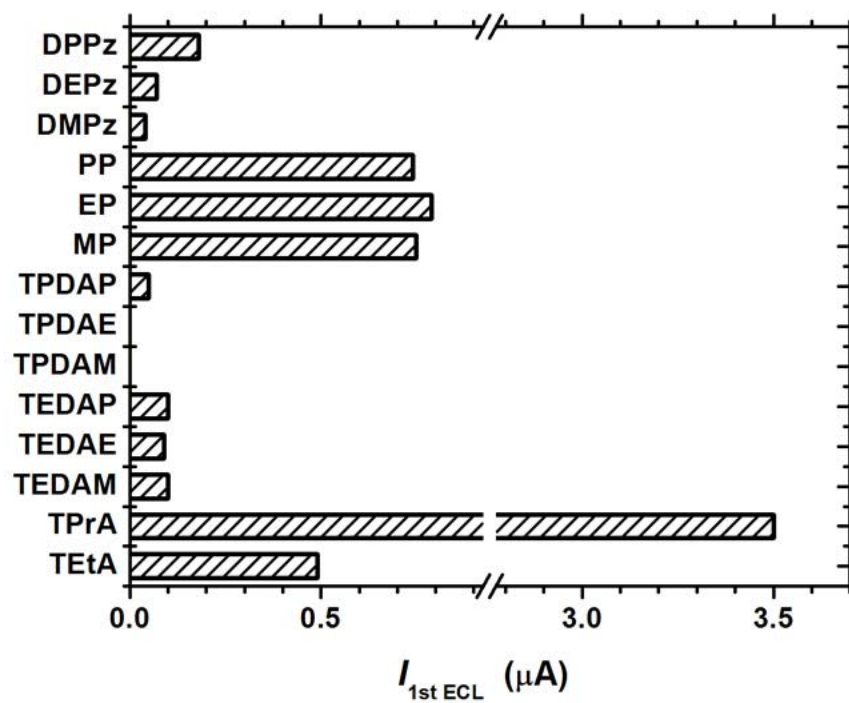


**Figure 3.7.** Comparison of the first ECL wave intensities of  $1\ \mu M$   $Ru(bpy)_3^{2+}$  generated with various amine coreactants (10 mM) in pH 7.5 PBS. Scan rate = 0.1 V/s. A GCE (area =  $0.07\ cm^2$ ) was used.

(TEDAM, TEDAE, TEDAP, TPDAM, TPDAE, TPDAP, DMPz, DEPz, and DPPz). In order to produce a first ECL wave, the radical cations of amine coreactants must have the proper value of  $E^\circ$  for eq. (3.10) as well as a fairly long lifetime, which is closely related on the stability of radical cations. This stability strongly depends on the structure of a molecule. At pH 7.5, one nitrogen atom of a diamine had to be protonated<sup>30</sup> and the oxidation would occur on the other nitrogen atom. When the radical cations of diamines were formed, the positive charge on the protonated nitrogen could induce a faster deprotonation of the radical cations. Therefore, the relative amount of diamine radical cations would be much smaller than that of monoamine radical cations. Thus, the ECL intensity of diamines was much weaker than that of monoamines.

*The second ECL.* The pH dependence of the second ECL wave were investigated in the range of pH 2.5 to 9.5, because the oxidation of  $\text{Ru}(\text{bpy})_3^{2+}$  became irreversible (Figure 3.3) and the unknown background emission (probably by the reaction of  $\text{Ru}(\text{bpy})_3^{3+}$  with  $\text{OH}^-$ )<sup>31</sup> was significant above at pH 10.5. Figures 3.8 – 3.12 show the pH dependence of the second ECL wave of  $\text{Ru}(\text{bpy})_3^{2+}$  produced by 14 different amine coreactants. Below at pH 6, relatively low ECL intensities were observed for most amine coreactants except for TPDAP, which generated the highest ECL intensity at pH 5.5, because the protonated forms of amines became predominant over deprotonated forms and the deprotonation step, reaction (3.11), proceeded more slowly in the acidic pH

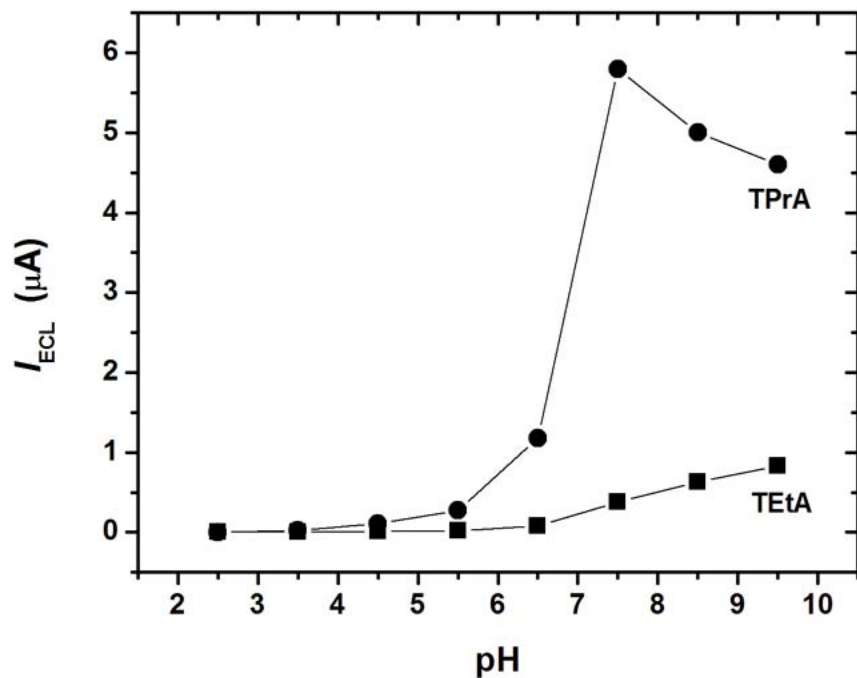


**Figure 3.8.** Dependence of the second ECL produced in a solution of 1  $\mu\text{M}$   $\text{Ru}(\text{bpy})_3^{2+}$  and 10 mM acyclic monoamine group coreactant (TEtA or TPrA) on the pH of PBS. Each data point is the average value of three measurements and contains less than 10 % deviation. A GCE (area = 0.07  $\text{cm}^2$ ) was used.

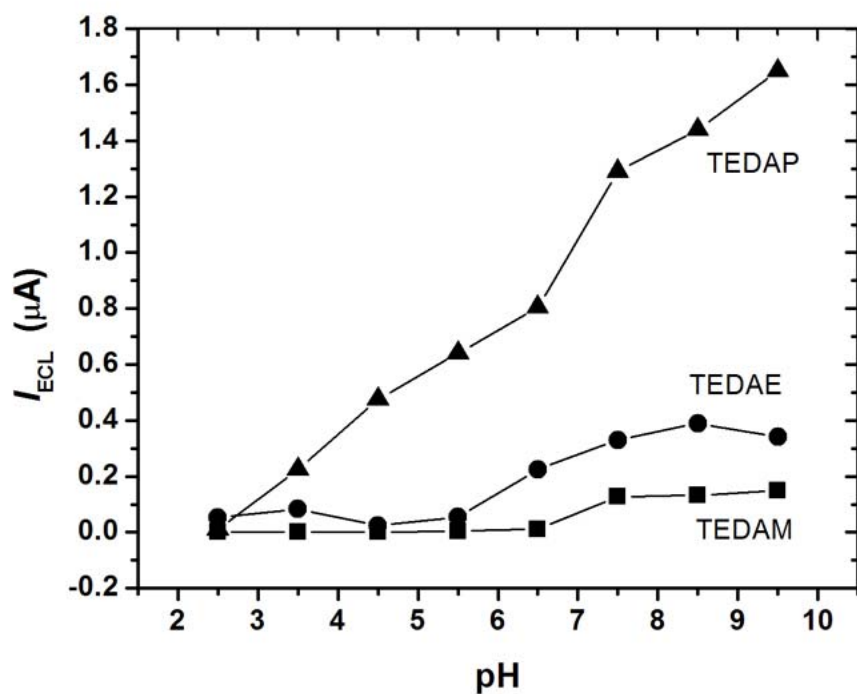


**Figure 3.9.** Dependence of the second ECL produced in a solution of 1  $\mu M$   $Ru(bpy)_3^{2+}$  and 10 mM acyclic  $N,N,N',N'$ -tetraethyldiamine group coreactant (TEDAM, TEDAE, or TEDAP) on the pH of PBS. Each data point is the average value of three measurements and contains less than 10 % deviation. A GCE (area = 0.07  $cm^2$ ) was used.

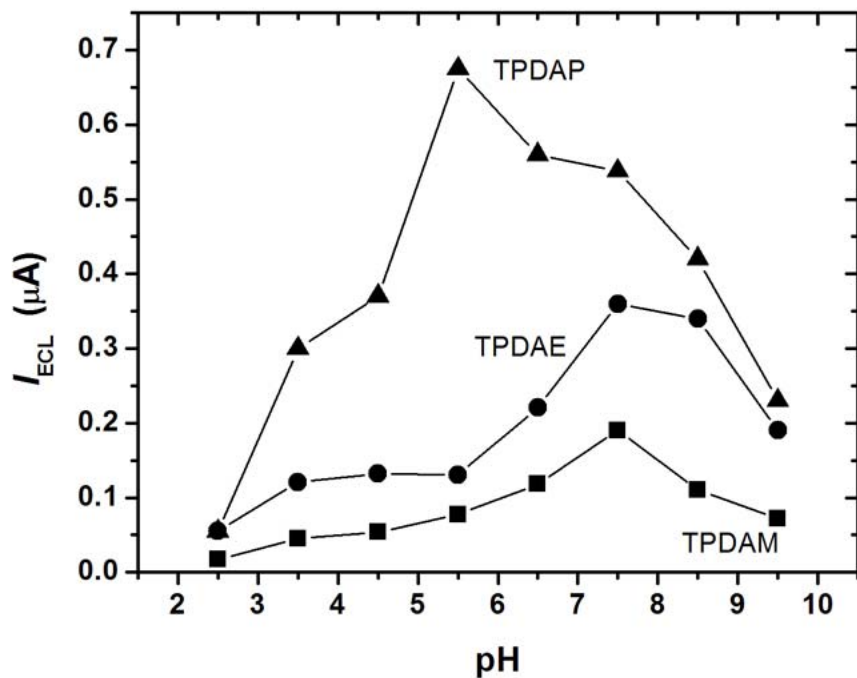


**Figure 3.10.** Dependence of the second ECL produced in a solution of 1  $\mu M$   $Ru(bpy)_3^{2+}$  and 10 mM acyclic  $N,N,N',N'$ -tetra-*n*-propyldiamine group coreactant (TPDAM, TPDAE, or TPDAP) on the pH of PBS. Each data point is the average value of three measurements and contains less than 10 % deviation. A GCE (area = 0.07 cm<sup>2</sup>) was used.

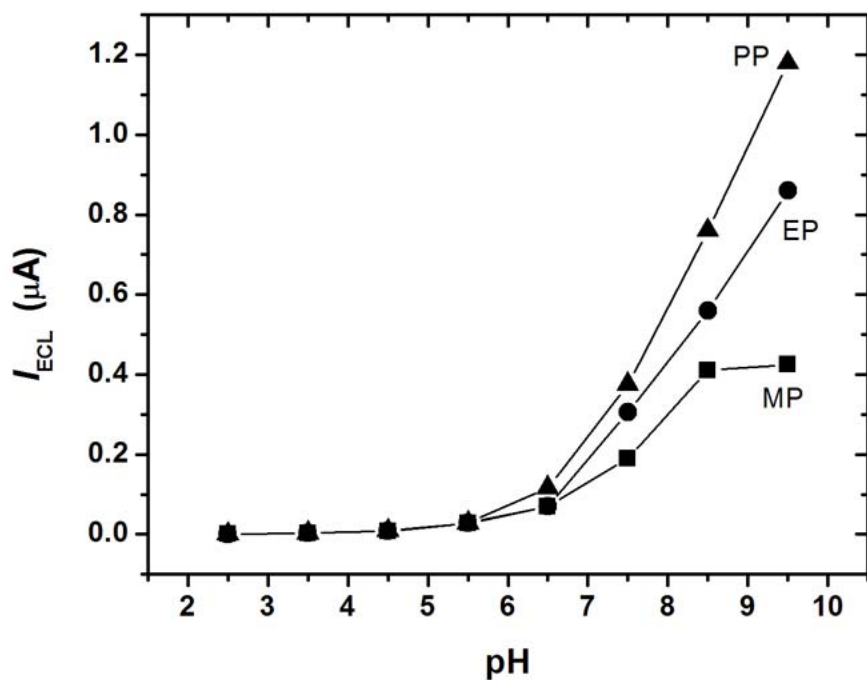


**Figure 3.11.** Dependence of the second ECL produced in a solution of 1  $\mu\text{M}$   $\text{Ru}(\text{bpy})_3^{2+}$  and 10 mM heteroalicyclic monoamine group coreactant (MP, EP, or PP) on the pH of PBS. Each data point is the average value of three measurements and contains less than 10 % deviation. A GCE (area = 0.07  $\text{cm}^2$ ) was used.

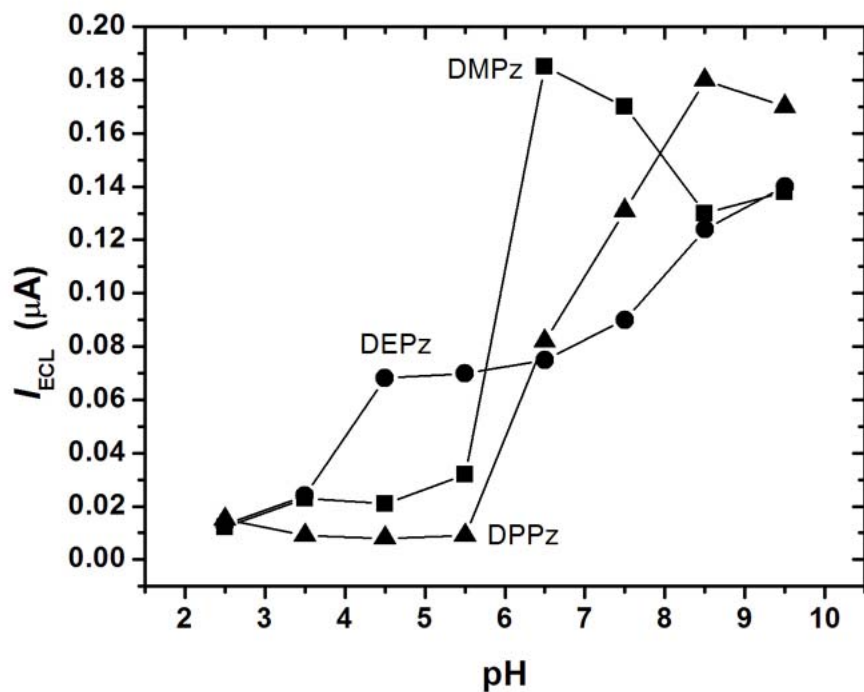


**Figure 3.12.** Dependence of the second ECL produced in a solution of 1  $\mu\text{M}$   $\text{Ru}(\text{bpy})_3^{2+}$  and 10 mM heteroalicyclic diamine group coreactant (DMPz, DEPz, or DPPz) on the pH of PBS. Each data point is the average value of three measurements and contains less than 10 % deviation. A GCE (area = 0.07  $\text{cm}^2$ ) was used.

region. In case of TPDAP, because of the hydrophobicity of TPDAP, the solubility of TPDAP in water decreased with the increasing pH of PBS. In fact, the oxidation peak current for TPDAP was highest at pH 5.5 (see Figure 3.13), so that its maximum ECL was shown at pH 5.5. On the other hand, the other amines generated their highest ECL intensities in a region of pH 7.5 – pH 9.5. Optimum pHs and the maximum ECL intensities of amine coreactants are summarized in Table 3.2.

Like the first ECL wave, monoamines gave a higher intensity of the second ECL wave than did diamines; the positive charge on the protonated nitrogen atom of a diamine molecule made the free radicals of diamines relatively less stable than those of monoamines. Except for DMPz, DEPz, and DPPz, the intensity of the second ECL wave tended to increase in order of methyl < ethyl < *n*-propyl substituent in the homolog of amines. Because of the electron-donating characteristics of alkyl group, amines having longer alkyl substituents produced more stable free radical and more intense ECL. However, the ECL tendency of DMPz, DEPz, and DPPz was totally unexpected.

The second ECL wave intensities of acyclic amines (e.g. TPrA and TEDAP) were higher than those of heterocyclic amines (PP and DPPz). The neutral molecule of an amine has the trigonal pyramid structure. When an amine molecule is oxidized, initially the loss of one electron occurs from the lone pair electrons on a nitrogen molecule and this causes the rearrangement of the amine

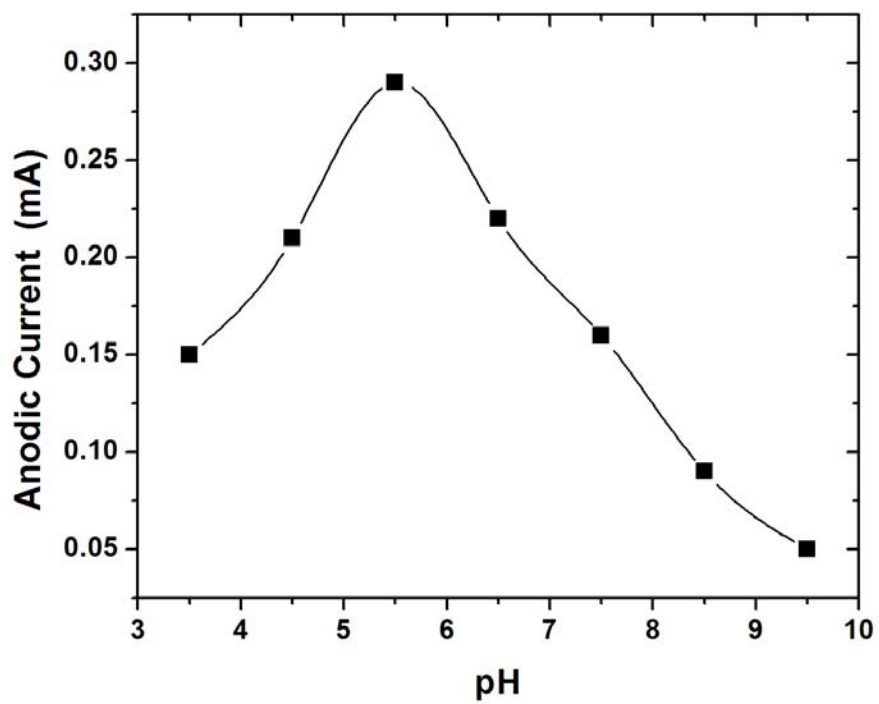


**Figure 3.13.** Dependence of the anodic current for the oxidation of 10 mM TPDAP on pH of PBS. Scan Rate = 0.1 V/s. A GCE (area = 0.07 cm<sup>2</sup>) was used.

**Table 3.2. List of  $pK_a$  Values of Coreactants, Optimum pH for the Second ECL and Its ECL intensities.**

Coreactants	$pK_a$	Optimum pH	$I_{ECL}^a$ ( $\mu A$ )
TtA	10.75 <sup>b</sup>	9.5	0.83 ± 0.05
TPrA	10.66 <sup>c</sup>	7.5	5.80 ± 0.07
TEDAM	< 1 <sup>d,f</sup> , 11.01 <sup>e,f</sup>	9.5	0.15 ± 0.03
TEDAE	6.54 <sup>d,f</sup> , 9.84 <sup>e,f</sup>	8.5	0.39 ± 0.05
TEDAP	8.20 <sup>d,g</sup> , 10.18 <sup>e,g</sup>	9.5	1.65 ± 0.07
TPDAM	- <sup>k</sup>	7.5	0.19 ± 0.04
TPDAE	- <sup>k</sup>	7.5	0.36 ± 0.04
TPDAP	9.6 <sup>e,h</sup>	5.5	0.68 ± 0.06
MP	10.38 <sup>b</sup>	9.5	0.43 ± 0.08
EP	10.45 <sup>b</sup>	9.5	0.86 ± 0.08
PP	10.41 <sup>i</sup>	9.5	1.18 ± 0.03
DMPz	4.10 <sup>d,j</sup> , 8.40 <sup>e,j</sup>	6.5	0.19 ± 0.07
DEPz	4.67 <sup>d,f</sup> , 8.83 <sup>e,f</sup>	9.5	0.14 ± 0.04
DPPz	- <sup>k</sup>	8.5	0.18 ± 0.06

*ECL was produced with 1  $\mu M$  Ru(bpy)<sub>3</sub><sup>2+</sup> and 10 mM each coreactant in PBS.*

*a.* Average values of 3 independent measurements for each coreactant. *b.* From ref. (32). *c.* From ref. (33). *d.*  $pK_{a,1}$ . *e.*  $pK_{a,2}$ . *f.* From ref. (34). *g.* From ref. (35). *h.* In this work. *i.* From ref. (36). *j.* From ref. (37). *k.* Not available.

molecule: the trigonal pyramid structure will be changed to the trigonal plane shape because the repulsion from the non-bonding orbital of nitrogen atom is diminished. Then, after deprotonation from the  $\alpha$ -carbon, another rearrangement must occur because the orbital of unpaired non-bonding electron is filled again. Therefore, the rate of amine oxidation depends on how easy the rearrangement of a molecule occurs. Because acyclic amines (TPrA and TEDAP) have more flexible movement of substituents than do heteroalicyclic amines (PP and DPPz), acyclic amine coreactants generated the more intense second ECL wave than did heteroalicyclic amines.

**ECL of  $\text{Ru}(\text{bpy})_3^{2+}$  in Coreactant Buffers.** The new concept of buffer (coreactant buffer) solutions for ECL was developed using various biological buffers. The coreactant buffer (CB) can be defined as an agent used for a coreactant as well as the control of pH. Therefore, use of a CB may be useful especially when an added coreactant causes a side-reaction with an analyte. CBs used in this work have various amine structures (Figure 3.2), offer a useful pH of  $\sim 7.5$  ( $\text{p}K_a$  6.9 – 8.4), and are inert with most biological molecules. Figure 3.14 shows the simultaneous CV and ECL of  $1 \mu\text{M}$   $\text{Ru}(\text{bpy})_3^{2+}$  in the CB solution (0.2 M DIPSO, 0.1 M NaCl) at 0.1 V/s. Because DIPSO is a tertiary amine, it could be electrochemically oxidized (Figure 3.14, CV) via Scheme 3.4 and produce both a radical cation and a free radical. The other CBs were also oxidized by this scheme. Like amine coreactants discussed in the previous section, DIPSO

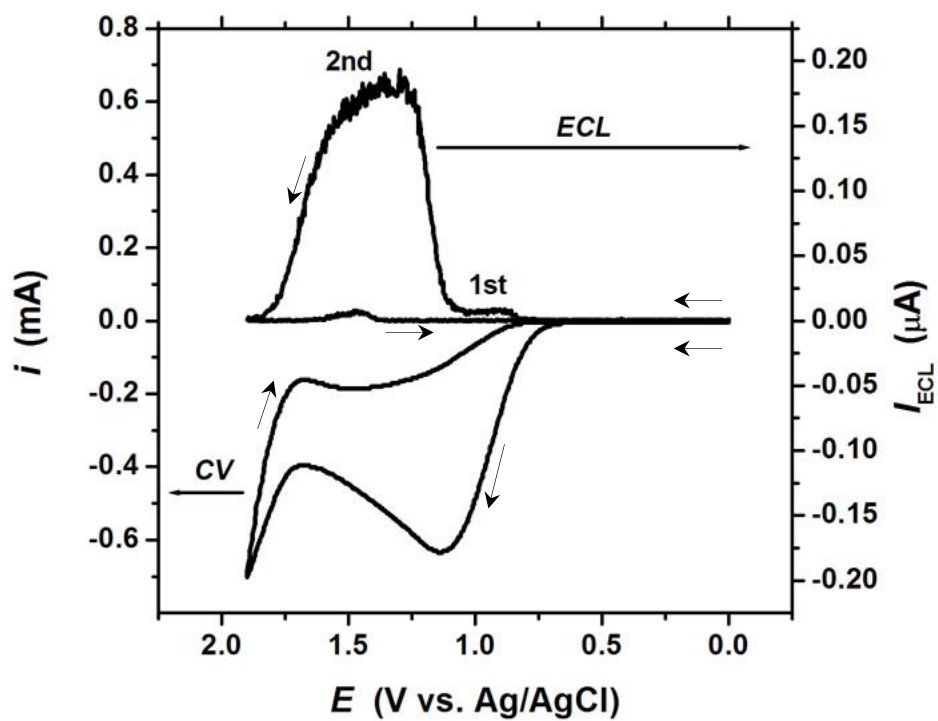


**Figure 3.14.** Simultaneous CV and ECL  $1 \mu\text{M Ru}(\text{bpy})_3^{2+}$  in pH 7.5 of DIPSO buffer (0.2 M) solution containing 0.1 M NaCl as a supporting electrolyte. Scan rate = 0.1 V/s. A GCE (area =  $0.07 \text{ cm}^2$ ) was used.

produced two ECL waves in a plot of the ECL intensity vs. potential (Figure 3.14, ECL) following the analogous mechanism to TPrA. Except for DIPSO, MOBS, and TEA, the other CBs did not show a first ECL wave because their oxidation occurred at more positive potentials (see Table 3.3) than  $\text{Ru}(\text{bpy})_3^{2+}$  oxidation ( $E_{1/2} = + 1.1 \text{ V vs. Ag/AgCl}$ ). All electrochemical and ECL data are summarized in Table 3.3.

Like amine coreactants, the stability of the radical cation of a CB plays an important role to produce the first ECL wave. It was reported that the radical cation or free radical of amine having electron-withdrawing groups near a nitrogen atom or an  $\alpha$ -carbon (within 2 carbon atoms) would be further destabilized.<sup>5,38</sup> As a result, MOBS produced the most intense first ECL among those that produced the first ECL waves because MOBS did not have any electron-withdrawing groups near a nitrogen atom in its molecular structure. In contrast, DIPSO and TEA have the  $-\text{CH}_2\text{CH}_2\text{OH}$  and  $-\text{CH}_2\text{CH}(\text{OH})-$  groups, which function as electron-withdrawing groups by an inductive effect of an electronegative atom,<sup>38,39</sup> on their nitrogen atoms. Therefore, their first ECL wave intensities were much less than that of MOBS.

All CBs produced a second ECL wave of  $\text{Ru}(\text{bpy})_3^{2+}$  by the same way of Schemes 3.2 and 3.3. The second ECL wave intensities of  $\text{Ru}(\text{bpy})_3^{2+}$  (1  $\mu\text{M}$ ) generated with various CBs were compared with that generated with 10 mM TPrA in pH 7.5 PBS by calculating the ratio of the second ECL intensities,

**Table 3.3.  $pK_a$ , Anodic Peak Potential ( $E_p$ ), the First and Second ECL wave Intensities, and the Relative second ECL wave Intensity ( $I_{CB}/I_{TPrA}$ ) of Coreactant Buffers.**

Buffer	$pK_a$	$E_p$ (V) <sup>a</sup>	1st ECL (nA)	2nd ECL ( $\mu$ A)	$I_{CB}/I_{TPrA}$ (%)
MOPSO	6.9	1.30	-	0.82	14.1
MOPS	7.2	1.52	-	1.00	17.2
MOBS	7.6	1.20	50	1.40	24.1
HEPES	7.5	- <sup>b</sup>	-	0.17	2.9
HEPPSO	7.8	- <sup>b</sup>	-	0.03	0.5
EPPS	8.0	- <sup>b</sup>	-	0.09	1.6
HEPBS	8.3	1.55	-	0.09	1.6
BES	7.1	1.20	-	0.09	1.6
DIPSO	7.6	1.03	15	0.18	3.1
TEA	7.8	0.95	10	0.26	4.5
BICINE	8.3	0.99	-	0.03	0.5
TES	7.4	1.44	-	0.18	3.1
TAPSO	7.6	1.40	-	0.24	4.1
TAPS	8.4	1.23	-	0.63	10.9
TRICINE	8.1	1.29	-	0.01	0.2
GLY-GLY	8.2	- <sup>b</sup>	-	0.01	0.2
BTP	6.8	1.43	-	0.88	15.2

*All buffer solutions contain 0.2 M buffering agents and 0.2 M NaCl.*

*a.* Oxidation peak potential measured from CV on the GCE at 0.1 V/s

*b.*  $E_p$  was not measurable due to the broadness of wave.

$I_{\text{CB}}/I_{\text{TPrA}}$ , (Table 3.3). Among them, MOPSO (14.1 %), BTP (15.2 %), MOPS (17.2 %), MOBS (24.1 %), and TAPS (10.9 %) generated more than 10 % of the second ECL produced with TPrA (10 mM) in PBS. Thus, these CBs could be candidates as substitutes of TPrA. In view of CB structures, a CB having an –OH group near at  $\alpha$ -carbon definitely produced a lower intensity of the second ECL wave than did a CB not having this group. In addition, as the number of –OH groups increased in the same molecular structure of CBs, the ECL intensity decreased. Although MOPSO, MOPS, and MOBS have heteroalicyclic structures (their base structure is a morpholine), their ECL intensities were not lower than those of acyclic CBs because the electron-donating group (–O–) in a ring further stabilized free radical form of MOPSO, MOPS, and MOBS.

### 3.4 Conclusion

The structures of amine coreactants were correlated with their reactivity to produce the ECL of  $\text{Ru}(\text{bpy})_3^{2+}$ . Of amine coreactants used in this work, TPrA generated the highest first and second ECL intensity of  $\text{Ru}(\text{bpy})_3^{2+}$ , indicating that TPrA had the optimized structure to keep stabilizing both the radical cation and the free radical. Generally, diamines and heteroalicyclic amines do not give more intense first and second ECL than acyclic tertiary amines. In addition, electron-withdrawing groups in an amine molecule decreased the second ECL wave by destabilizing the free radical of an amine, while the electron-donating group in an

amine molecule enhanced the second ECL wave by stabilizing the free radical of an amine.

Based on the ECL results in CB solutions, MOPSO, BTP, MOPS, MOBS, and TAPS generated comparable ECL of  $\text{Ru}(\text{bpy})_3^{2+}$  to TPrA. Generally, morpholine group coreactants produced the most efficient ECL among CBs. Therefore, they can be used especially in the ECL analysis of immunoassays or DNA-probe assays without employing additional coreactants. Furthermore, since they are well-known biological buffers and there are no other components besides analytes and ECL labels, the biological reactivity of biomolecules, such as interaction between antibody and antigen, will not be interfered, and the decomposition or denaturalization of biomolecules is not expected.

## References

- (1) Faulkner, L. R.; Bard, A. J. In *Electroanalytical Chemistry*; Bard, A. J., Ed.; Marcel Dekker: New York, 1977; Vol. 10, p. 1.
- (2) Knight, A. W.; Greenway, G. M. *Analyst* **1994**, *119*, 879.
- (3) Bard, A. J.; Debad, J. D.; Leland, J. K.; Sigal, G. B.; Wilber, J. L.; Wohlstadter, J. N. In *Encyclopedia of Analytical Chemistry: Applications, Theory, and Instrumentation*; Meyers, R. A., Ed.; John Wiley & Sons: New York, 2000, Vol. 11, p. 9842.
- (4) Leland, J. K.; Powell M. J. *J. Electrochem. Soc.* **1990**, *137*, 3127.
- (5) Knight, A. W.; Greenway, G. M. *Analyst* **1996**, *121*, 101R.
- (6) Kanoufi, F.; Zu, Y.; Bard, A. J. *J. Phys. Chem. B* **2001**, *105*, 210.
- (7) Zu, Y.; Bard, A. J. *Anal. Chem.* **2001**, *73*, 3960.
- (8) Gross, E. M.; Pastore, P.; Wightman, R. M. *J. Phys. Chem. B* **2001**, *105*, 8732.
- (9) Zu, Y.; Bard, A. J. *Anal. Chem.* **2000**, *72*, 3223.
- (10) Miao, W.; Choi, J. -P.; Bard, A. J. *J. Am. Chem. Soc.* **2002**, *124*, 14478.
- (11) Noffsinger, J. B.; Danielson, N. D. *Anal. Chem.* **1987**, *59*, 865.
- (12) Downey, T. M.; Nieman, T. A. *Anal. Chem.* **1992**, *64*, 261.
- (13) Christian, G. D.; Purdy, W. C. *J. Electroanal. Chem.* **1962**, *3*, 363.
- (14) Tokel-Takvoryan, N. E.; Hemingway, R. E.; Bard, A. J. *J. Am. Chem. Soc.* **1973**, *95*, 6582.
- (15) Gillard, R. D.; Hughes, C. T.; Williams, P. A. *Transition Met. Chem.* **1976**, *1*, 51.
- (16) Sagüés, J. A. A.; Gillard, R. D.; Lancashire, R. J.; Willaims, P. A. *J. Chem. Soc. Dalton Trans.* **1979**, 193.
- (17) Constable, E. C.; Seddon, E. A. *J. Chem. Soc. Chem. Comm.* **1982**, 34.
- (18) Constable, E. C. *Polyhedron* **1983**, *2*, 551.
- (19) Creutz, C.; Sutin, N. *Proc. Nat. Acad. Sci.* **1975**, *72*, 2858.

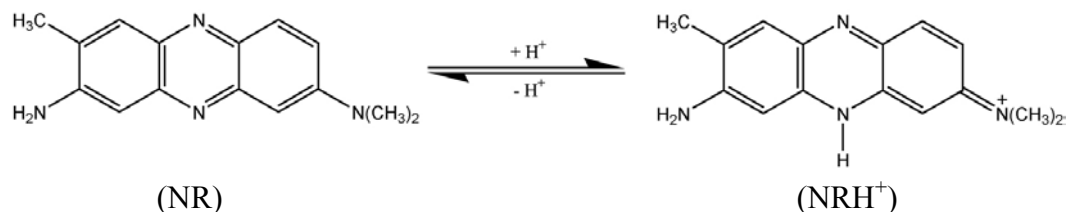
- (20) Serpon, N.; Bolletta, F. *Inorg. Chim. Acta.* **1983**, *75*, 189.
- (21) Serpon, N.; Ponterini, G.; Jamieson, M. A.; Bolletta, F.; Maestri, M. *Coord. Chem. Rev.* **1983**, *50*, 209.
- (22) For a general review on an nonaromatic amine oxidation, Chow, Y. L.; Danen, W. C.; Nelsen, S. F.; Rosenblatt, D. H. *Chem. Rev.* **1978**, *78*, 243.
- (23) Mann, C. K. *Anal. Chem.* **1964**, *36*, 2424.
- (24) Masui, M.; Sayo, H.; Tsuda, Y. *J. Chem. Soc. B* **1968**, 973.
- (25) Portis, L. C.; Bhat, V. V.; Mann, C. K. *J. Org. Chem.* **1970**, *35*, 2175.
- (26) Ross, S. D. *Tetrahedron Lett.* **1973**, *14*, 1237.
- (27) Bard, A. J.; Faulkner, L. R. In *Electrochemical Method, 2nd Ed.* Wiley & Sons: New York, 2001, Chapter 6.
- (28) Calculated from an equation:  $E^\circ [\text{R}_3\text{N}/\text{R}_3\text{N}^{\bullet+}] = E_s + E^\circ [\text{Ru}(\text{bpy})_3^{2+/+}] + 0.1$  eV where  $E_s$  is the excited singlet energy of  $\text{Ru}(\text{bpy})_3^{2+}$  and 0.1 eV is the entropy correction term.
- (29) Kalyanasundaram, K. *Coord. Chem. Rev.* **1982**, *46*, 159.
- (30) The first  $pK_a$ 's of most diamines are below 5 and the second  $pK_a$ 's are above 9.
- (31) Hercules, D. M.; Lytle F. E. *J. Am. Chem. Soc.* **1966**, *88*, 4745.
- (32) In *CRC Handbook of Chemistry and Physics, 83rd Ed.*, Lide, D. R. Ed., CRC Press: Boca Raton, FL, 2002/03, Section 8.
- (33) Dean, J. A. In *Lange's Handbook of Chemistry, 15th Ed.*, McGraw-Hill, Inc.: New York, 1999, Section 8.
- (34) Yu, Q.; Kandegedara, A.; Xu, Y.; Rorabacher, D. B. *Anal. Biochem.* **1997**, *253*, 50.
- (35) Gero, A. *J. Am. Chem. Soc.* **1954**, *76*, 5158.
- (36) Perrin, D. D. In *Dissociation Constants of Organic Bases in Aqueous Solution*. Butterworths: London, 1965.

- (37) Dega-Szafran, Z.; Jaskólski, M.; Kurzyca, I.; Barczyński, P.; Szafran, M. *J. Mol. Struct.* **2002**, *614*, 23.
- (38) Brune, S. N.; Bobbitt, D. R. *Anal. Chem.* **1992**, *64*, 166.
- (39) March, J. In *Advanced Organic Chemistry: Reactions, Mechanisms, and Structure*, 4th Ed. Wiley & Sons: New York, 1992, Chapter 9.

## Chapter 4: Acid-Base Properties, Electrochemistry, and Electrogenerated Chemiluminescence of Neutral Red in Acetonitrile

### 4.1 Introduction

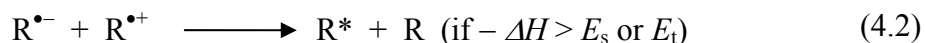
3-Amino-7-dimethylamino-2-methylphenazine, also known as neutral red (NR), has been well known in biological systems: especially as an intracellular pH indicator<sup>1,2</sup>, a nontoxic stain<sup>3,4</sup>, and a probe material<sup>5-7</sup>. In aqueous solutions, neutral red is under equilibrium between a protonated form (NRH<sup>+</sup>) and a deprotonated form (NR) depending on the concentration of H<sup>+</sup> as shown below and its p*K*<sub>a</sub> value was reported as 6.81.<sup>8</sup>



In addition, the electronic absorption spectrum of NR at low pH (e.g. pH 3.5) shows a maximum absorption at 531 nm, whereas a blue shift of ~ 80 nm is observed in the absorption spectrum at high pH (e.g. pH 10.5).<sup>8</sup> A distinctive

color change is seen at around pH 7; the color of a NR solution changes from yellow to red as the solution changes from basic to acidic.

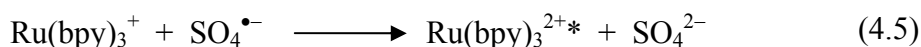
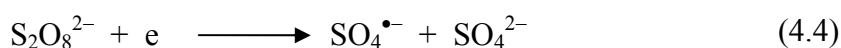
Electrogenerated chemiluminescence (ECL)<sup>9</sup> is a phenomenon where an energetic electron transfer reaction of electrogenerated species produces the excited state usually with the regeneration of emitters. In ECL, the excited state can be generated by either ion annihilation or use of a coreactant. The ECL produced by ion annihilation usually involves the generation of both stable radical anions ( $R^{\bullet-}$ ) and radical cations ( $R^{\bullet+}$ ) by alternating or sweeping the electrode potential. Then these two species can react to produce the excited state ( $R^*$ ) in the diffusion layer of an electrode, depending on the energy ( $-\Delta H$ ) available in ion annihilation.



where R is an ECL emitter,  $E_s$  is the lowest excited singlet state energy, and  $E_t$  is the triplet state energy. This method requires the electrochemical generation of both stable  $R^{\bullet-}$  and  $R^{\bullet+}$ .

However, ECL is still producible even if either stable  $R^{\bullet-}$  or  $R^{\bullet+}$  is not produced. ECL can be generated in the presence of a coreactant by pulsing or sweeping the electrode potential in only one direction, either cathodic or anodic.

A coreactant is a species able to produce a strong oxidizing or a reducing agent while it is electrochemically reduced or oxidized. For example, tris(2,2'-bipyridine)ruthenium(II),  $\text{Ru}(\text{bpy})_3^{2+}$  (bpy = 2,2'-bipyridine), can generate its ECL in the presence of peroxydisulfate ion ( $\text{S}_2\text{O}_8^{2-}$ ) by sweeping the potential in the cathodic direction (*vide infra*).<sup>10-12</sup>



or



ECL is one of the versatile analytical techniques having high sensitivity and selectivity. Understanding ECL mechanisms and optimizing conditions for generating ECL are very important for the application of ECL as an analytical method, such as an immunoassay analysis or DNA-probe assay analysis.<sup>13,14</sup> In addition, developing new ECL emitters and coreactants is also important to employ them as ECL label systems in such analyses. To be a good candidate as an ECL emitter, the compound must have a reversible one-electron redox reaction resulting in either stable  $\text{R}^{\bullet-}$  or  $\text{R}^{\bullet+}$  and a sufficiently fast ECL reaction. In case of

coreactants, they must be chemically inert with an ECL emitter, undergo electrochemical reactions in a proper potential range, and produce reducing or oxidizing agents without any side-reactions with ECL emitters.

In this chapter, it is discussed how the ECL of NR and  $\text{Ru}(\text{bpy})_3^{2+}$  is generated by use of a coreactant, benzoyl peroxide (BPO), in acetonitrile (MeCN). The spectroscopic behavior and electrochemistry of protonated and deprotonated NRs are also described. In addition, the ECL mechanism and quenching effect with BPO coreactant were studied.

## 4.2 Experimental Section

**Materials.** The hydrochloride form (NR-HCl, high purity) of neutral red (NR) was purchased from Acros (Houston, TX). Because the commercial NR-HCl is a mixture of NR and NR-HCl, it was purified by the following procedure before use. Three mg of NR-HCl was dissolved in 50 ml of deionized water. A saturated NaOH solution was then added until the reddish brown precipitate of NR was formed. This precipitate was filtered and washed thoroughly with deionized water. Then, the filtered precipitate was dried in a vacuum oven at 70 °C for 24 hr. Anhydrous acetonitrile (MeCN, 99.93 % in a sure-sealed bottle), trifluoroacetic acid (TFA, 99+ %), perchloric acid (70 %, double distilled), acetic anhydride (99.5 %), glacial acetic acid (99.8 %), tetra-*n*-butylammonium perchlorate (TBAP), and benzoyl peroxide (BPO, see Supporting Information

Figure 4.1 for structure) were obtained from Aldrich (Milwaukee, WI) and used as received. Anhydrous 1 M perchloric acid ( $\text{HClO}_4$ ) in acetic acid was made by heating a solution of 70 % aqueous  $\text{HClO}_4$  (8.6 ml) in glacial acetic acid (72.4 ml) with acetic anhydride (19 ml). This stock solution was standardized by titration with potassium hydrogen phthalate in acetic acid using crystal violet as an indicator. Acetic acid introduced in anhydrous  $\text{HClO}_4$  standard solution did not interfere with electronic absorption spectra of NR, because acetic acid is an extremely weak acid in  $\text{MeCN}$ <sup>15</sup>. TBAP and BPO were dried at 30 °C in a vacuum oven before being transferred to an inert atmosphere drybox (Vacuum Atmospheres Co., Hawthorne, CA).

**Spectroscopy.** Electronic absorbance spectra were taken with a Beckman DU 640 Spectrophotometer (Fullerton, CA). Fluorescence spectra were obtained with an ISA Spex Fluorolog-3 (JY Horiba, Edison, NJ) with absorbance maxima as an excitation source. A quartz cuvette with a 1 cm path length was used for all spectroscopic measurements. All solutions used for absorbance and fluorescence spectra were prepared in a drybox or purged by a nitrogen ( $\text{N}_2$ ) gas.

**Electrochemistry.** Electrochemical measurements were performed with either the Model 660 Electrochemical Workstation (CH Instruments, Austin, TX) or the PAR model 173/175. For cyclic voltammetry, a conventional three-electrode electrochemical cell was used. A platinum (Pt) ultramicroelectrode of 25  $\mu\text{m}$  diameter was used for steady-state voltammetry and a Pt disk electrode of

2 mm diameter was used for cyclic voltammetry or ECL. A Pt wire and silver (Ag) wire were employed as the auxiliary electrode and quasi-reference electrode (QRE), respectively. All electrode potentials were calibrated by using the ferrocene(Fc)/ferrocenium ( $\text{Fc}^+$ ) redox couple and converted to V vs. SCE by taking  $E^\circ (\text{Fc}/\text{Fc}^+) = 0.424 \text{ V vs. SCE}^{16}$ . All electrodes were polished with 0.05  $\mu\text{m}$  alumina suspension (Buehler, Lake Bluff, IL), and sonicated in deionized water and ethanol. Then all electrodes were dried in an oven at 120  $^\circ\text{C}$  for at least 20 minutes. Immediately after drying procedure, they were transferred into the drybox.

**Electrogenerated Chemiluminescence (ECL).** All ECL spectra were measured as previously reported.<sup>17</sup> A charge-coupled device (CCD) camera (Photometrics CH260, Tucson, AZ) cooled to  $-110 \text{ }^\circ\text{C}$  and interfaced to a computer was used to obtain ECL spectra. The CCD camera was focused on the exit slit of a grating spectrometer (concave grating) having a 1 mm entrance slit (Holographics, Inc.). For simultaneous CV and integrated ECL signals, a photomultiplier tube (PMT, Hamamatsu R4220p) was used. A voltage of  $-750 \text{ V}$  was supplied to the PMT with a high-voltage power supply series 225 (Bertan High Voltage Corp., Hicksville, NY). All ECL spectra were produced by pulsing potentials from 0 V to the cathodic peak potential of NR and all integrated ECL signals were produced by sweeping potentials from 0 V to a potential sufficiently negative to generate the radical anion of NR.

### 4.3 Results and Discussion

**Acid-Base Properties of NR in MeCN.** To characterize the acid-base properties of NR in MeCN, anhydrous perchloric acid (HClO<sub>4</sub>) was used as a titrant because it is completely dissociated in MeCN<sup>18</sup>. Figure 4.1 shows the electronic absorption spectra of 10 μM NR titrated with anhydrous HClO<sub>4</sub> in MeCN. Like electronic absorption spectra measured in water solution, NR has one absorption band with the maximum at 441 nm and the color of 10 μM NR solution in MeCN was bright yellow. As the concentration of HClO<sub>4</sub> increased in a NR solution, the absorption band of 441 nm decreased and a new absorption band appeared with a maximum at 533 nm. In addition, an isosbestic point was found at 468 nm, indicating that only two forms (NR and NRH<sup>+</sup>) were under equilibrium in the solution. When 10 μM of HClO<sub>4</sub> was added, the absorption band of 441 nm disappeared and the color of this solution became red.

The acid dissociation constant ( $K_a$ ) for the acid-base reaction of NR can be calculated from the electronic absorption spectra in Figure 4.1.<sup>18</sup> The reaction between NR and a proton (H<sup>+</sup>) in MeCN is represented in eq. (4.1).



The equilibrium constant ( $1/K_a$ ) of this reaction is

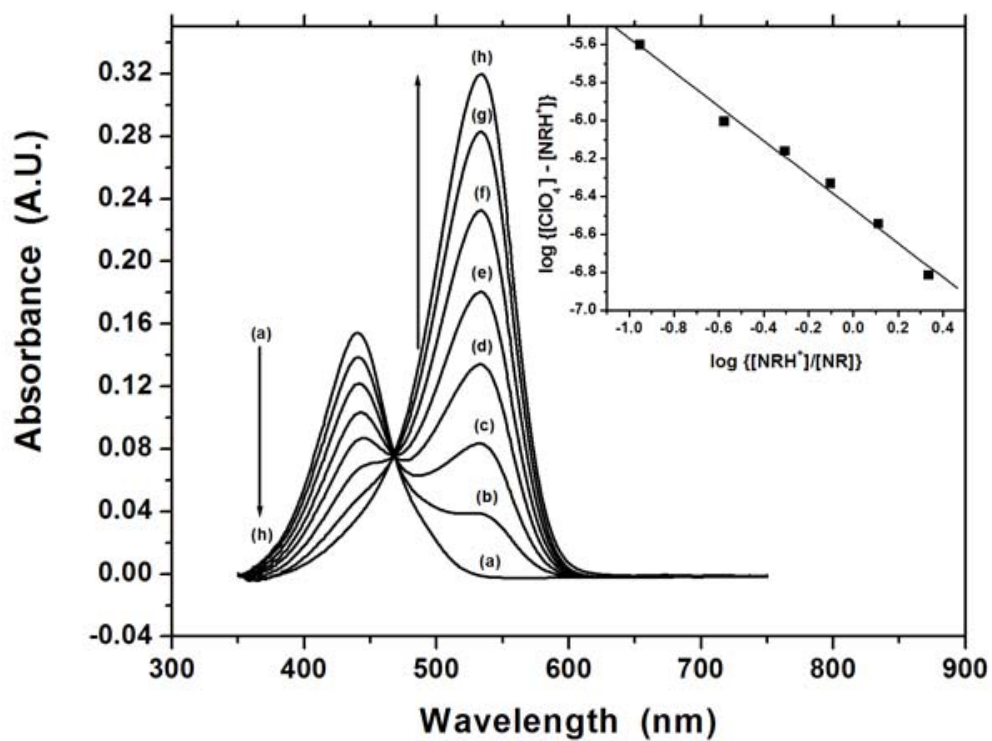


**Figure 4.1.** Electronic absorption spectra of 10  $\mu\text{M}$  NR titrated with (a) 0  $\mu\text{M}$  (b) 2  $\mu\text{M}$  (c) 3  $\mu\text{M}$  (d) 4  $\mu\text{M}$  (e) 5  $\mu\text{M}$  (f) 6  $\mu\text{M}$  (g) 7  $\mu\text{M}$  (h) 10  $\mu\text{M}$  of anhydrous  $\text{HClO}_4$  in MeCN. Inset is a plot of  $\log \{[\text{ClO}_4^-] - [\text{NRH}^+]\}$  vs.  $\log \{[\text{NRH}^+]/[\text{NR}]\}$ .

$$\frac{1}{K_a} = \frac{[\text{NRH}^+]f_{\text{NRH}^+}}{[\text{NR}][\text{H}^+]f_{\text{NR}}f_{\text{H}^+}} \cong \frac{[\text{NRH}^+]}{[\text{NR}][\text{H}^+]} \quad (4.2)$$

where  $f$  represents the activity coefficient. In a dilute solution, the  $f$  for  $\text{NRH}^+$  cancels with the  $f$  for  $\text{H}^+$  and the  $f$  for  $\text{NR}$  is 1 because of the uncharged species. Therefore,  $K_a$  will be a function of concentration. Because  $\text{HClO}_4$  is completely dissociated in MeCN,  $[\text{H}^+]$  would be

$$[\text{H}^+] = [\text{ClO}_4^-] - [\text{NRH}^+] \quad (4.3)$$

If eq. (4.3) is plugged into eq. (4.2) and then the logarithm is applied,

$$\log\{[\text{ClO}_4^-] - [\text{NRH}^+]\} = \log \frac{[\text{NRH}^+]}{[\text{NR}]} + \log K_a \quad (4.4)$$

where  $K_a$  denotes the acid dissociation constant.  $[\text{NRH}^+]$  and  $[\text{NR}]$  can be calculated from the absorption spectra by Beer's law and  $[\text{ClO}_4^-]$  is same as the concentration of  $\text{HClO}_4$  added in the NR solution. Therefore, a plot of  $\log\{[\text{ClO}_4^-] - [\text{NRH}^+]\}$  vs.  $\log\{[\text{NRH}^+]/[\text{NR}]\}$  should be linear [inset of Figure 4.1] and the  $\text{p}K_a$  value of NR can be estimated from the  $y$ -intercept of that plot. The estimated  $\text{p}K_a$  value was 6.5 in MeCN.

**Electrochemistry of NR and NRH<sup>+</sup>.** There have been several reports<sup>19-21</sup> on the electrochemistry of NR in aqueous solution, and these mainly focused on the electrochemical reduction of NRH<sup>+</sup> in aqueous solutions. The electrochemistry of NR and NRH<sup>+</sup> in organic solvents, however, has not been investigated, even though NR was first synthesized in 1878<sup>22</sup>. Figures 4.2 and 4.3 show the cyclic voltammograms of 1 mM NR in MeCN containing 0.1 M TBAP at 0.1 V/s and the scan rate dependence of peak potentials and peak currents for the NR reduction. When the electrode potential was swept in the anodic direction, three irreversible electrochemical oxidation waves were found at + 0.74, + 1.18, and + 1.55 V vs. SCE (See Figure 4.2). In contrast, the electrochemical reduction of NR was reversible (See Figure 4.2) because the peak potentials ( $E_p$ ) are independent of the square root of scan rate ( $\nu$ ) (See Figure 4.3). The cathodic peak currents ( $i_{pc}$ ) and corresponding anodic peak currents ( $i_{pa}$ ) of NR for reduction were linearly dependent on  $\nu^{1/2}$ , indicating that this reduction is diffusion-controlled (See Figure 4.3). In addition, the current ratio ( $\sim 0.9$ ),  $i_{pa}/i_{pc}$ , of this reduction was close to the unity. The half-wave potential ( $E_{1/2}$ ) of NR reduction was found at  $- 1.64$  V vs. SCE. However, the continuous scan from the anodic (oxidation of NR) to the cathodic direction (reduction of NR) in CV did not reproduce the reversible reduction of NR, indicating the decomposition of NR radical cation (NR<sup>•+</sup>).

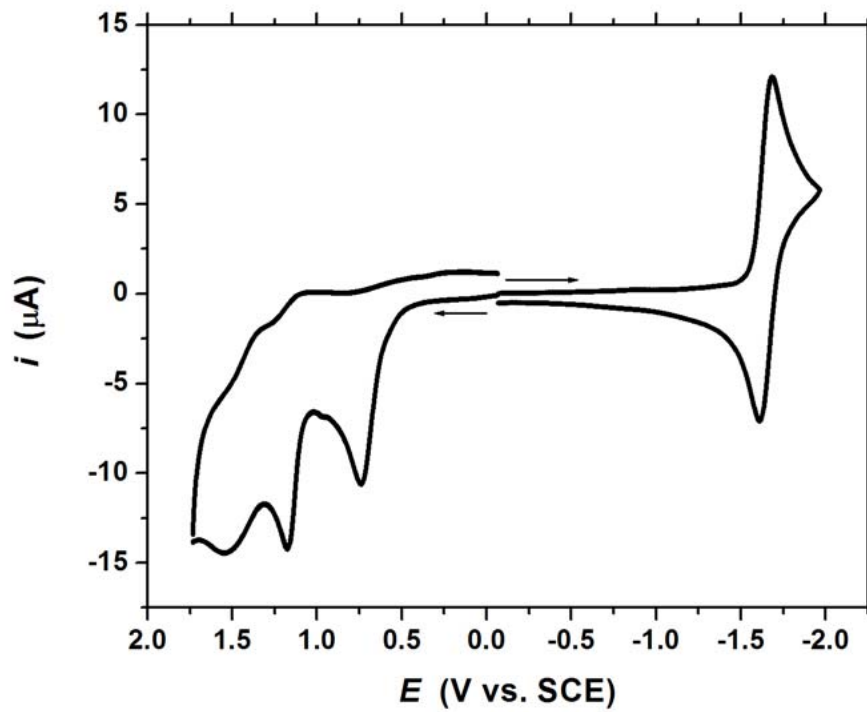


**Figure 4.2.** Cyclic voltammograms of 1 mM neutral red (NR) in 0.1 M TBAP/MeCN. Scan rate = 0.1 V/s. A Pt electrode was used (area = 0.03 cm<sup>2</sup>).

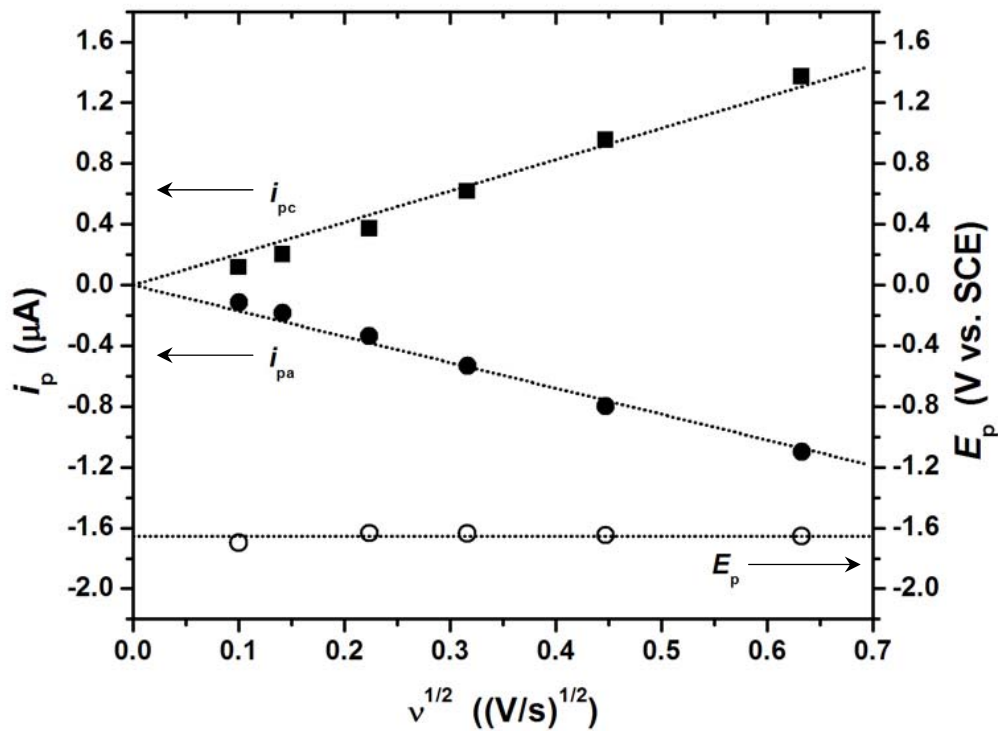


**Figure 4.3.** Dependence of peak potentials ( $E_p$ ) and peak currents ( $i_{pc}$  and  $i_{pa}$ ) for the NR reduction on the scan rate ( $v$ ).  $i_{pc}$  represents the reduction peak current of NR and  $i_{pa}$  denotes the corresponding oxidation current of reduced NR. 1mM NR in 0.1 M TBAP/MeCN and a Pt electrode (area =  $7.9 \times 10^{-3} \text{ cm}^2$ ) were used.

The electrochemical reduction of NR was investigated under the different concentrations of trifluoroacetic acid (TFA). Figure 4.4 shows the cyclic voltammograms for the electrochemical reduction of 1 mM NR in 0.1 M TBAP/MeCN with various concentrations of TFA at 0.1 V/s. As the concentration of TFA increased, the original reduction peak at  $-1.47$  V vs. Ag QRE diminished and a new reduction wave developed at a much more positive potential (1.11 V shift) than the original reduction peak potential. In addition, both of the reduction peak currents ( $i_p$ ) were linearly dependent on the concentrations of TFA up to 1.8 mM [Figure 4.5]. Then the new  $i_p$  was independent of the concentration of TFA at higher than 2.2 mM of TFA, and the original reduction peak totally disappeared, because all NR molecules were protonated by TFA. Therefore, the new reduction peak was not associated with the reduction of  $H^+$  but the reduction of  $NRH^+$ ; in fact,  $H^+$  reduction occurred at a more negative potential than the new reduction peak potential. In Figure 4.5,  $i_p$  of NR measured without TFA is distinctly lower than that of  $NRH^+$  at 3 mM TFA, indicating that the reduction mechanism of  $NRH^+$  may be different from that of NR.

To characterize electrochemical reductions of NR and  $NRH^+$ , the unknown diffusion coefficient ( $D$ ) and the number of electron transferred during reduction ( $n$ ) were estimated from the steady-state current and the chronoamperometric diffusion current (transient current) of an ultramicroelectrode (UME).<sup>23</sup> The steady-state current of UME is<sup>24,25</sup>

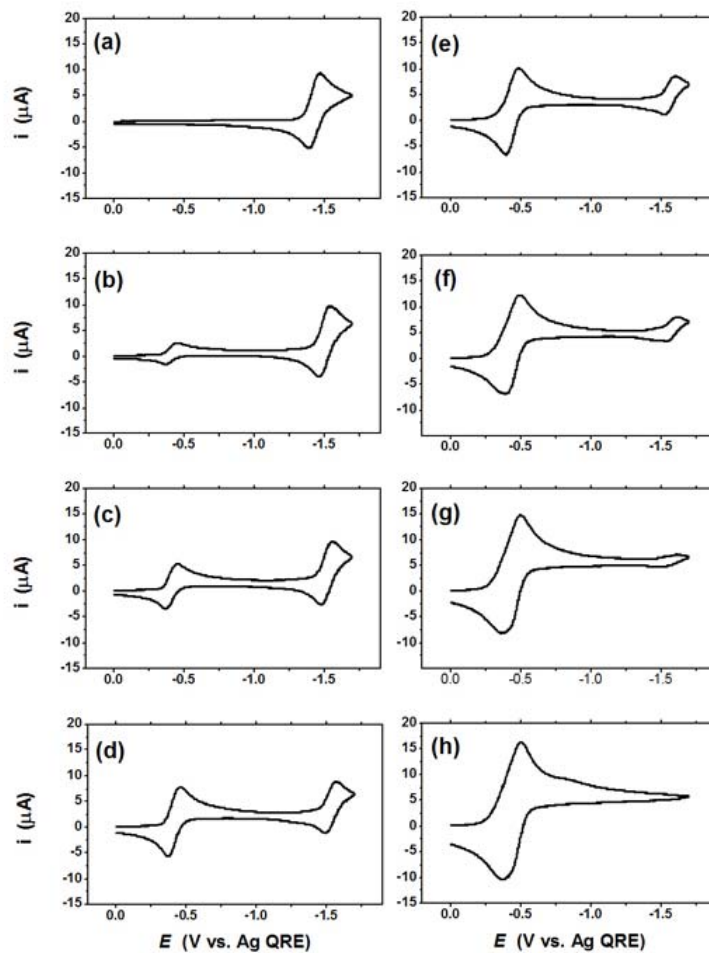


**Figure 4.4.** Cyclic voltammograms of 1 mM neutral red (NR) with (a) 0.00 mM, (b) 0.26 mM, (c) 0.52 mM, (d) 0.78 mM, (e) 1.04 mM, (f) 1.30 mM, (g) 1.56 mM, and (h) 1.82 mM trifluoroacetic acid (TFA) in 0.1 M TBAP/MeCN. Scan Rate = 0.1 V/s. The same Pt electrode was used for each measurement (area = 0.03 cm<sup>2</sup>).

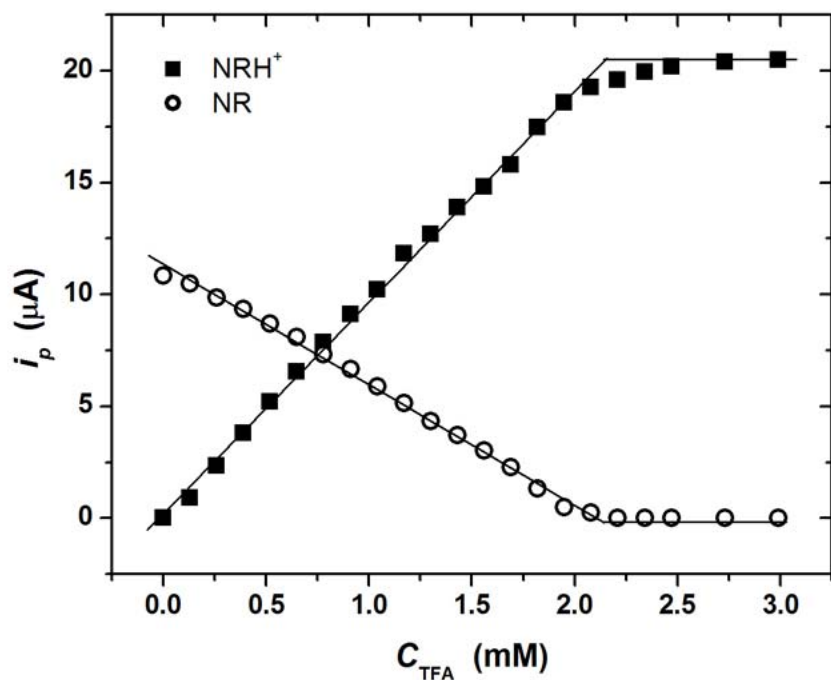


**Figure 4.5.** Dependence of reduction peak currents ( $i_p$ ) NR and NRH<sup>+</sup> on the concentration of TFA in 0.1 M TBAP/MeCN. 1 mM NR was titrated with 0.13 M TFA/0.1 M TBAP /MeCN stock solution. Scan rate = 0.1 V/s. A same Pt electrode was used for each measurement (area = 0.03 cm<sup>2</sup>).

$$i_{ss} = 4nFDC^*a \quad (4.5)$$

where  $C^*$  is the bulk concentration of analyte and  $a$  is the radius of an UME. Because the current response at an UME having a radius  $a$  is same as that of a hemisphere electrode having  $r_s = 2a/\pi$ ,<sup>26,27</sup> the chronoamperometric diffusion current,  $i_d(t)$ , is defined as

$$i_d(t) = \pi^{1/2}nFD^{1/2}C^*a^2t^{-1/2} + 4nFDC^*a \quad (4.6)$$

By normalizing eq. (4.6) with eq. (4.5), the normalized current,  $i_d(t)/i_{ss}$ , at an UME is

$$i_d(t)/i_{ss} = (\pi^{1/2}/4)a(Dt)^{-1/2} + 1 \quad (4.7)$$

Therefore,  $i_d(t)/i_{ss}$  is a function of  $t^{-1/2}$  and a plot of  $i_d(t)/i_{ss}$  vs.  $t^{-1/2}$  should be linear.  $D$  can be estimated from the slope of this plot and  $n$  can also be calculated by plugging the  $D$  value into eq. (4.5), if  $C^*$  is known.<sup>23</sup>

Figure 4.6 shows the steady state currents of  $\text{NRH}^+$  and NR reductions. Although  $i_{\text{ss}}$  was not well characterized for  $\text{NRH}^+$  because of the cathodic current of the  $\text{H}^+$  reduction, it was still possible to approximate the  $i_{\text{ss}}$  of  $\text{NRH}^+$  reduction. The measured  $i_{\text{ss}}$  was 9.9 nA for  $\text{NRH}^+$  and 4.7 nA for NR. Because  $i_{\text{ss}}$  for  $\text{NRH}^+$  is two times as large as that for NR, the  $n$  value of  $\text{NRH}^+$  may be two times larger than that of NR.

Figure 4.7 shows the plots of  $i_{\text{d}}(t)/i_{\text{ss}}$  vs.  $t^{-1/2}$  for NR and  $\text{NRH}^+$ . In the very short time region, the experimental data points of Figure 4.7 deviated from linearity because of double layer charging of the electrode, finite rise time of the potentiostat and current follower, and finite heterogeneous electron transfer kinetics. For the relatively long time region, however,  $i_{\text{d}}(t)/i_{\text{ss}}$  was a linear function of  $t^{-1/2}$  and its slope was extracted by a linear regression. The calculated slopes were 0.180 for NR and 0.182 for  $\text{NRH}^+$  and the calculated  $D$  values were  $9.5 \times 10^{-6} \text{ cm}^2/\text{s}$  for NR and  $9.3 \times 10^{-6} \text{ cm}^2/\text{s}$ . As was expected, both  $D$  values were not much different. Then, the  $n$  values calculated from eq. (4.5) were 1.02 electron for NR and 2.20 electrons for  $\text{NRH}^+$ .  $E_{1/2}$ ,  $n$ , and  $D$  values for the reductions of NR and  $\text{NRH}^+$  are summarized in Table 4.1.

The electrochemical reduction mechanisms of NR and  $\text{NRH}^+$  are postulated as shown in Scheme 4.1. Because NR is a derivative of phenazine, its electrochemical reduction mechanism may be similar to that of phenazine.<sup>28</sup>

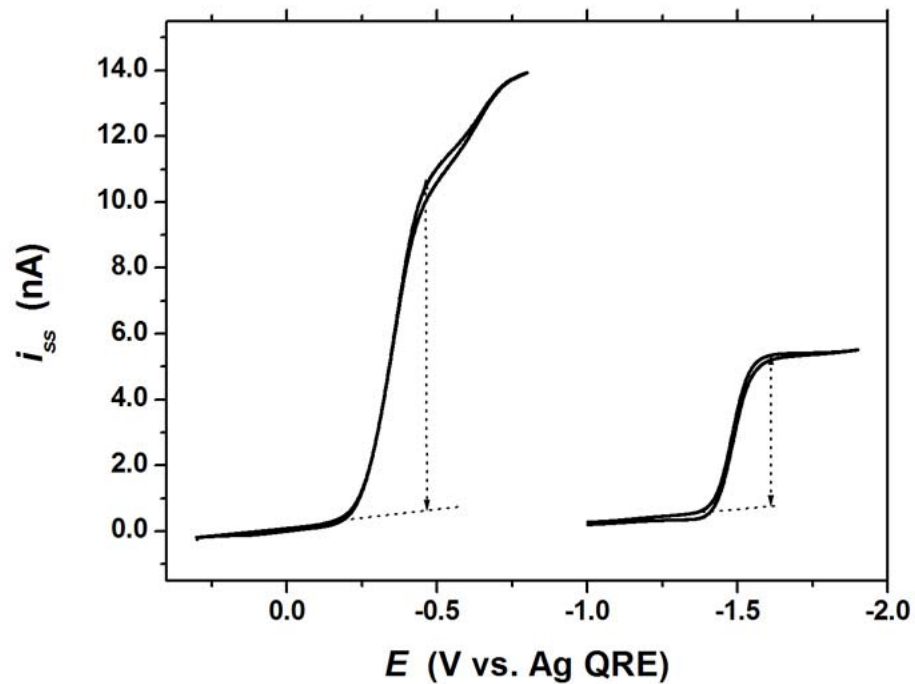


**Figure 4.6.** Cyclic voltammograms of 1 mM NR and  $\text{NRH}^+$  produced by adding 2 mM TFA in 0.1 M TBAP/MeCN. A Pt-UME of  $25\mu\text{m}$  ( $a = 12.5\ \mu\text{m}$ ) was used. Scan rate = 10 mV/s.

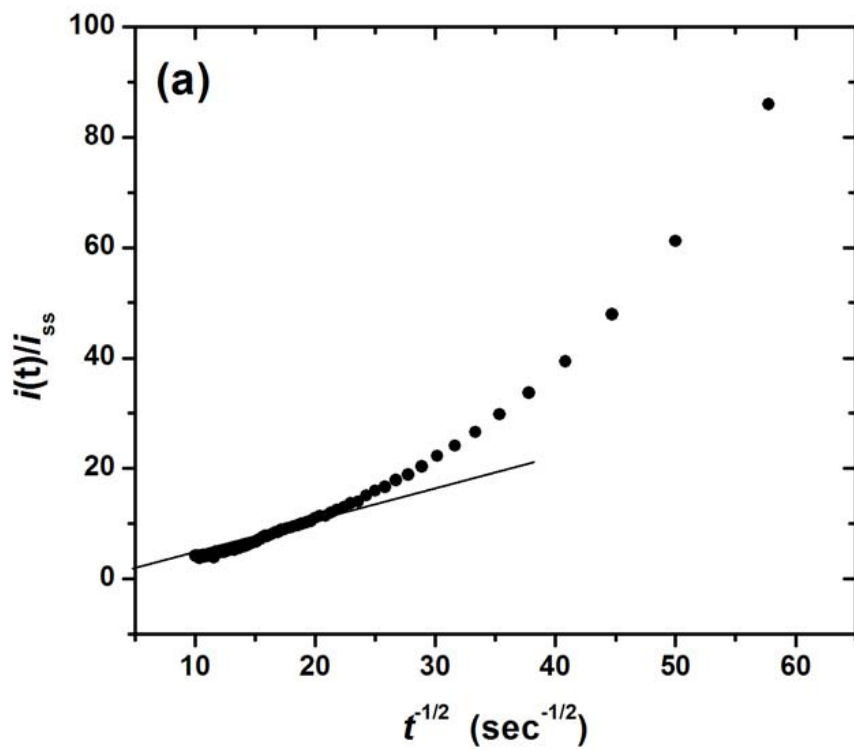
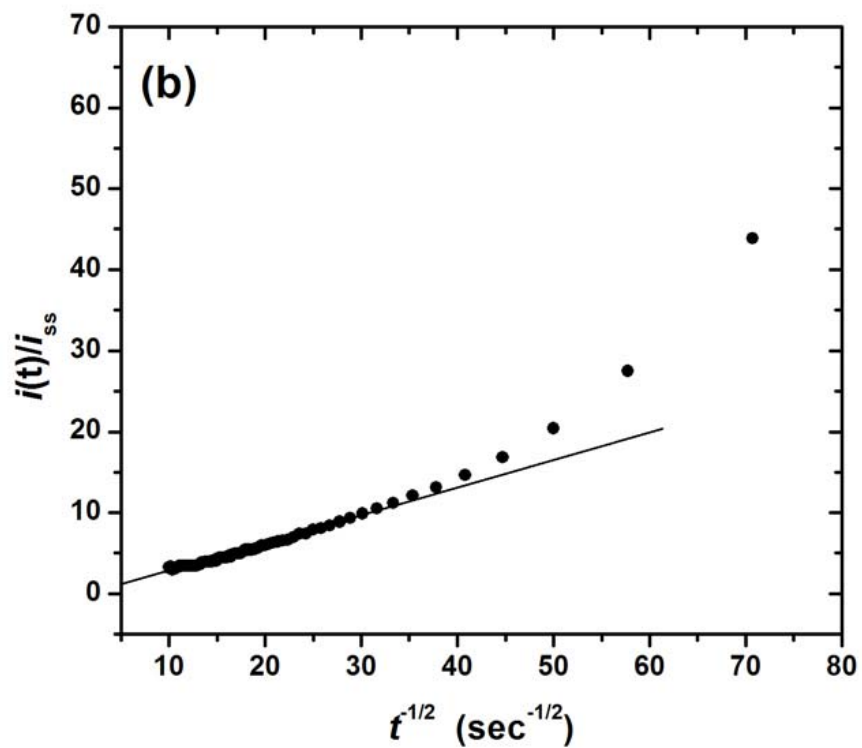


Figure 4.7. Continued on the next page.



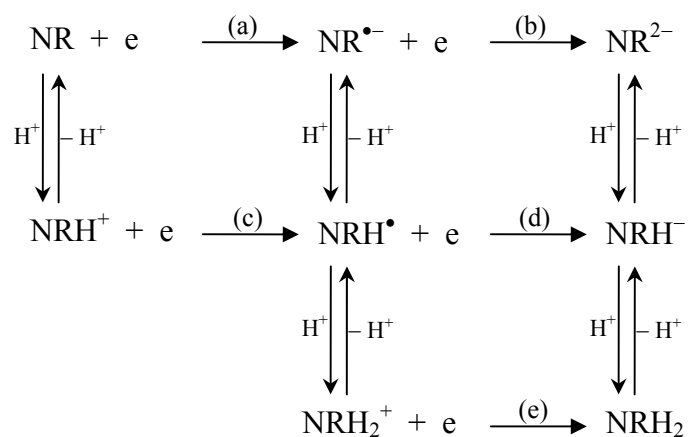
**Figure 4.7. (Cont.)** Plots of the normalized current ratio,  $i_d(t)/i_{ss}$ , against the inverse square root of time for the reductions of (a) 1 mM NR and (b) 1 mM  $\text{NRH}^+$  in 0.1 M TBAP/MeCN. The sampling rate is 100  $\mu\text{sec}$  per point. 12.5  $\mu\text{m}$  radius Pt-UME employed.

**Table 4.1. Summary of  $E_{1/2}$ ,  $n$ , and  $D$  for the Reductions of NR and NRH<sup>+</sup>.**

	$E_{1/2}$ (V vs. SCE)	$n$	$D$ (cm <sup>2</sup> /s)
NR	-1.64	1.02	$9.5 \times 10^{-6}$
NRH <sup>+</sup>	-0.53	2.20	$9.3 \times 10^{-6}$

Therefore, it is speculated that two successive one-electron reductions of NR can occur [paths (a) and (b) in Scheme 4.1]. Similarly, NRH<sup>+</sup> is supposed to be reduced as same manner. However, if the heterogeneous electron transfer rate of path (d) is very fast and path (d) occurs at same or more positive potential than the one for path (c), a two-electron reduction process of NRH<sup>+</sup> is expected. In our system, path (e) might be negligible because there was not a sufficient concentration of H<sup>+</sup>. Similar phenomena were observed in electrochemical reductions of phenazine and protonated phenazine in DMF or DMSO.<sup>28</sup>

**Scheme 4.1**



In summary, electrochemical reductions of NR and NRH<sup>+</sup> in MeCN are occurs as follows.



**Electrogenerated Chemiluminescence (ECL) of NR.** ECL by ion annihilation was not produced because neither NR nor  $\text{NRH}^+$  generated stable radical cations (no reversible oxidation shown in their CVs). Therefore, benzoyl peroxide (BPO) was used as a coreactant because it produced a sufficiently strong oxidizing agent, benzoate radical ( $\text{C}_6\text{H}_5\text{CO}_2^\bullet$ ), via the ECE process.

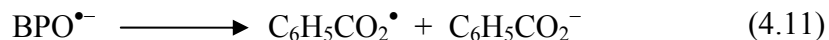
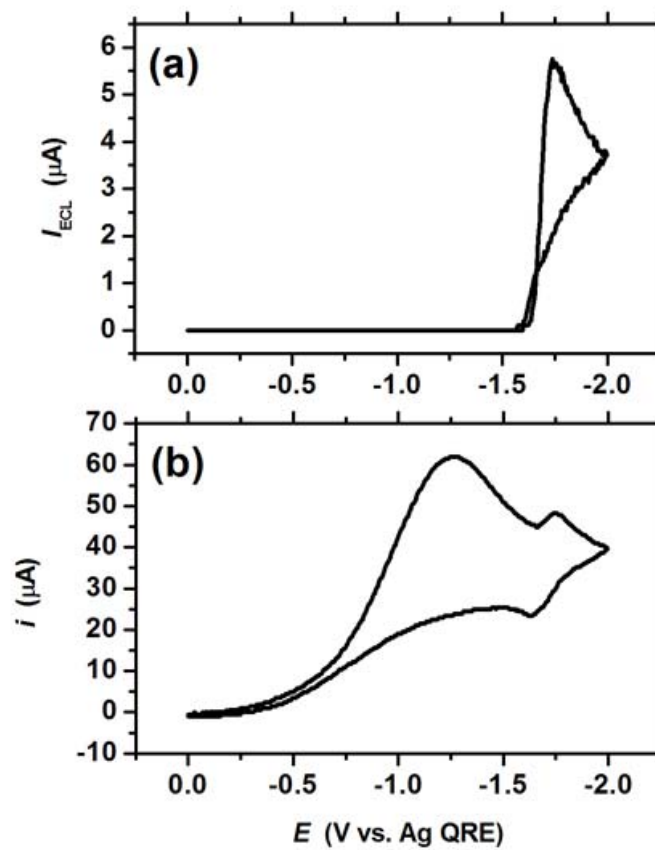


Figure 4.8 shows the simultaneous CV and ECL response of the 1 mM NR/5 mM BPO system in MeCN containing 0.1 M TBAP at 0.1 V/s. From the CV, BPO was reduced at  $-1.25$  V vs. Ag QRE prior to the NR reduction and no ECL was found at this potential, indicating that no luminescence was generated by only BPO reduction. When the electrode potential approached to the reduction potential of NR, ECL emitted by NR was detected at the PMT.

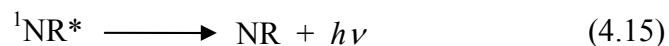
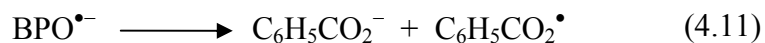
The proposed ECL mechanism of NR generated with BPO is shown in Scheme 4.2. The electrochemical reduction of BPO displayed an irreversible



**Figure 4.8.** Simultaneous (a) ECL and (b) CV of 1 mM NR and 5 mM BPO in 0.1 M TBAP/MeCN at 0.1 V/s. A Pt electrode was used (area = 0.03 cm<sup>2</sup>).

reduction wave in CV [Figure 4.8], and followed an ECE mechanism<sup>29</sup>, [eq. (4.10) through eq. (4.12)] which was analogous to the one proposed by Chandross,<sup>30</sup> *et. al.*, where BPO is reduced by hydrocarbon radical anions. The generated  $C_6H_5CO_2^\bullet$  was a sufficiently strong oxidizing agent, whose  $E^\circ$  ( $C_6H_5CO_2^\bullet/C_6H_5CO_2^-$ ) values were reported as either + 0.8 V<sup>31</sup> or + 1.5 V<sup>30</sup> vs. SCE. Once NR was reduced,  $C_6H_5CO_2^\bullet$  oxidized  $NR^{\bullet-}$  to  $NR^*$  [eq. (4.14)].

#### Scheme 4.2



To check the energetic feasibility, the energy ( $-\Delta H_{co}$ )<sup>32</sup> available in the reaction between  $C_6H_5CO_2^\bullet$  and  $NR^{\bullet-}$  was calculated using  $E_{1/2}$  ( $NR/NR^{\bullet-}$ ) and  $E^\circ$  ( $C_6H_5CO_2^\bullet/C_6H_5CO_2^-$ ), and compared with the lowest excited singlet state energy ( $E_s$ ) of NR, which was determined from the fluorescence spectrum of NR.

From the equation (4.16),

$$-\Delta H_{\text{co}} = E^\circ (\text{C}_6\text{H}_5\text{CO}_2^\bullet/\text{C}_6\text{H}_5\text{CO}_2^-) - E_{1/2} (\text{NR}/\text{NR}^{\bullet-}) - 0.1 \text{ eV} \quad (4.16)$$

where 0.1 eV is an estimate of the temperature-entropy approximation term ( $T\Delta S$ ) at 25 °C, the calculated  $-\Delta H_{\text{co}}$  is 2.34 eV if  $E^\circ (\text{C}_6\text{H}_5\text{CO}_2^\bullet/\text{C}_6\text{H}_5\text{CO}_2^-)$  is + 0.8 V ( $-\Delta H_{\text{co}} = 3.04 \text{ eV}$  if  $E^\circ$  of  $\text{C}_6\text{H}_5\text{CO}_2^\bullet$  is + 1.5 V), which is larger than  $E_s$  (2.21 eV) of NR. Therefore, the lowest excited singlet state ( $^1\text{NR}^*$ ) of NR can be directly generated.

In contrast, no ECL signal was obtained with  $\text{NRH}^+$  and BPO. Because the electrochemical reduction of  $\text{NRH}^+$  is a two-electron transfer reaction and  $-\Delta H_{\text{co}}$  (1.93 eV) estimated from the maximum value (+ 1.5 V) of  $E^\circ (\text{C}_6\text{H}_5\text{CO}_2^\bullet/\text{C}_6\text{H}_5\text{CO}_2^-)$  is less than  $E_s$  (2.06 eV) of  $\text{NRH}^+$ , it is energetically unfavorable to directly generate  $^1\text{NRH}^{+\bullet}$ .

To determine that the observed ECL was emitted from NR, ECL spectra were measured with a CCD camera and compared with its fluorescence. Figure 4.9 shows the ECL spectrum of 1 mM NR with 10 mM BPO produced by pulsing the electrode potential between 0 V and  $-1.6 \text{ V}$  vs. Ag QRE with the 0.1 sec pulse width and the fluorescence spectra of NR (5  $\mu\text{M}$ ) and  $\text{NRH}^+$  (5  $\mu\text{M}$ ). The fluorescence maxima of NR and  $\text{NRH}^+$  were found at 561 nm and 601 nm, respectively. Interestingly, the observed ECL spectrum of NR, which had a maximum intensity at 610 nm, corresponded to the fluorescence of  $\text{NRH}^+$  rather

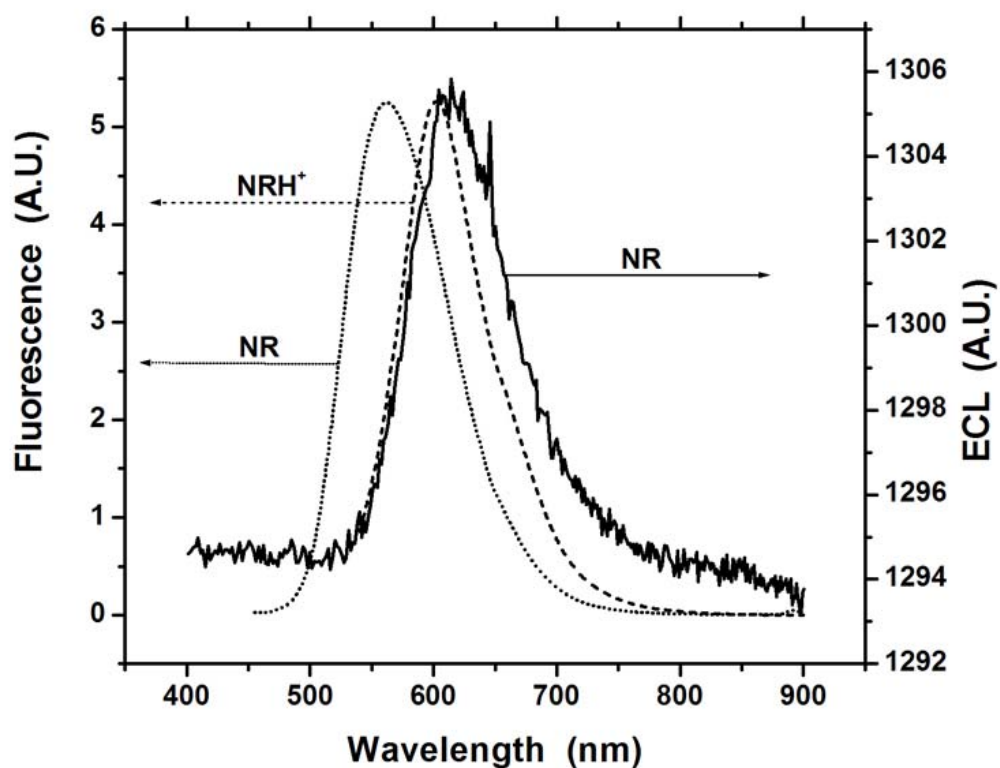


**Figure 4.9.** ECL (solid line) spectrum of 1 mM NR and fluorescence spectra of 5  $\mu\text{M}$  NR (dotted line) and 5  $\mu\text{M}$   $\text{NRH}^+$  (dashed line). ECL was generated with 10 mM BPO by pulsing the electrode potential between 0 V and  $-1.6$  V vs. Ag QRE (0.1 sec pulse-width and 5 min integration).  $\lambda_{\text{ex}}$  for NR and  $\text{NRH}^+$  were 440 nm and 530 nm, respectively.

than NR. To check the presence of unknown fluorescing species produced during ECL, absorbance and fluorescence measurements were carried out again with the same NR/BPO solution as soon as the ECL experiment was finished. The resulting absorption and fluorescence spectra were identical with those measured before ECL experiments, suggesting that no emissive bulk by-product was formed during the ECL reaction. However, there may be still possibility that a small amount of by-products can be formed at (or near) the electrode during the ECL reaction.

Singh, *et. al.* reported the dual solvatochromism of NR in fluorescence.<sup>33</sup> They observed that the fluorescence maxima shifted to the longer wavelength region as the solvent polarity became higher, and suggested the existence of two closely spaced electronic excited states<sup>33</sup>. To check the solvatochromic effect on the NR ECL, several solvents having different polarities (dielectric constants) were used. Unlike in MeCN, the electrochemical reduction of NR was not reversible in tetrahydrofuran (THF) and benzonitrile (Bz) (See Supporting Information Figure 4.2), indicating that the radical anions of NR were not stable in these solvents. As well, no ECL was observed in THF and Bz. However, NR was reversibly reduced in CH<sub>2</sub>Cl<sub>2</sub> (See Supporting Information Figure 4.2) and its ECL was produced with BPO at 575 nm. Figure 4.10 shows the ECL spectra of 1 mM NR with 10 mM BPO in MeCN and CH<sub>2</sub>Cl<sub>2</sub>. Because MeCN usually provides better stability for radical anions than CH<sub>2</sub>Cl<sub>2</sub>,<sup>32</sup> the ECL produced in

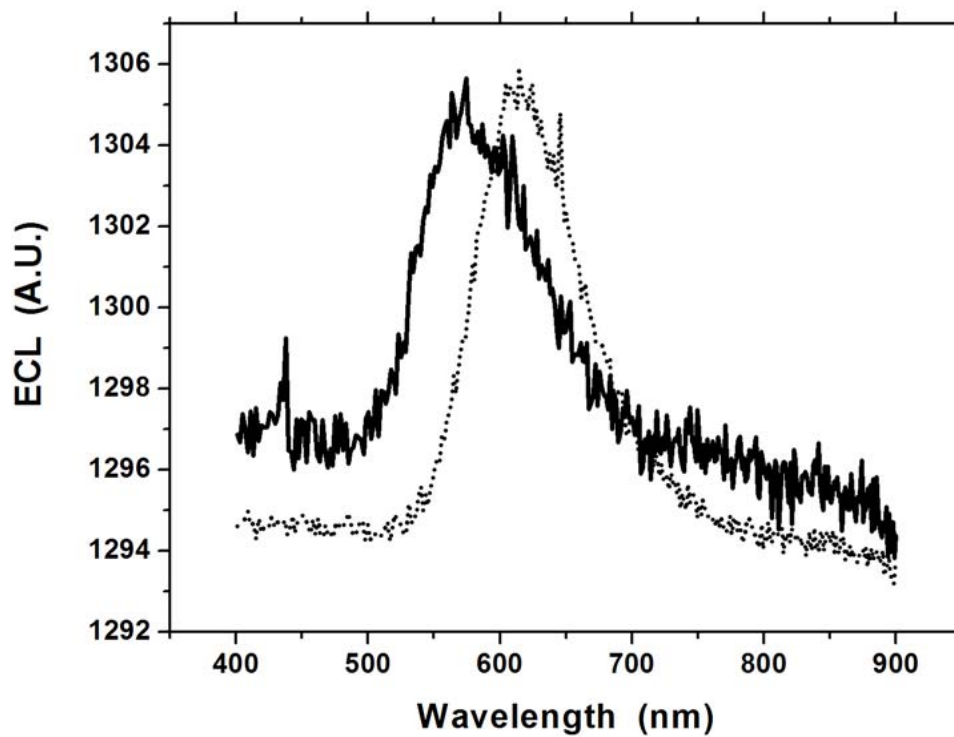


**Figure 4.10.** ECL spectra of 1 mM NR with 10 mM BPO in MeCN (dotted line) and CH<sub>2</sub>Cl<sub>2</sub> (solid line). ECL was generated by pulsing the potential between 0 V and -1.6 V vs. Ag QRE with 5 min integration time. The same Pt electrode was used for each measurement (area =0.03 cm<sup>2</sup>).

MeCN is higher than that produced in CH<sub>2</sub>Cl<sub>2</sub> with the same concentrations of NR and BPO. The ECL of NR in CH<sub>2</sub>Cl<sub>2</sub> occurred at a ~ 30 nm shorter wavelength than in MeCN. This wavelength shift in the NR ECL is likely due to the difference in the dielectric constants ( $\epsilon$ ) of CH<sub>2</sub>Cl<sub>2</sub> ( $\epsilon = 9.1$ ) and MeCN ( $\epsilon = 37.5$ ).

**Concentration effects on the ECL of NR.** The ECL of NR strongly depends on the concentrations of NR, H<sup>+</sup>, and BPO. Figure 4.11 displays the concentration effect of NR on its ECL produced with 5 mM BPO. Each ECL was measured with a PMT by sweeping the electrode potential. The measured ECL intensities were linearly proportional to the concentrations of NR up to 0.25 mM. However, the ECL intensities gradually decreased from 0.5 mM to 2 mM of NR because of the inner filter effect (self-absorption) and self-quenching at such high concentrations. Generally, the inner filter effect occurs when the wavelength of emission overlaps an absorption band and becomes significant with an increasing concentration of emitter. The rate of self-quenching is expected to increase with increasing concentration of emitter because the average distance between emitting molecules is shorter so that probability of collisions between excited state molecules is greater at high concentration. Therefore, radiationless energy transfer becomes significant.

The ECL intensity of NR was strongly dependent on the concentration of H<sup>+</sup>, because the protonated form of NR did not produce ECL. Figure 4.12 shows

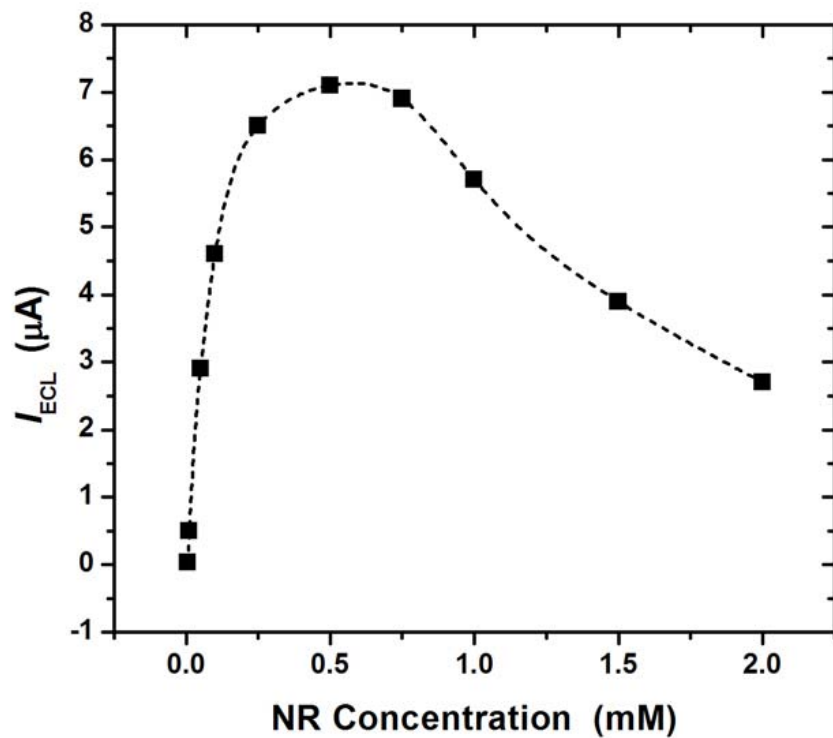


**Figure 4.11.** Effect of NR concentrations on its ECL produced with a fixed 5 mM BPO. ECL was measured with a PMT and by sweeping an electrode potential at 0.1 V/s. The same Pt electrode was used for each measurement (area =0.03 cm<sup>2</sup>).

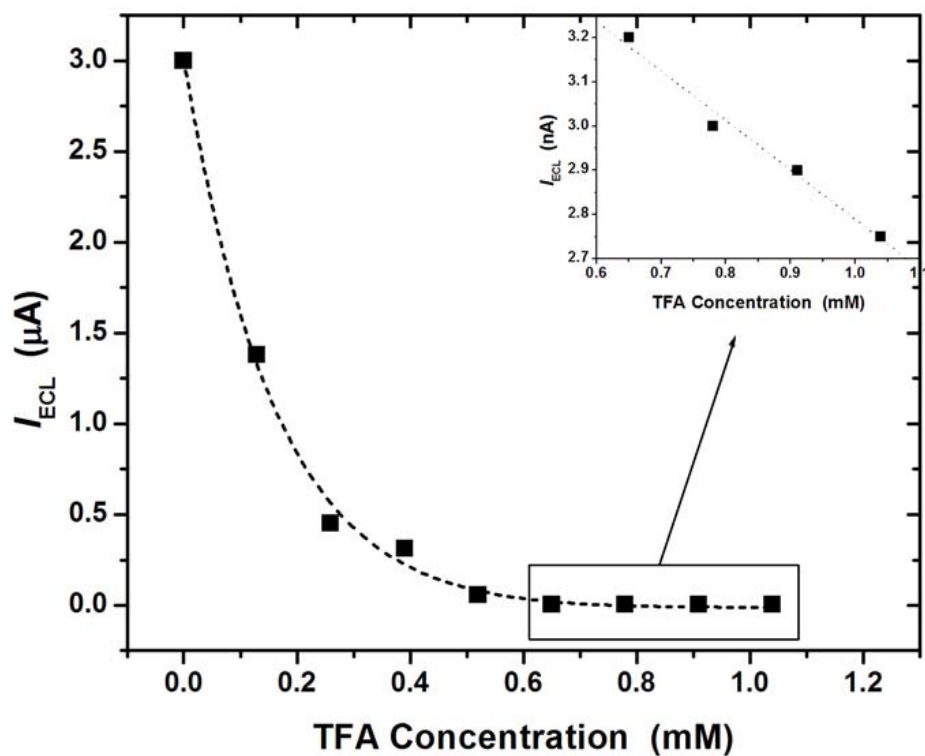


**Figure 4.12.** Effect of TFA concentrations on the ECL of 1 mM NR produced with 5 mM BPO. ECL was measured with a PMT and by sweeping an electrode potential at 0.1 V/s. The same Pt electrode was used for each measurement (area = 0.03 cm<sup>2</sup>).

the effect of  $H^+$  concentrations on the ECL of 1 mM NR using TFA as a  $H^+$  donor. As shown in Figure 4.12, the initial ECL intensities were dramatically affected by the small amount of acid and the total ECL intensity decayed exponentially although it decreased linearly in the relatively high concentration region [inset of Figure 4.12]. The decay of the ECL intensity by adding TFA is caused not only by the formation of  $NRH^+$  but also by the inner filter effect of formed  $NRH^+$ . Because the absorption band (533 nm) of  $NRH^+$  is located more closely to the ECL band (610 nm) of NR than that (441 nm) of NR, the inner filter effect by  $NRH^+$  could occur more efficiently than by NR. In fact, larger portion of the absorption band of  $NRH^+$  overlapped the ECL spectrum of NR than did the absorption band of NR: 15.8 % of NR ECL was overlapped to the  $NRH^+$  absorption band, but 2.8 % to the NR absorption band (See Supporting Information Figure 4.3).

Figure 4.13 shows the ECL intensity of 0.5 mM NR as a function of the BPO concentration. The ECL intensity of 0.5 mM NR was linearly proportional to the concentration of BPO from 0 to 10 mM. Then the ECL intensities decreased as the concentration of BPO increased from 10 mM, implying that the ECL of NR was quenched by BPO in such high concentrations. It has already been reported that BPO was used as an effective quencher for the fluorescence of  $Ru(bpy)_3^{2+}$  and aromatic hydrocarbons.<sup>34,35</sup> Similarly, ECL quenching might occur by electron transfer (ET) as follows;

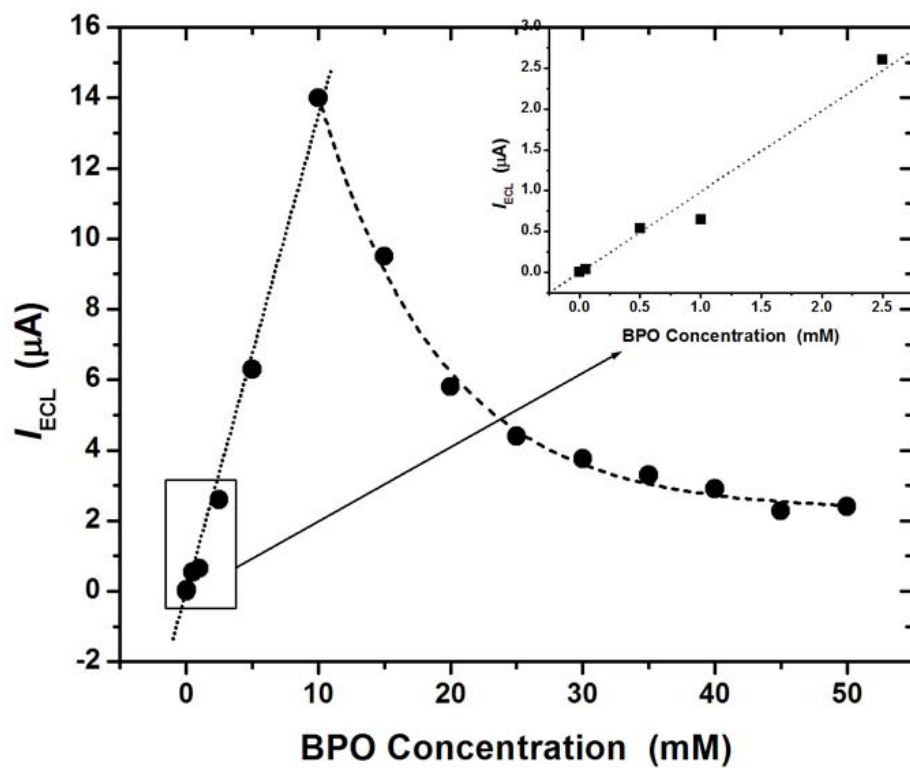
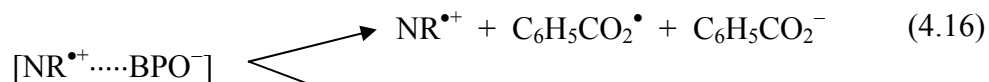


**Figure 4.13.** Effect of BPO concentrations on the ECL of 0.5 mM NR. ECL was measured with a PMT and by sweeping the electrode potential at 0.1 V/s. Inset represents the low concentration region (0 mM to 2.5 mM BPO). The same Pt electrode was used for each measurement (area = 0.03 cm<sup>2</sup>).



Once the intermediate state,  $[\text{NR}^{\bullet+} \cdots \text{BPO}^-]$ , as shown in eq. (4.15) was formed, both the decomposition reaction [eq. (4.16)] and the back electron transfer reaction [eq. (4.17)] could occur. The quenching effect by BPO seemed not to be efficient below 10 mM BPO against the ECL of 0.5 mM NR.

The quenching experiments were performed with the fluorescence of NR to check whether NR was a quencher. The quenching effect of BPO was also observed in the fluorescence of NR. The fluorescence quenching rate constant ( $k_q$ ) can be estimated from the Stern–Volmer relationship<sup>36</sup> in the absence of molecular oxygen as defined by

$$\frac{I_0}{I} = 1 + K_{\text{SV}}[\text{BPO}] = 1 + k_q \tau^s [\text{BPO}] \quad (4.18)$$

where  $I$  and  $I_0$  denote the fluorescence intensity with BPO and the initial fluorescence intensity without BPO, respectively,  $K_{\text{SV}}$  is the Stern-Volmer quenching constant,  $k_q$  is the quenching rate constant, and  $\tau^s$  is the lifetime of the

lowest excited singlet state. Figure 4.14 shows the Stern-Volmer plot of the NR fluorescence quenching. From the slope of this plot,  $K_{SV}$  and  $k_q$  were calculated as  $68.95 \text{ M}^{-1}$  and  $1.64 \times 10^{10} \text{ M}^{-1}\text{s}^{-1}$ , respectively, by taking  $\tau^s$  as  $4.2 \text{ ns}^{33}$ .

**ECL of  $\text{Ru}(\text{bpy})_3^{2+}$  with BPO and ECL Efficiency.** The new coreactant BPO was also applied to tris(2,2'-bipyridine)ruthenium(II),  $\text{Ru}(\text{bpy})_3^{2+}$  (bpy = 2,2'-bipyridine), which is a well-known ECL emitter. As shown in Figure 4.15, the  $\text{Ru}(\text{bpy})_3^{2+}$ /BPO system produced ECL in 0.1 M TBAP/MeCN. When the electrode potential was swept in the cathodic direction, BPO was first reduced and followed by the production of  $\text{C}_6\text{H}_5\text{CO}_2^\bullet$ . No luminescence occurred until  $\text{Ru}(\text{bpy})_3^{2+}$  was reduced. Three reversible reductions for the  $\text{Ru}(\text{bpy})_3^{2+/+}$ ,  $\text{Ru}(\text{bpy})_3^{+/0}$ , and  $\text{Ru}(\text{bpy})_3^{0/-}$  couples were observed in order [Figure 4.15 (a)] and  $\text{Ru}(\text{bpy})_3^{2+*}$  ( $2.12 \text{ eV}^{37}$ ) was produced by the energetic ET reaction ( $-\Delta H_{\text{co}} =$  at least  $2.2 \text{ eV}^{38}$ ) with  $\text{C}_6\text{H}_5\text{CO}_2^\bullet$  [Figure 4.15 (b)]. The produced ECL gave the orange emission having a maximum intensity at 623 nm [inset of Figure 4.15 (b)]. Although ECL was also produced at the potential where  $\text{Ru}(\text{bpy})_3^0$  and  $\text{Ru}(\text{bpy})_3^-$  were generated, only the first ECL produced by  $\text{Ru}(\text{bpy})_3^+$  would be considered here for the proposed ECL mechanism shown in Scheme 4.2. Besides the direct generation of  $\text{Ru}(\text{bpy})_3^{2+*}$  [eq. (4.20)],  $\text{Ru}(\text{bpy})_3^{2+*}$  can be produced by annihilation reaction. If the  $E^\circ$  value of  $\text{C}_6\text{H}_5\text{CO}_2^\bullet$  is taken as  $+1.5 \text{ V vs. SCE}^{30}$ , it is energetically feasible for  $\text{C}_6\text{H}_5\text{CO}_2^\bullet$  to oxidize  $\text{Ru}(\text{bpy})_3^{2+}$  to  $\text{Ru}(\text{bpy})_3^{3+}$  ( $E^\circ = +$

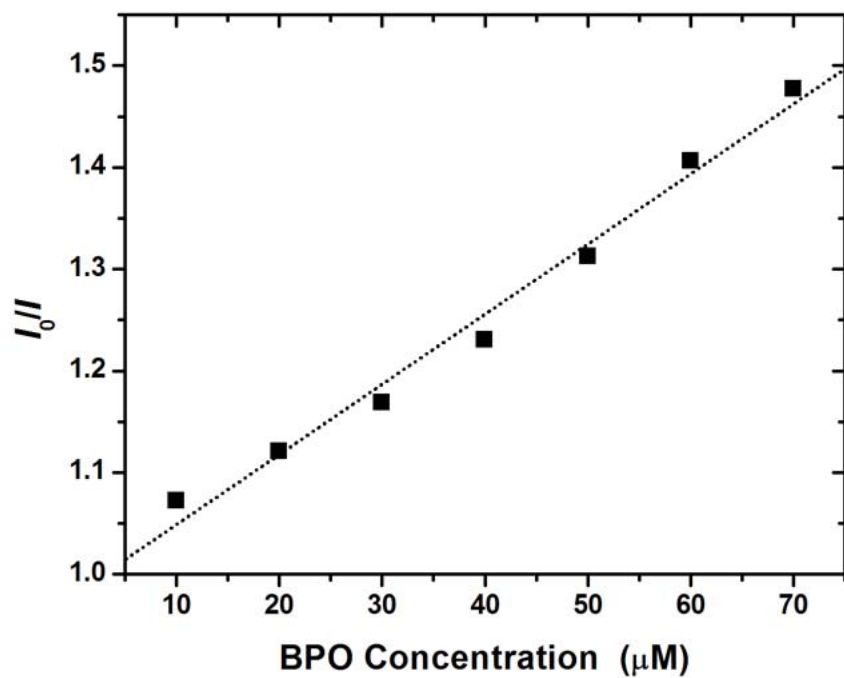


**Figure 4.14.** Stern-Volmer plot of the NR fluorescence quenching by BPO in the absence of molecular oxygen.  $C_{\text{NR}} = 1 \mu\text{M}$ .  $\lambda_{\text{ex}} = 440 \text{ nm}$ .

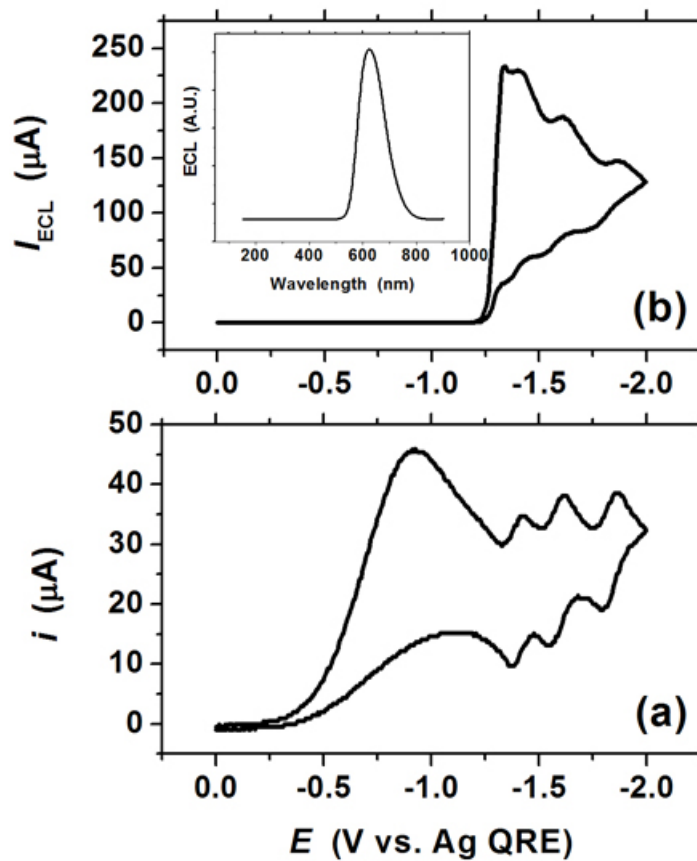
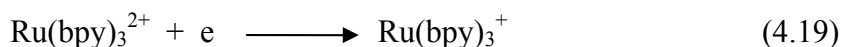
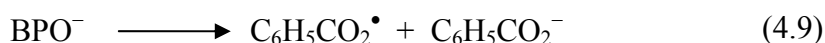


**Figure 4.15.** Simultaneous (a) cyclic voltammogram and (b) ECL wave of 1 mM  $\text{Ru}(\text{bpy})_3^{2+}$  and 5 mM BPO in 0.1 M TBAP/MeCN at 0.1 V/s. Inset of (b) represents the ECL spectra measured under the same condition.

1. 29 V vs. SCE) [eq. (4.21)]. Therefore, electrochemically generated  $\text{Ru}(\text{bpy})_3^+$  can be annihilated by  $\text{Ru}(\text{bpy})_3^{3+}$  to produce  $\text{Ru}(\text{bpy})_3^{2+*}$  [eq. (4.22)].

### Scheme 4.3



or



In general, the ECL efficiency ( $\phi_{\text{ECL}}$ ) is defined as photons emitted per redox event that is related to the total charge applied. In the NR/BPO ECL system,  $\phi_{\text{ECL}}$  could not be estimated because the total charge did not represent the number of redox reactions between  $\text{NR}^{\bullet-}$  and  $\text{C}_6\text{H}_5\text{CO}_2^\bullet$ . Therefore, the integrated ECL intensity of the NR/BPO system was compared with a reference ECL emitter/BPO system. For this comparison,  $\text{Ru}(\text{bpy})_3^{2+}$  was employed as a reference because the ECL efficiency of the  $\text{Ru}(\text{bpy})_3^{2+}$  is well known ( $\sim 5\%$ <sup>39-42</sup>). The integrated ECL intensity of NR was compared with that of  $\text{Ru}(\text{bpy})_3^{2+}$ .

obtained under the identical condition (0.5 mM NR/10 mM BPO and 0.5 mM Ru(bpy)<sub>3</sub><sup>2+</sup>/10 mM BPO). The relative intensity ratio ( $I_{\text{NR}}/I_{\text{Ru(II)}}$ ) was  $\sim 0.05$ .

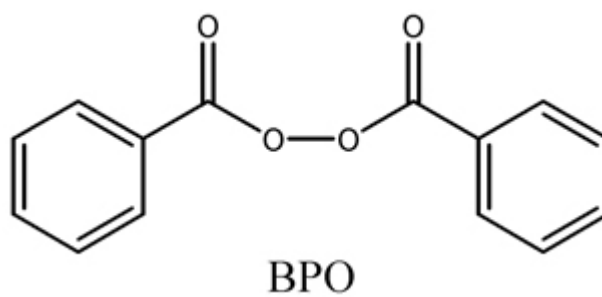
#### 4.4 Conclusion

NR can be used as an pH indicator ( $pK_a = 6.5$ ) showing the yellow-to-red color change when a NR solution is titrated with acids. In addition, NR that generates the stable radical anion (NR<sup>•-</sup>) can also be used as a new ECL emitter ( $\lambda_{\text{em}} = 610 \text{ nm}$ ) in MeCN. Although NR produces the low ECL intensity ( $I_{\text{NR}}/I_{\text{Ru(II)}} = \sim 5 \%$ ), it may be useful for an ECL label in immunoassay or DNA-probe assay analyses because of its non-toxic stain property for biological cells and pH indicator property in MeCN. The protonated form (NRH<sup>+</sup>) of NR does not produce ECL because of its two-electron reduction and lack of sufficient energy for ECL generation.

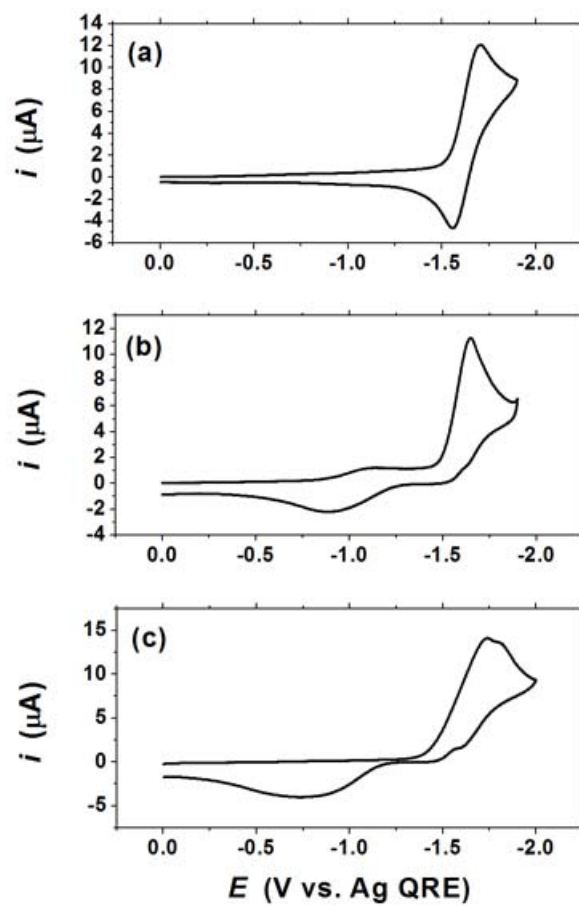
BPO is introduced as a new coreactant. The chemical and electrochemical reduction of BPO generates a strong oxidizing agent, C<sub>6</sub>H<sub>5</sub>CO<sub>2</sub><sup>•</sup>, which oxidizes the radical anions of NR and Ru(bpy)<sub>3</sub><sup>2+</sup> to their excited states. The relatively high concentration of BPO (e.g. >10 mM compared to 5 mM NR) quenches both ECL and fluorescence. The optimum condition for NR to produce ECL is 0.5 mM NR/10 mM BPO in the absence of proton donors and molecular oxygens.

### Supporting Information

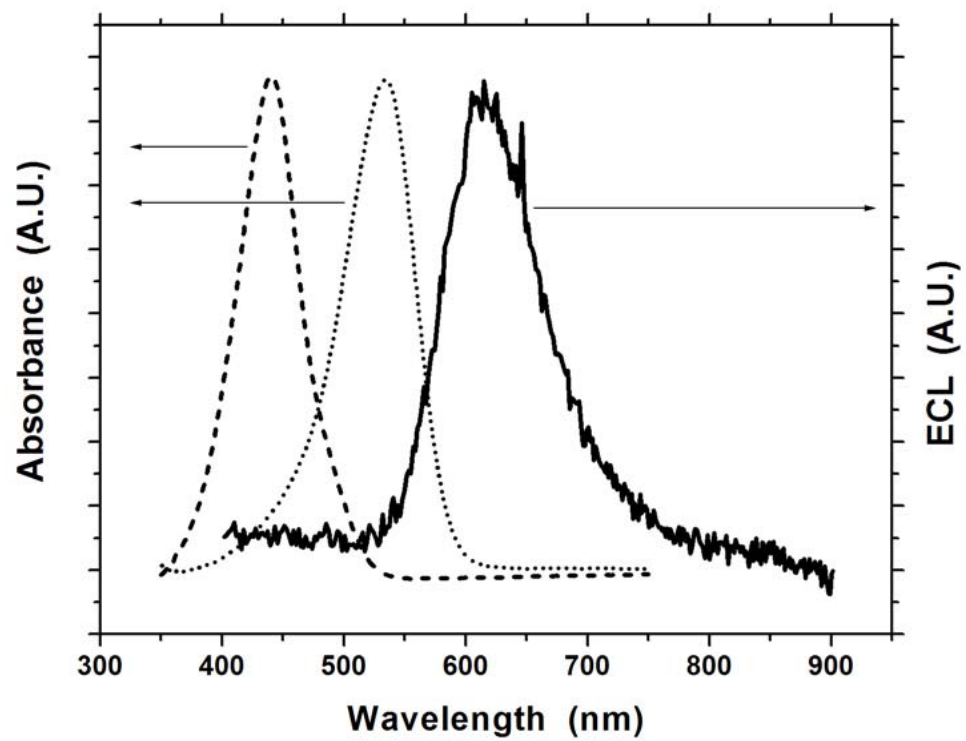
The molecular structure of BPO, CVs of NR taken in various solvents, and the inner filter effect of NR and  $\text{NRH}^+$  in ECL are available in this section.



**Supporting Information Figure 4.1.** Molecular structure of benzoyl peroxide.



**Supporting Information Figure 4.2.** Cyclic voltammograms of 1 mM NR in (a)  $\text{CH}_2\text{Cl}_2$ , (b) benzonitrile, and (c) tetrahydrofuran (THF). Supporting electrolyte: 0.1 M TBAP. S.R. = 0.1 V/s



**Supporting Information Figure 4.3.** Electronic absorbance spectra of 10  $\mu\text{M}$  NR (dashed line) and  $\text{NRH}^+$  (dotted line) in MeCN and ECL spectrum of 1 mM NR (solid line) with 10 mM BPO in MeCN.

## References

- (1) Lamanna, J. C.; McCracken, K. A. *Anal. Biochem.* **1984**, *142*, 117.
- (2) Haumann, M.; Junge, W. *Biochemistry*, **1994**, *33*, 864.
- (3) Osborne, R.; Perkins, M. A. *Food Chem. Toxicol.* **1994**, *32*, 133.
- (4) Gaullier, J. M.; Geze, M.; Santus, R.; Sa e Melo, T.; Maziere, J. C.; Bazin, M.; Morliere, P.; Dubertret, L. *Photochem. Photobiol.* **1995**, *62*, 114.
- (5) Woodburn, K. W.; Vardaxis, N. J.; Hill, J. S.; Kaye, A. H.; Phillips, D. R. *Photochem. Photobiol.* **1991**, *54*, 725.
- (6) Chen, G.; Hanson, C. L.; Ebner, T. J. *J. Neurophysiol.* **1996**, *76*, 4169.
- (7) Okada, D. *J. Neurosci. Methods* **2000**, *101*, 85.
- (8) Walz Jr., F. G.; Terenna, B.; Rolince, D. *Biopolymers*, **1975**, *14*, 825.
- (9) For general reviews, (a) Faulkner, L. R.; Glass, R. S. In *Chemical and Biological Generation of Excited States*, Adam, W.; Cilento, G., Eds.; Academic Press: New York, Chapter 6, 1982, p. 191. (b) Knight, A. W.; Greenway, G. M. *Analyst* **1994**, *119*, 879. (c) Bard, A. J.; Debad, J. D.; Leland, J. K.; Sigal, G. B.; Wilbur, J. L.; Wohlstadter, J. N. In *Encyclopedia of Analytical Chemistry: Applications, Theory, and Instrumentation*, Meyer, R. A. Ed.; John Wiley & Sons: New York, 2000, p. 9842.
- (10) White, H. S.; Bard, A. J. *J. Am. Chem. Soc.* **1982**, *104*, 6891.
- (11) Bolleta, F.; Ciano, M.; Balzani, V.; Serpone, N. *Inorg. Chim. Acta.* **1982**, *62*, 207.
- (12) Becker, W. G.; Seung, H. S.; Bard, A. J. *J. Electroanal. Chem.* **1984**, *167*, 127.
- (13) Bard, A. J.; Whitesides, G. M. *U.S. Patents* 5 221 605, 1993; 5 238 808, 1993; and 5 310 687, 1994.

- (14) Blackburn, G. F.; Shah, H. P.; Kenien, J. H.; Leland, J.; Kamin, R. A.; Link, J.; Peterman, J.; Powell, M. J.; Shah, A.; Talley, D. B.; Tyagi, S. K.; Wilkins, E.; Wu, T. -G.; Massey, R. J. *J. Clin. Chem.* **1991**, *37*, 1534.
- (15) Coetzee, J. F.; Kolthoff, I. M. *J. Am. Chem. Soc.* **1957**, *79*, 6110.
- (16) Debad, J. D.; Morris, J. S.; Magnus, P.; Bard, A. J. *J. Org. Chem.* **1997**, *62*, 530.
- (17) McCord, P.; Bard, A. J. *J. Electroanal. Chem.* **1991**, *318*, 91.
- (18) Kolthoff, I. M.; Bruckenstein, S.; Chantooni, M. K. *J. Am. Chem. Soc.* **1961**, *83*, 3927.
- (19) Halliday, C. S.; Matthews, D. B. *Aust. J. Chem.* **1983**, *36*, 507.
- (20) Bauldrey, J. M.; Archer, M. D. *Electrochim. Acta* **1983**, *28*, 1515.
- (21) Creager, S. E.; Marks, G. T.; Aikens, D. A.; Richtol, H. H. *J. Electroanal. Chem.* **1983**, *152*, 197.
- (22) Witt, E. *Ber. Dtsch. Chem. Ges.* **1878**, *12*, 931.
- (23) Denuault, G.; Mirkin, M. V.; Bard, A. J. *J. Electroanal. Chem.* **1991**, *308*, 27.
- (24) Wightman, R. M.; Wipf, D. O. In *Electroanalytical Chemistry*; Bard, A. J., Ed.; Marcel Dekker: New York, 1988, Vol. 15. p. 267.
- (25) Bard, A. J.; Fan, F. -R.; Kwak, J.; Lev, O. *Anal. Chem.* **1989**, *61*, 132.
- (26) Oldham, K. B. *J. Electroanal. Chem.* **1981**, *122*, 1.
- (27) Oldham, K. B.; Zoski, C. G. *J. Electroanal. Chem.* **1988**, *256*, 11.
- (28) Sawyer, D. T.; Komai, R. Y. *Anal. Chem.* **1972**, *44*, 715.
- (29) Bard, A. J.; Faulkner, L. R. In *Electrochemical Methods*, 2nd Ed., John Wiley & Sons: New York, 2001, Chapter 12, p 476.
- (30) Chandross, E. A.; Sonntag, F. I. *J. Am. Chem. Soc.* **1966**, *88*, 1089.
- (31) Akins, D. L.; Birke, R. L. *Chem. Phys. Lett.* **1974**, *29*, 428.

- (32) Faulkner, L. R.; Bard, A. J. In *Electroanalytical Chemistry*; Bard, A. J., Ed; Marcel Dekker: New York, 1977; Vol. 10, p 1.
- (33) Singh, M. K.; Pal, H.; Bhasikuttan, A. C.; Sapre, A. V. *Photochem. Photobiol.* **1998**, *68*, 32.
- (34) Oishi, S.; Tajime, K.; Shiojima, I. *J. Mol. Catal.* **1982**, *14*, 383.
- (35) Urano, T.; Kitamura, A.; Sakuragi, H.; Tokumaru, K. *J. Photochem.* **1984**, *26*, 69.
- (36) Wilkinson, F. In *Fluorescence: Theory, Instrumentation, and Practice*; Guilbault, G. G., Ed; Marcel Dekker: New York, 1967; Chapter 1.
- (37) Kalyanasundaram, K. *Coor. Chem. Rev.* **1982**, *46*, 159.
- (38) Calculated by eq. (4.14) with  $E^\circ(\text{C}_6\text{H}_5\text{CO}_2^\bullet/\text{C}_6\text{H}_5\text{CO}_2^-) = +0.8\text{ V}$  from ref. (30) and  $E^\circ(\text{Ru}(\text{bpy})_3^{2+/+}) = -1.5\text{ V}$  from ref. (10)
- (39) Tokel-Takvoryan, N. E.; Hemingway, R. E.; Bard, A. J. *J. Am. Chem. Soc.* **1973**, *95*, 6582.
- (40) Wallace, W. L.; Bard, A. J. *J. Phys. Chem.* **1979**, *83*, 1350.
- (41) Itoh, K.; Honda, K. *Chem. Lett.* **1979**, 99.
- (42) Luttmer, J. D.; Bard, A. J. *J. Phys. Chem.* **1981**, *85*, 1155.

## Chapter 5: Electrogenerated Chemiluminescence of Ter(9,9-diarylfluorene)s: Excited Singlet State Emission vs. Excimer Emission

### 5.1 Introduction

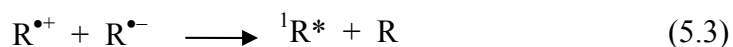
Fluorene-based macromolecules, such as terfluorenes<sup>1-3</sup>, oligomeric fluorenes<sup>3-5</sup>, and polyfluorenes<sup>6-9</sup>, are of interest in organic light-emitting devices (OLED) because of their efficient blue light emitting characteristics and good chemical and thermal stabilities. Among these, the ter(9,9-diarylfluorene)s show good optical and electrochemical properties<sup>1</sup>, such as high fluorescence quantum yields in solution (99 %) as well as in thin films (~90 %) of interest in OLEDs. They also have good carrier transport properties and show high mobility of both electrons and holes in amorphous films.<sup>10</sup> These ter(9,9-diarylfluorene)s are therefore good candidates for blue-light emitters in electrogenerated chemiluminescence (ECL).

ECL is light emission produced by an energetic electron transfer reaction between electrochemically generated species at an electrode. There are two general methods for producing ECL:

(1) *An ion annihilation reaction that involves the generation of radical cations and radical anions on the electrode by alternating or sweeping potentials.*

The two oppositely charged species can undergo an electron transfer (ET) reaction (ion annihilation) in the diffusion layer of the electrode to produce the excited singlet or triplet state depending on the energy of the reaction. If the magnitude of the enthalpy ( $\Delta H_{\text{ann}}$ ) of an ion annihilation reaction is larger than the energy ( $E_s$ ) needed for the excited singlet state, the direct generation of excited singlet state is possible as shown in Scheme 5.1; this is called the S-route or an energy-sufficient system<sup>11</sup>.

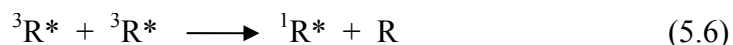
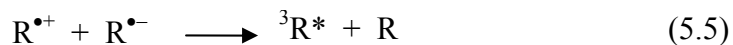
#### Scheme 5.1



where R is an emitter.

If  $-\Delta H_{\text{ann}}$  of ion annihilation reaction is lower than  $E_s$  of excited singlet state but higher than the triplet state energy ( $E_t$ ), the generation of an excited singlet state is still possible by triplet-triplet annihilation reaction as shown in Scheme 5.2 (a T-route or energy-deficient system).<sup>11</sup>

### Scheme 5.2



where R is an emitter.

(2) *Use of a coreactant (a compound that can produce a strong reducing or oxidizing agent by a reaction that follows the electrochemical ET reaction).*

These agents must be energetic enough to reduce or oxidize radical ions of emitters to their excited states. Typical coreactants for oxidations are tri-*n*-propylamine (TPrA), which produces a strong reducing agent (TPrA free radical, TPrA $\bullet$ )<sup>12-15</sup> and a relatively strong oxidizing agent (TPrA radical cation, TPrA $\bullet+$ )<sup>16</sup> and oxalate ion (C<sub>2</sub>O<sub>4</sub><sup>2-</sup>), which produces a strong reducing agent (CO<sub>2</sub> $\bullet-$ ).<sup>17-19</sup> Peroxydisulfate (S<sub>2</sub>O<sub>8</sub><sup>2-</sup>) produces a strong oxidizing agent (SO<sub>4</sub> $\bullet-$ )<sup>20-22</sup> upon reduction. The general ECL mechanism for a coreactant reduction is shown in Scheme 5.3.

### Scheme 5.3



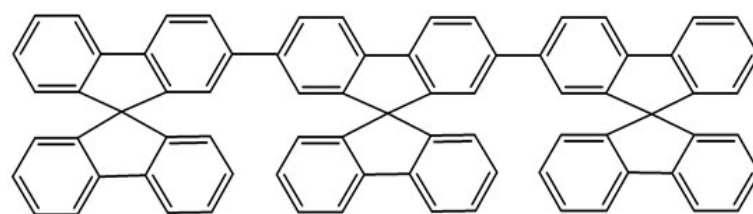
where R is an emitter, CR is a coreactant, X is a reactive oxidizing agent produced from CR radical anion, and X' is a reaction product of X.

For ion annihilation ECL, both the radical cations and radical anions should be relatively stable, but for coreactant ECL only one of the emitter radical ions needs to be stable.

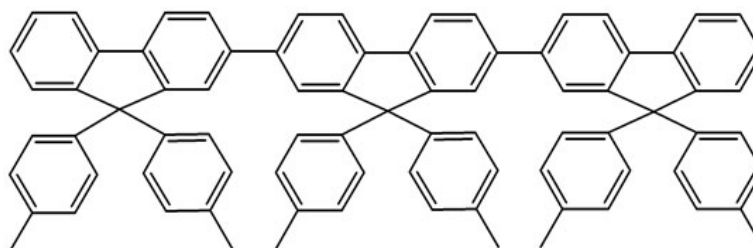
In this chapter, the photophysical properties, electrochemistry, and ECL of two different ter(9,9-diarylfluorene)s, TDAF-1 and TDAF-2 shown in Figure 5.1 are discussed. Moreover, ECL by both ion annihilation and coreactant ECL processes are described. Evidence for excimer emission of TDAF-1 and TDAF-2 is also demonstrated by comparing the ECL spectra obtained by both approaches and, in addition, to their fluorescence spectra.

## 5.2 Experimental Section

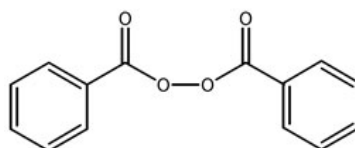
**Chemicals.** The synthesis of TDAF-1 and TDAF-2 has been described.<sup>1</sup> Anhydrous acetonitrile (MeCN, 99.93% in a sure-sealed bottle), anhydrous



TDAF-1



TDAF-2



BPO

**Figure 5.1.** Molecular structures of TDAF-1, TDAF-2 and BPO.

benzene (Bz, 99.9% in a sure-sealed bottle), tetra-*n*-butylammonium perchlorate (TBAP), and benzoyl peroxide (BPO) were obtained from Aldrich (St. Louis, MO) and used as received. TBAP and BPO were dried at 30 °C in a vacuum oven before transferred to an inert atmosphere drybox (Vacuum Atmospheres Co., Hawthorne, CA).

**Apparatus and Instrumentation.** UV-Vis absorption and photoluminescence spectra were taken with a Milton Roy Spectronic 3000 array spectrophotometer and a Fluorolog-3 spectrofluorimeter (ISA-Jobin Yvon Hariba, Edison, NJ) using an 1 cm path-length quartz cuvette, respectively. The phosphorescence spectrum was measured by an ultrasensitive detection system coupled with a laser excitation source. Briefly, an Nd:YAG (355 nm, 8 ns, Continuum Surelite II) pumped optical parametric oscillator coupled with a second harmonic device serves as a tunable excitation source. The resulting emission was detected by an intensified charge coupled device camera (ICCD, Princeton Instrument, Model 576G/1). The delay between pump laser and high voltage pulse amplifier (Princeton Instrument, PG 200) used to gate ICCD was controlled by a programmable delay pulse generator (SRS Model DG-535). The sample for the phosphorescence study was prepared in methylcyclohexane that forms a clear glass at 77 K, and was degassed via three freeze-pump-thaw cycles prior to the measurement.

Cyclic voltammograms were measured with a CH Instruments Electrochemical Work Station (Austin, TX) using a three-electrode conventional electrochemical cell. Platinum disk (area, 0.12 cm<sup>2</sup>) and Pt wire served as the working and auxiliary electrodes, respectively. A silver (Ag) wire was used as a quasi-reference electrode and all potentials were calibrated by adding ferrocene (Fc) as an internal reference and quoting all potentials vs. SCE by taking Fc<sup>+</sup>/Fc as 0.424 V. vs. SCE.<sup>23</sup>

All ECL measurements were performed as previously reported.<sup>24</sup> The ECL spectra were taken using a charge-coupled device (CCD) camera (Photometrics CH 260, Photometrics-Roper Scientific, Tucson, AZ). The CCD camera was aligned with the outlet of a grating spectrometer (concave grating, 1 mm entrance slit) calibrated with a mercury lamp emission. ECL spectra were obtained with 0.1 s potential pulses and at least 5 min of integration time.

**Calculations.** The optimized radical structures of TDAF-1 and TDAF-2 were obtained using the Spartan® software package.

### 5.3 Results and Discussion

**Absorbance, Fluorescence, and Phosphorescence.** Absorption, fluorescence, and phosphorescence spectra of TDAF-1 and TDAF-2 are shown in Figure 5.2. The absorption and fluorescence spectra were obtained in the same solvent system, a 1:1 volume mixture of MeCN and Bz, which was also used for

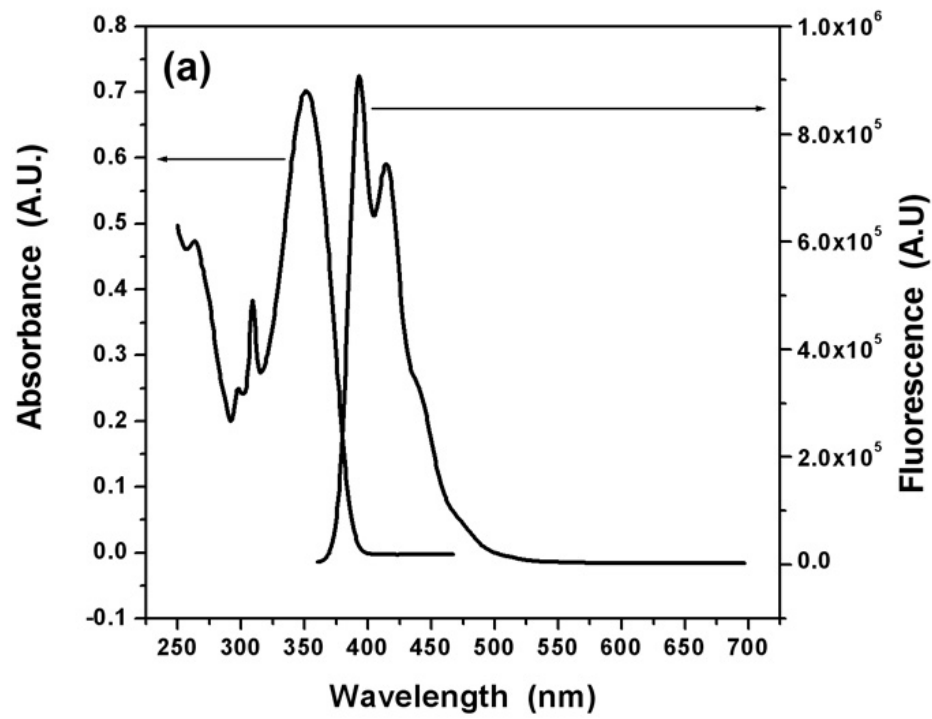


Figure 5.2. Continued on the next page.

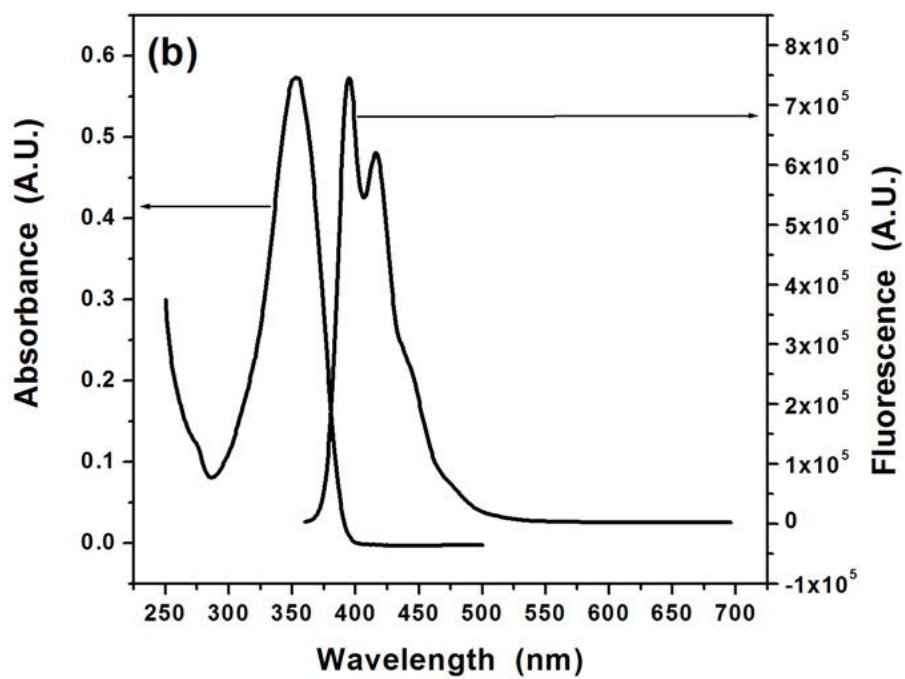
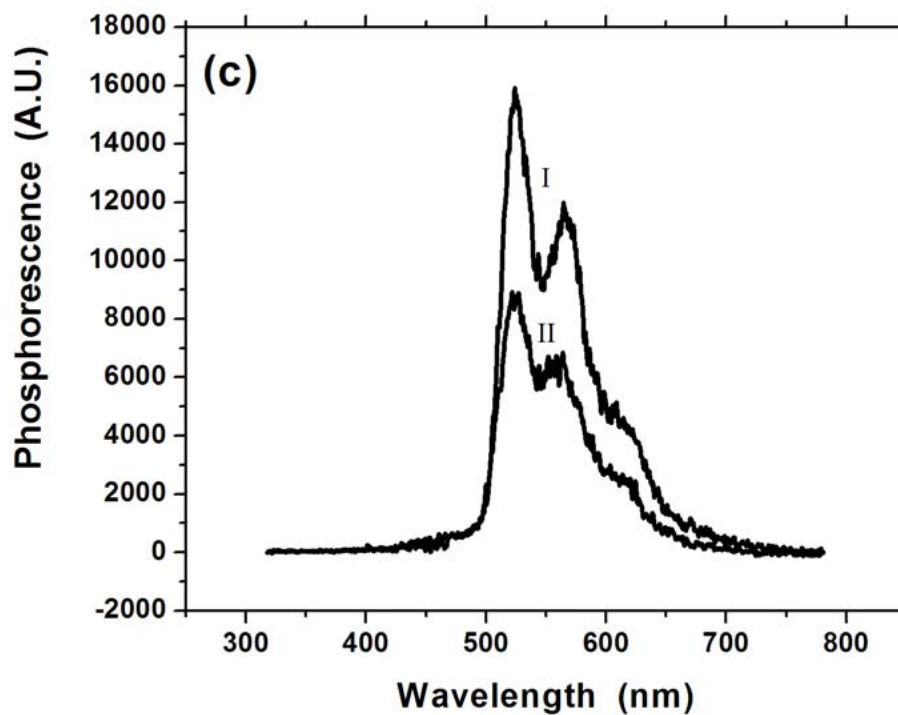


Figure 5.2. (Cont.) Continued on the next page.



**Figure 5.2. (Cont.)** Absorption and fluorescence ( $\lambda_{\text{ex}} = 350$  nm) spectra of (a) TDAF-1 and (b) TDAF-2 in MeCN:Bz (1:1,v:v) at room temperature under atmospheric conditions. Absorbance: 10  $\mu\text{M}$  of TDAF; fluorescence: 1  $\mu\text{M}$  of TDAF. (c) Phosphorescence ( $\lambda_{\text{ex}} = 355$  nm) spectra of 10.1  $\mu\text{M}$  TDAF-1 (I) and 9.8  $\mu\text{M}$  TDAF-2 (II) obtained at 77 K in deoxygenated methylcyclohexane. The spectra were taken at a delay time of 5 ms.

all electrochemical and ECL measurements. TDAF-1 and TDAF-2 gave absorption maxima at 351 and 353 nm, respectively, with the onset of these bands at around 398 nm [Figure 5.2, (a) and (b)]. Unlike TDAF-2, the absorption spectrum of TDAF-1 shows three additional absorption peaks at 263, 298, and 309 nm besides the most intense absorption band at 351 nm. A comparison of the two absorbance spectra taken in 10  $\mu$ M and 0.25 mM indicated that no aggregation of the ground states occurred at the higher concentration. There were no wavelength shifts found for TDAF-1 and TDAF-2 up to 0.25 mM. (See Supporting Information Figure 5.1) The fluorescence of the TDAFs, taken with excitation at the absorption maxima, displayed almost identical emission spectra with two well-resolved vibronic peaks and one shoulder (Figure 5.2, (a) and (b)). No other luminescence above 520 nm was found. Phosphorescence spectra (Figure 5.2, (c)) were obtained in a 77 K glassy methylcyclohexane medium with excitation at 355 nm. Phosphorescence maxima were observed at 525 nm for both TDAF-1 and TDAF-2 and the shape of phosphorescence peak was very similar to that of the fluorescence. No phosphorescence could be observed at room temperature. All spectroscopic data are summarized in Table 5.1.

**Electrochemistry.** All electrochemical measurements were carried out in 1:1 volume mixture of MeCN and Bz with 0.1 M TBAP as supporting electrolyte with a Pt disk electrode. TDAF-1 and TDAF-2 show low solubility in pure MeCN. Although have good solubility in  $\text{CH}_2\text{Cl}_2$  and tetrahydrofuran (THF),<sup>1</sup>

**Table 5.1. Summary of Spectroscopic Data.**

	<b>Absorbance (nm)</b>	<b>Fluorescence (nm)</b>	<b>Phosphorescence (nm)</b>
TDAF-1	263(p), 298(p), 309(p), 351(p)	393(p), 414(p), 440 (s)	525(p), 570(p), 620(s)
TDAF-2	353(p)	395(p), 416(p), 442(s)	525(p), 567(p), 620(s)

(p) represents peak and (s) represents shoulder.

these solvents are not appropriate for ECL because they have narrow potential windows. Cyclic voltammograms (CV) of TDAF-1 and TDAF-2 are shown in Figure 5.3. When the potential was anodically swept at 0.1 V/s, two oxidation peaks were observed at 1.54 V and 1.71 V (TDAF-1) and at 1.57 V and 1.71 V vs. SCE (TDAF-2). For a cathodic sweep two reduction peaks were observed at -1.96 V and -2.09 V (TDAF-1) and at -1.90 V and -2.07 V vs. SCE (TDAF-2). Although the cathodic reduction waves of TDAF-1 were not well-resolved, a differential pulse voltammogram (DPV, inset of Figure 5.3 (a)) showed that TDAF-1 had two cathodic reductions like TDAF-2. These electrochemical results are in good agreement with previous results in  $\text{CH}_2\text{Cl}_2$  (oxidation) and THF (reduction).<sup>1</sup>

The oxidations and reductions of the TDAFs are essentially nernstian one-electron steps as judged from the peak potential separation ( $\Delta E_p$ ) compared to that of ferrocene (Fc) as an internal reference. Because of the ohmic drop caused by our solvent,  $\Delta E_p$  is larger than the theoretical value of 59 mV. Under the same conditions,  $\Delta E_p$  of Fc, which undergoes a nernstian reaction in this solvent, was 100 mV and this was about the same as the  $\Delta E_p$  values of the TDAFs. The small potential separation between the first and the second reductions prevented a precise measurement of the current ratio even at a slow scan rates (e.g. 20 mV/s). All half-wave potentials ( $E_{1/2}$ ) of oxidations and reductions are summarized in Table 5.2.

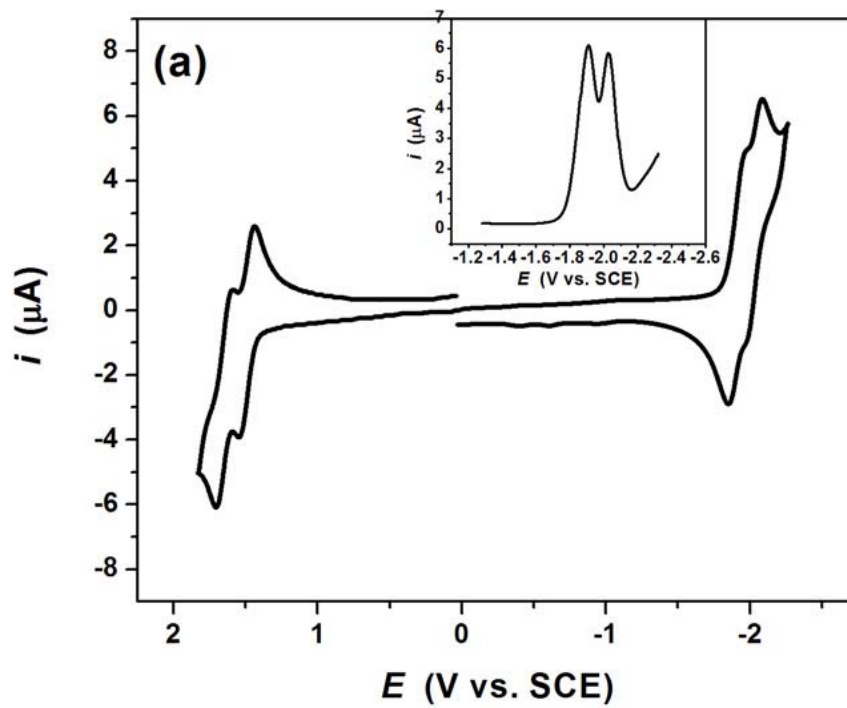


**Figure 5.3.** *Continued on the next page.*

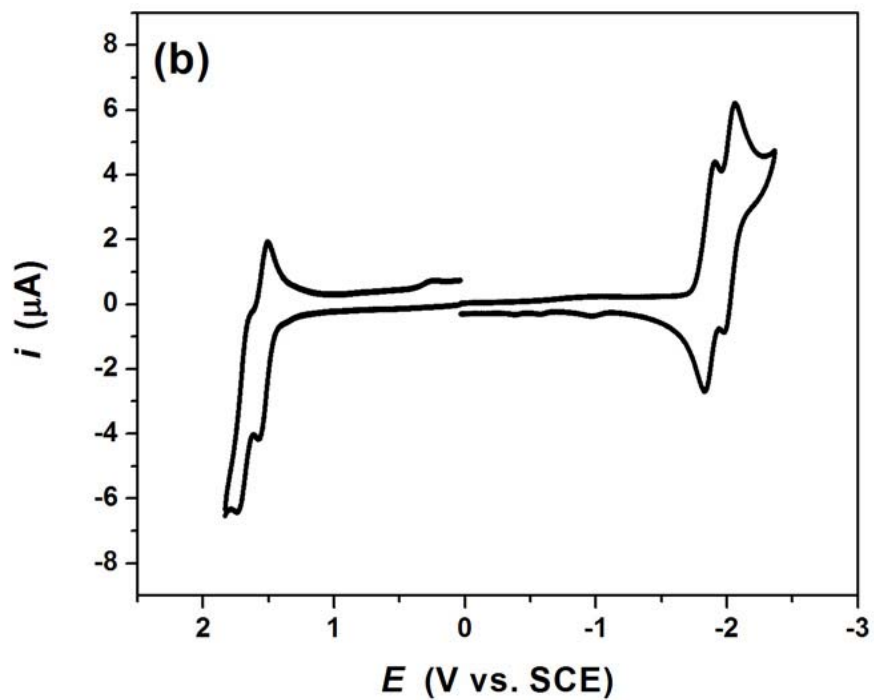


**Figure 5.3. (Cont.)** Cyclic voltammograms of (a) 0.5 mM TDAF-1 and (b) 0.5 mM TDAF-2 in MeCN:Bz (1:1,v:v)/0.1 M TBAP at 0.1 V/s. Inset: differential pulse voltammogram (DPV) with increment potential, 4 mV, amplitude, 0.05 V, pulse width, 0.05 s.

**Table 5.2. Summary of Electrochemical Data.**

	Oxidation		Reduction	
	$E_{1/2}^{2nd}$ (V <sup>a</sup> )	$E_{1/2}^{1st}$ (V <sup>a</sup> )	$E_{1/2}^{1st}$ (V <sup>a</sup> )	$E_{1/2}^{2nd}$ (V <sup>a</sup> )
TDAF-1	+ 1.66	+ 1.49	- 1.91	- 2.02
TDAF-2	+ 1.70	+ 1.54	- 1.87	- 2.03

*a.* V vs. SCE. Scan Rate = 0.1 V/s. In MeCN: Bz (1:1, v:v) containing 0.1 M TBAP

### **Electrogenerated Chemiluminescence (ECL)- Ion annihilation.**

Because the electrochemical results show that the electrogenerated radical ions of both TDAFs are stable, ECL was initially performed by ion annihilation. The energy available in this ion annihilation reaction is given by :<sup>11</sup>

$$-\Delta H_{\text{ann}} \cong E_p(\text{TDAF/TDAF}^{\bullet+}) - E_p(\text{TDAF/TDAF}^{\bullet-}) - 0.1 \quad (5.10)$$

For S-route ion annihilation,  $-\Delta H_{\text{ann}}$  must be larger than the lowest excited singlet energy ( $E_s$ ), as calculated from the fluorescence emission peak; data for the TDAFs, summarized in Table 5.3 suggest that ECL via the S-route is possible.

ECL was obtained by continuously pulsing (pulse width = 0.1 s) the potential of a Pt working electrode between + 1.58 V and – 1.95 V vs. Ag QRE for TDAF-1 or +1.54 V and – 1.97 V vs. Ag QRE for TDAF-2. The ECL of the TDAFs [Figure 5.4], unlike their fluorescence (which showed no emission beyond 500 nm) produced the most intense emissions at much longer wavelengths. The emission bands were quite broad and centered at 522 nm for TDAF-1 and 583 nm for TDAF-2. The band width at a half emission intensity was about 300 nm. Less intense ECL emissions corresponding to the fluorescence, at 406 nm for TDAF-1 and 410 nm for TDAF-2 were also present. The lack of resolution in the ECL spectra at the shorter wavelengths compared to the fluorescence can be ascribed to the wide entrance slit (1 mm) of a grating spectrometer used for ECL because of

**Table 5.3. Physical Data of Ion Annihilation Reaction and Coreactant Reaction for ECL.**

	$E_{p,a}$ (V) <sup>a</sup>	$E_{p,c}$ (V) <sup>b</sup>	$-\Delta G$ (eV) <sup>c</sup>	$-\Delta H$ (eV) <sup>d</sup>	$E_s$ (eV) <sup>e</sup>	$E_t$ (eV) <sup>e</sup>	$\Delta E^*$ (eV) <sup>f</sup>
TDAF-1	+ 1.54	- 1.96	3.50	3.40	3.16	2.38	-
TDAF-1	+ 1.5 <sup>g</sup>	- 1.96	3.46	3.36	3.16	2.38	- 0.29
+ BPO	+ 0.8 <sup>h</sup>	- 1.96	2.76	2.66	3.16	2.38	
TDAF-2	+ 1.57	- 1.90	3.47	3.37	3.16	2.38	-
TDAF-2	+ 1.5 <sup>g</sup>	- 1.90	3.40	3.30	3.16	2.38	- 0.32
+ BPO	+ 0.8 <sup>h</sup>	- 1.90	2.70	2.60	3.16	2.38	

*a.* Anodic peak potential, V vs. SCE. In MeCN:Bz (1:1, v:v) containing 0.1 M TBAP. *b.* Cathodic peak potential of TDAFs, V vs. SCE. *c.*  $-\Delta G = E_{p,a} - E_{p,c}$ . *d.*  $-\Delta H_{ann}$  or  $-\Delta H_{co}$ .  $-\Delta H = -\Delta G - 0.1$ . *e.* Calculated from the spectroscopic data. *f.*  $\Delta E^* = E_t + E_p(\text{BPO/BPO}^-) - E_p(\text{TDAF/TDAF}^{\bullet+}) + 0.1$ . *g.*  $E^\circ$  of  $\text{C}_6\text{H}_5\text{CO}_2^\bullet$  from ref. 28. *h.*  $E^\circ$  of  $\text{C}_6\text{H}_5\text{CO}_2^\bullet$  from ref. 30.

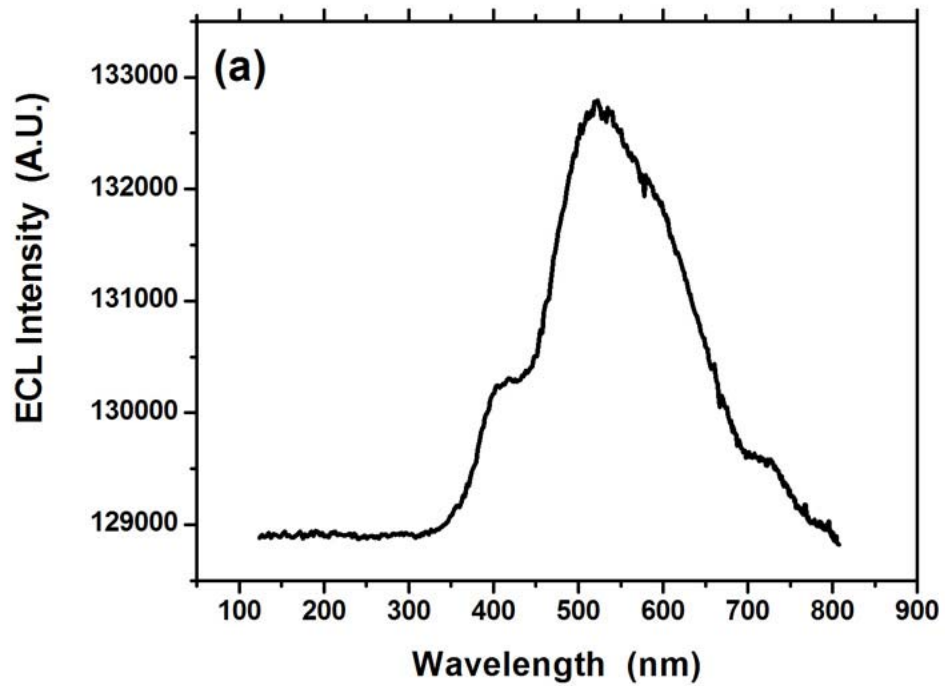
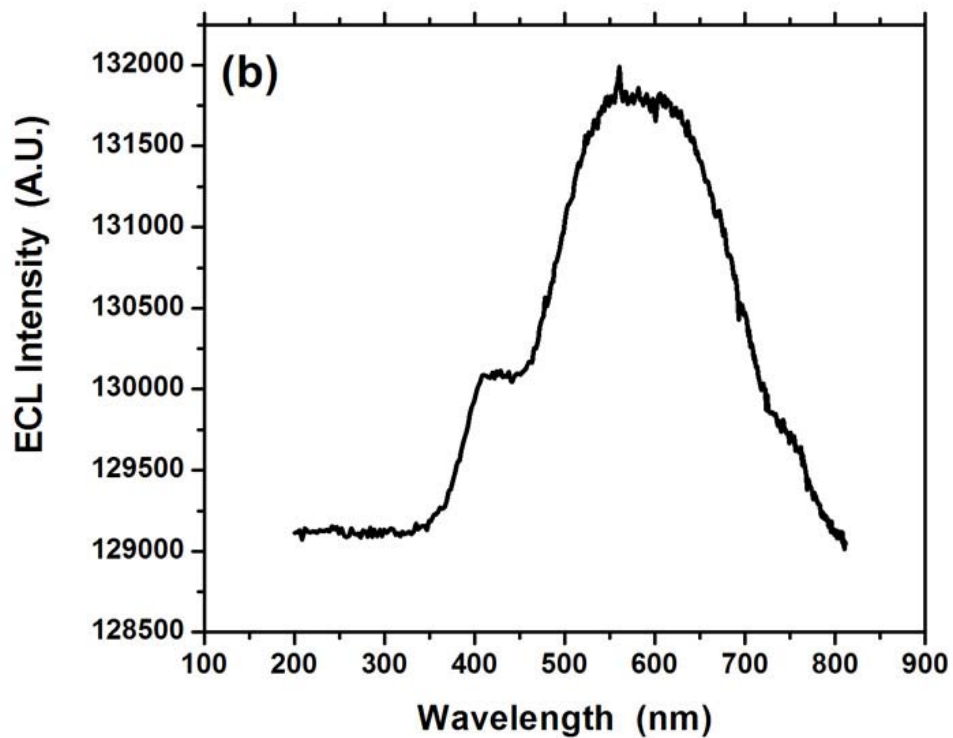


Figure 5.4. *Continued on the next page.*



**Figure 5.4. (Cont.)** ECL spectra of (a) 0.5 mM TDAF-1 and (b) 0.5 mM TDAF-2 in MeCN:Bz (1:1,v:v)/0.1 M TBAP. 0.1 s pulses by alternating between + 1.58 V and - 1.95 V vs. Ag QRE for (a) and + 1.54 V and - 1.97 V vs. Ag QRE for (b). All spectra were obtained with an integration time of 5 min.

the low ECL intensity. Thus the shorter wavelength ECL with a shoulder at ~400 nm can be ascribed to emission from the lowest singlet state (Figure 5.5 path a).

The unusually broad ECL emission of the TDAFs could come from by-products from side reactions of the radical ions, excimers, or triplet states. Immediately after the ECL experiments, the solution fluorescence spectra were measured again and found to be identical to those measured before ECL experiments, suggesting there were no side-reactions to produce bulk by-products fluorescing at longer wavelengths (although small amounts produced in the diffusion layer near the electrode that emit is still a possibility). (See Supporting Information Figure 5.2.)

The second possibility is the formation of an excimer. Generally, excimers generate structureless broad emission bands. Although the ECL spectra of the TDAFs were quite broad (~ 300 nm band-width), they were not structureless and appear to have shoulders at around 750 nm in addition to the broad bands (Figure 5.4). These shoulders, however, are artifacts caused by the second harmonic signals of the lowest excited singlet state emissions. If a long-wavelength pass (LP) filter of 425 nm was placed in front of the CCD camera and ECL by ion annihilation was measured, the spectra did not show these shoulders (See Supporting Information Figure 5.3). The formation of excimer is more favorable in this ECL than in photoluminescence, because ion annihilation involves the collision of oppositely charged radical ions. The proposed mechanism for excimer

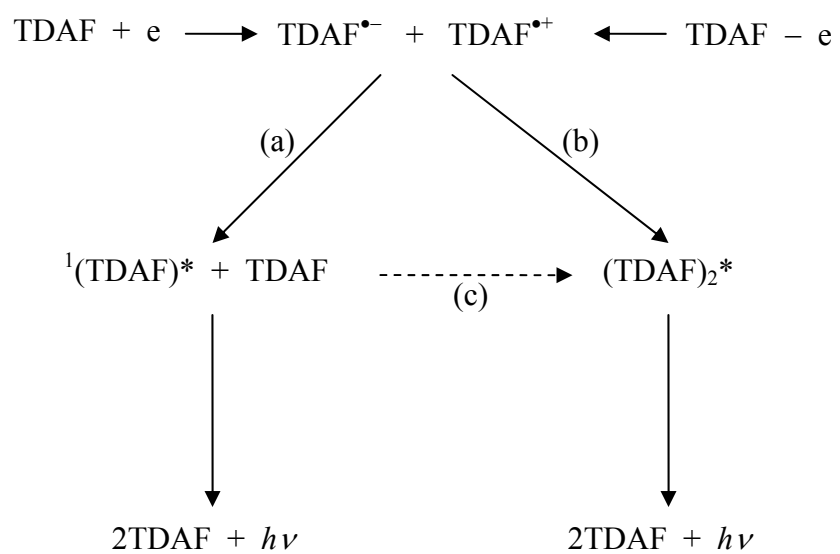


**Figure 5.5.** Schematic diagram of ECL and excimer formation mechanism.

formation in ECL is shown in Figure 5.5 path (b). Most excimers were formed through the path (b) route rather than by reaction of excited state and ground state (Figure 5.5 path (c)), because no excimer emission was found in the fluorescence spectra. Lack of excimer formation in fluorescence can be ascribed to the relatively short radiative lifetimes (840 ps, TDAF-1 and 790 ps, TDAF-2) compared with average fluorescence lifetime<sup>25</sup> of  $10^{-9}$  to  $10^{-8}$  s for a singlet excited state. Thus the rate of decay of  $^1(\text{TDAF})^*$  was probably so fast that excimer formation by path (c) would be negligible in both fluorescence and ECL. In addition, the bulky substituent groups (biphenyl for TDAF-1 and *p*-toluenyl for TDAF-2) would make path (c) much slower due to the steric hindrance. Similar results were reported for a polyfluorene.<sup>26</sup>

**Electrogenerated Chemiluminescence (ECL)- Coreactant.** To test for the importance of annihilation in the production of excimer, an ECL experiment was performed using the coreactant, benzoyl peroxide (BPO). When BPO is electrochemically reduced at  $-1.23$  V vs. SCE, the reaction proceeds through the ECE route<sup>27</sup> to produce the benzoate radical ( $\text{C}_6\text{H}_5\text{CO}_2^\bullet$ ) that is a strong oxidizing agent (Scheme 5.4). This follows an early study by Chandross and Sonntag<sup>28</sup> where BPO was reduced stepwise by hydrocarbon radical anions rather than at an electrode.

#### Scheme 5.4

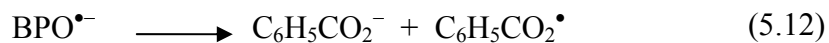


Figure 5.6 shows the ECL spectra (solid line) of the TDAFs in MeCN:Bz (1:1, v:v) / 0.1 M TBAP at a Pt electrode with 0.1s potential pulses from 0 V to – 1.96 V vs. Ag QRE for TDAF-1 or 0 V to – 1.98 V vs. Ag QRE for TDAF-2. Under these conditions only radical anions of TDAF-1 and TDAF-2 and  $\text{C}_6\text{H}_5\text{CO}_2^{\bullet}$  were produced. Unlike the ECL spectra by ion annihilation, these ECL spectra displayed only emission corresponding to the fluorescence emission (dotted line in Figure 5.6) with no evidence of excimer emission.

The energy available in the reaction between the radical anions and  $\text{C}_6\text{H}_5\text{CO}_2^{\bullet}$  can be calculated by eq. (5.10), using  $E^\circ(\text{C}_6\text{H}_5\text{CO}_2^{\bullet}/\text{C}_6\text{H}_5\text{CO}_2^-)$ . Two different  $E^\circ$  values for a  $\text{C}_6\text{H}_5\text{CO}_2^{\bullet}/\text{C}_6\text{H}_5\text{CO}_2^-$  couple have been reported: + 1.5 V vs. SCE<sup>28</sup> and + 0.8 V vs. SCE.<sup>29</sup> If we use the larger value, the energy of reaction (16) was 3.36 eV for TDAF-1 and 3.30 eV for TDAF-2, in both cases sufficient to form the lowest excited singlet state (3.16 eV) directly and the suggested mechanism is in Scheme 5.5.

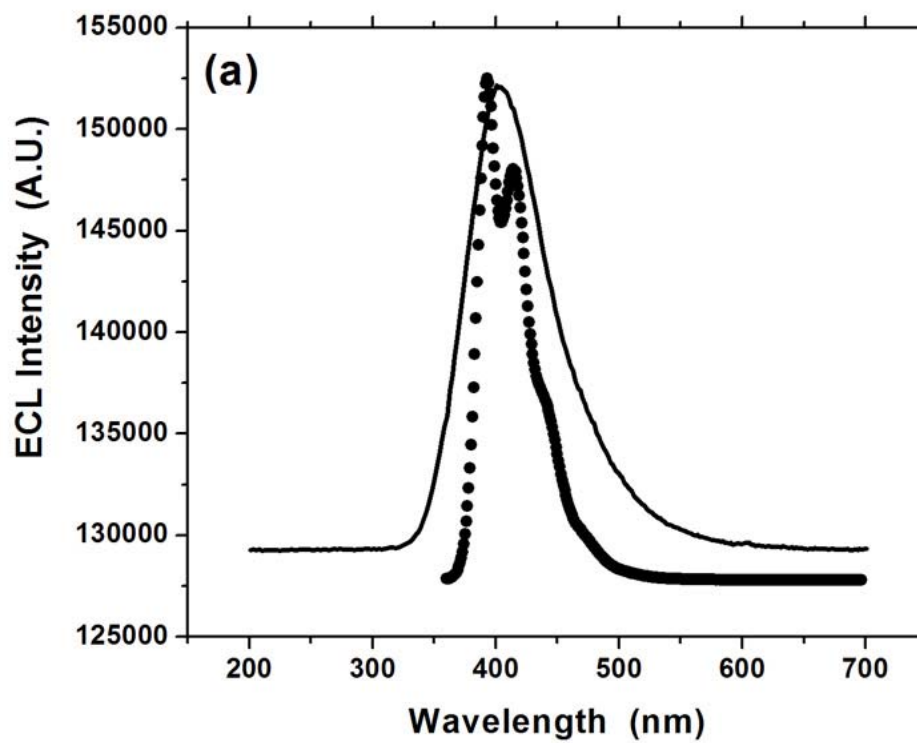
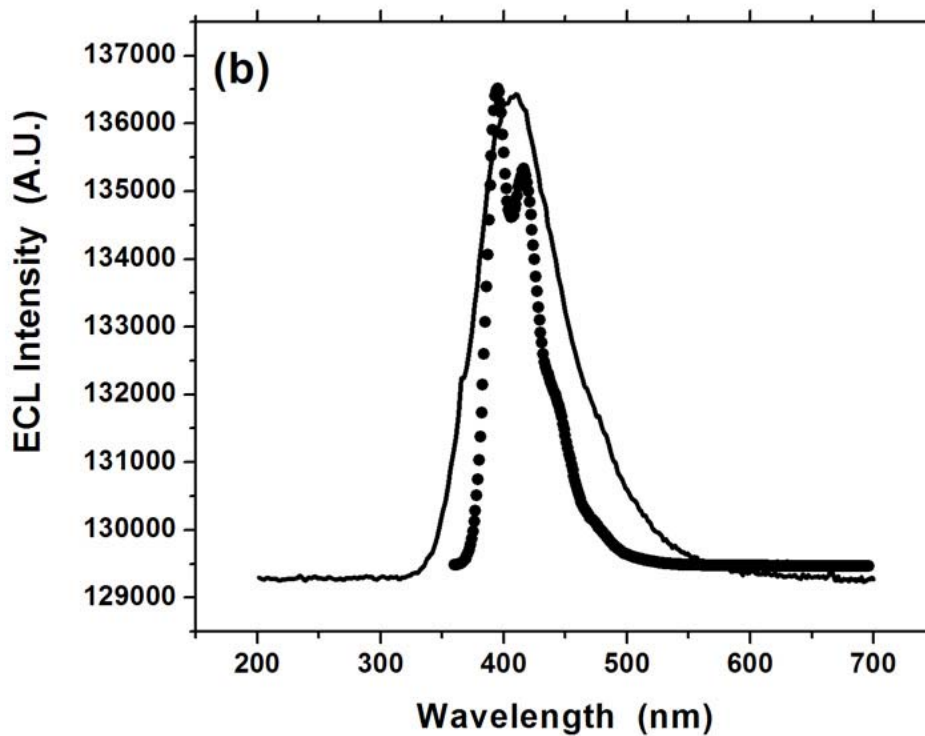
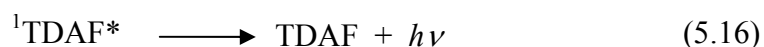


Figure 5.6. Continued on the next page.

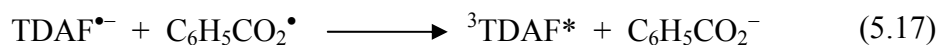


**Figure 5.6. (Cont.)** ECL (solid line) spectra of (a) 0.5 mM TDAF-1 and (b) 0.5 mM TDAF-2 with 5 mM BPO in MeCN:Bz (1:1,v:v)/ 0.1 M TBAP. 0.1 s pulses alternating 0 V and  $-1.96$  V vs. Ag QRE for (a) and  $+0$  V and  $-1.98$  V vs. Ag QRE for (b). All ECL spectra were obtained with an integration time of 5 min. Fluorescence spectra (dotted line) were obtained with (a)  $1 \mu\text{M}$  TDAF-1 and (b)  $1 \mu\text{M}$  TDAF-2 without BPO.  $\lambda_{\text{ex}} = 350$  nm for both (a) and (b).

**Scheme 5.5**



If + 0.8 V vs. SCE is used as  $E^\circ (\text{C}_6\text{H}_5\text{CO}_2^\bullet/\text{C}_6\text{H}_5\text{CO}_2^-)^{29}$ , the energy is 2.66 eV for TDAF-1 and 2.60 eV for TDAF-2. These energies are below that of the lowest singlet excited state (3.16 eV), so one cannot produce  ${}^1\text{TDAF}^*$  directly. However, both 2.66 and 2.60 eV are large enough to produce  ${}^3\text{TDAF}^*$  (2.38 eV) with  ${}^1\text{TDAF}^*$  generated by triplet-triplet annihilation:



Once the triplet state is formed, it is possible to produce  $\text{TDAF}^{\bullet+}$  by triplet state quenching, eq. (5.19), which could then lead to some excimer formation. To determine the energy change ( $\Delta E^*$ ) for eq. (5.19), the triplet state energy,  $E_t$ , of TDAF and the free energy of eq. (5.20) were used.



$$\Delta E^* = E_t + E_p(\text{BPO}/\text{BPO}^-) - E_p(\text{TDAF}/\text{TDAF}^{\bullet+}) + 0.1 \quad (5.21)$$

The  $E^\circ$  of BPO/BPO<sup>-</sup> couple is needed to calculate the enthalpy for reaction (5.20), but the electrochemical reduction of BPO occurs via ECE reaction and is irreversible as described previously. The irreversible peak potential (-1.23 V vs. SCE) of BPO/BPO<sup>-</sup> is less negative than  $E^\circ_{\text{BPO}/\text{BPO}^-}$ , so it would represent a lower limit for the energy of (5.20).<sup>30</sup>  $\Delta E^*$  values calculated in this way are summarized in Table 5.3; these suggest that reaction (5.19) is non-spontaneous. However this estimate is compromised by the use of the experimental irreversible  $E_p$ -value. The radical C<sub>6</sub>H<sub>5</sub>CO<sub>2</sub><sup>•</sup> could oxidize TDAF to TDAF<sup>•+</sup> and lead to the formation of excimers, but this reaction is energetically marginal, because for C<sub>6</sub>H<sub>5</sub>CO<sub>2</sub><sup>•</sup>/C<sub>6</sub>H<sub>5</sub>CO<sub>2</sub><sup>-</sup>,  $E^\circ = +1.5$  V (maximum) and for TDAF<sup>•+</sup>/TDAF,  $E^\circ = +1.54$  V (at least). Therefore, the absence of TDAF<sup>•+</sup> and excimers in ECL by BPO is understandable.

**Modeling the excimer.** The presence of bulky substituent groups in a molecule can prevent formation of excimers<sup>31</sup> and high dielectric constant solvents, such as MeCN and DMSO, typically show less excimer emission than

low dielectric solvents like THF.<sup>32</sup> However formation of excimers in ECL by ion annihilation can be a very efficient process, because the excited state is formed by two reactants in close proximity, just as with exciplexes studied by ECL.<sup>32</sup> The rate of exciplex formation is governed by the overlap of  $\pi$  orbitals in the molecules and coulombic interactions between oppositely charged species.<sup>33</sup> Therefore, formation of TDAF excimers can be very efficient in ion annihilation, even if the TDAFs have bulky substituents and a high dielectric solvent is used.

To model the proposed excimer, geometric optimization calculations were performed for [TDAF-1]<sup>•+</sup> and [TDAF-1]<sup>•-</sup> using molecular dynamics and then an excimer model was manually constructed by manipulating the orientation of the two radical ions and placing them in close proximity. Figure 5.7 shows a possible ionic dimer before the excimer is produced by ion annihilation. Here, the fluorene backbones totally overlap to allow a  $\pi$ - $\pi$  orbital stacking as well of the biphenyl groups, and this dimer can be stabilized by coulombic interaction between [TDAF-1]<sup>•+</sup> and [TDAF-1]<sup>•-</sup>. Although there is some steric hindrance between the biphenyl groups, some rearrangement could occur to minimize it.

**Triplet ECL Emission.** It is unlikely that the long wavelength ECL emission is triplet state emission, which is generally very weak at room temperature because of its long radiative lifetime ( $> 1.0$  s) and quenching by molecular oxygen and other species. Rothe and Monkman<sup>34</sup> investigated the

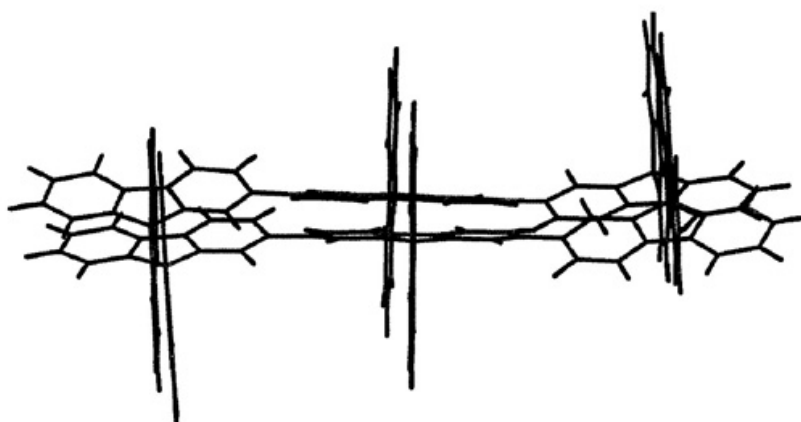


**Figure 5.7.** Model of a dimer of TDAF-1 from radical ions.

temperature dependence of phosphorescence of poly(9,9-di(ethylhexyl)fluorene), which was similar to TDAF, and did not observe phosphorescence above 80 K. No phosphorescent emission of the TDAFs was found above 77 K in our experiments. Moreover, if the long wavelength ECL emission were from the triplet state, it should appear in the ECL spectra with a coreactant as well as by ion annihilation.

**ECL Efficiency.** The relative ECL efficiency ( $\phi_{ECL}$ ) was calculated from eq. (5.23)<sup>35</sup> using a  $\phi_{ECL}^{\circ}$  ( $\sim 5\%$ )<sup>36</sup> for  $\text{Ru}(\text{bpy})_3^{2+}$  as a reference,

$$\phi_{ECL} = (\phi_{ECL}^{\circ} \cdot I_{ECL} \cdot Q_{a,c}^{\circ}) / (I_{ECL}^{\circ} \cdot Q_{a,c}) \quad (5.23)$$

where  $I_{ECL}$  is the integrated ECL intensity and  $Q_{a,c}$  is the total anodic or cathodic charge. The estimated  $\phi_{ECL}$  was 0.05 % for TDAF-1 and 0.01 % for TDAF-2 by ion annihilation ECL. However, it was not possible to calculate  $\phi_{ECL}$  in coreactant ECL, because the total charge did not represent the number of reactions between  $\text{TDAF}^{\bullet-}$  and  $\text{C}_6\text{H}_5\text{CO}_2^{\bullet}$ . Therefore, ECL of  $\text{Ru}(\text{bpy})_3^{2+}$  with BPO was employed as a reference, although this ECL system has not been previously reported. The generation of  $\text{Ru}(\text{bpy})_3^{2+*}$  can be described by a similar mechanism as that in Scheme 5.5; the electrochemically generated  $\text{Ru}(\text{bpy})_3^{+}$  reacts with  $\text{C}_6\text{H}_5\text{CO}_2^{\bullet}$  to produce  $\text{Ru}(\text{bpy})_3^{2+*}$ . Since  $\text{C}_6\text{H}_5\text{CO}_2^{\bullet}$  ( $E^{\circ} = + 1.5$  V vs. SCE) is sufficiently

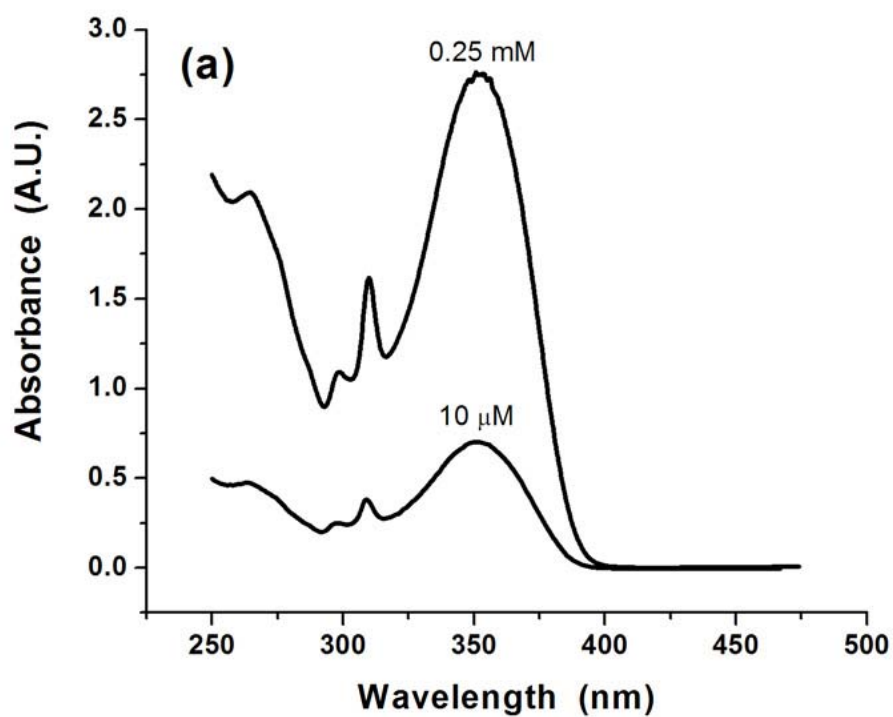
energetic,  $\text{Ru}(\text{bpy})_3^{2+}$  could also be oxidized to  $\text{Ru}(\text{bpy})_3^{3+}$  ( $E^\circ$  of  $\text{Ru}(\text{bpy})_3^{2+/3+} = + 1.25 \text{ V vs. SCE}^{37}$ ) As a result,  $\text{Ru}(\text{bpy})_3^{2+*}$  could also be produced by the annihilation reaction of  $\text{Ru}(\text{bpy})_3^{3+}$  and  $\text{Ru}(\text{bpy})_3^+$ . The integrated ECL intensity ratio of TDAF to  $\text{Ru}(\text{bpy})_3^{2+}$  under the exactly same experimental conditions (0.5 mM TDAF or  $\text{Ru}(\text{bpy})_3^{2+}/5 \text{ mM BPO}$ ) was expressed instead of  $\phi_{\text{ECL}}$ . The estimated percentage of  $I(\text{TDAF})/I(\text{Ru}(\text{bpy})_3^{2+})$  was 8 % for TDAF-1 and 3 % for TDAF-2. Because of the lack of excimer formation, ECL produced with BPO yielded a stronger and purer blue emission than ECL by ion annihilation.

#### 5.4 Conclusions

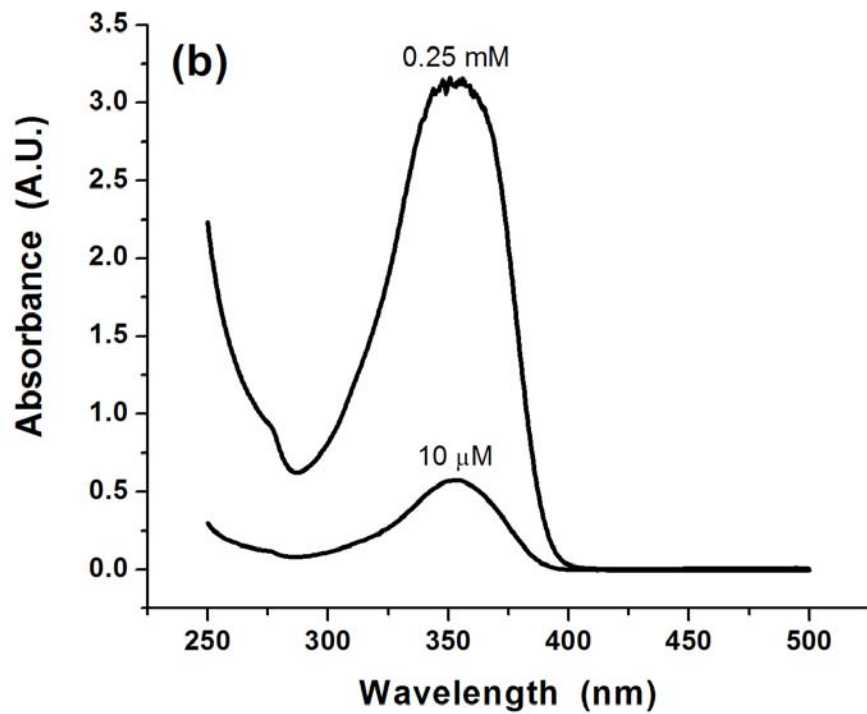
TDAF-1 and TDAF-2 are new blue ECL emitters. For both compounds, ECL by ion annihilation produced excimer emission, which was not seen in the fluorescence spectra. In this process, the formation of excimers was mainly from a reaction of oppositely charged radical ions [Figure 5.6, path (b)]. ECL produced by reduction in the presence of BPO coreactant only produced emission at the fluorescence (monomer) wavelengths, supporting the formation of excimer only by ion annihilation.

## Supporting Information

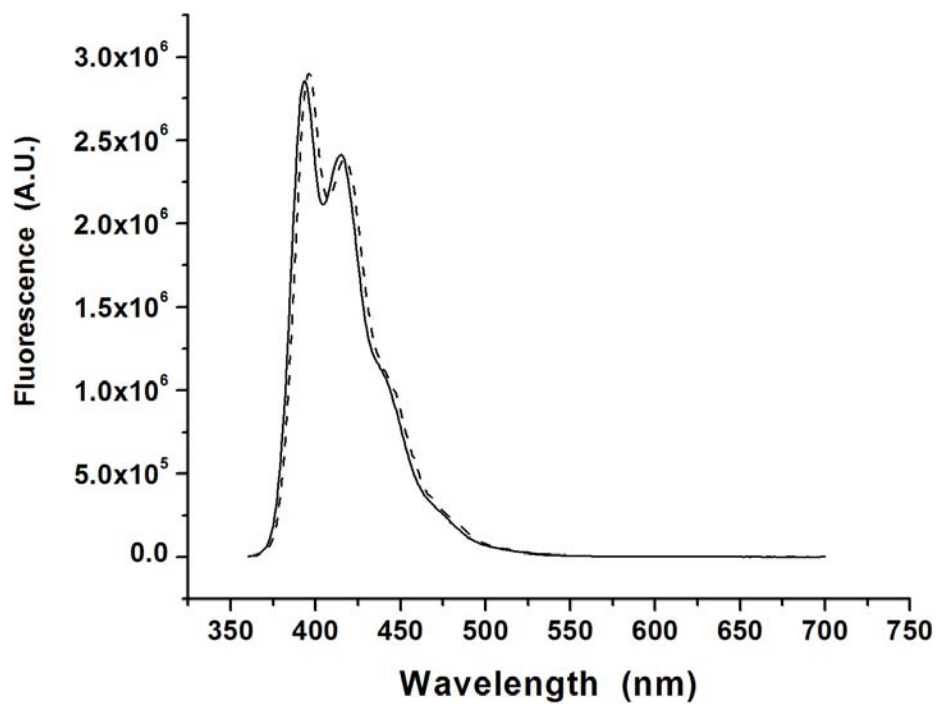
UV-Vis spectra of TDAF at low and high concentrations, fluorescence spectra measured before and after ECL experiments, and filtered and unfiltered ECL spectra are available in this section.



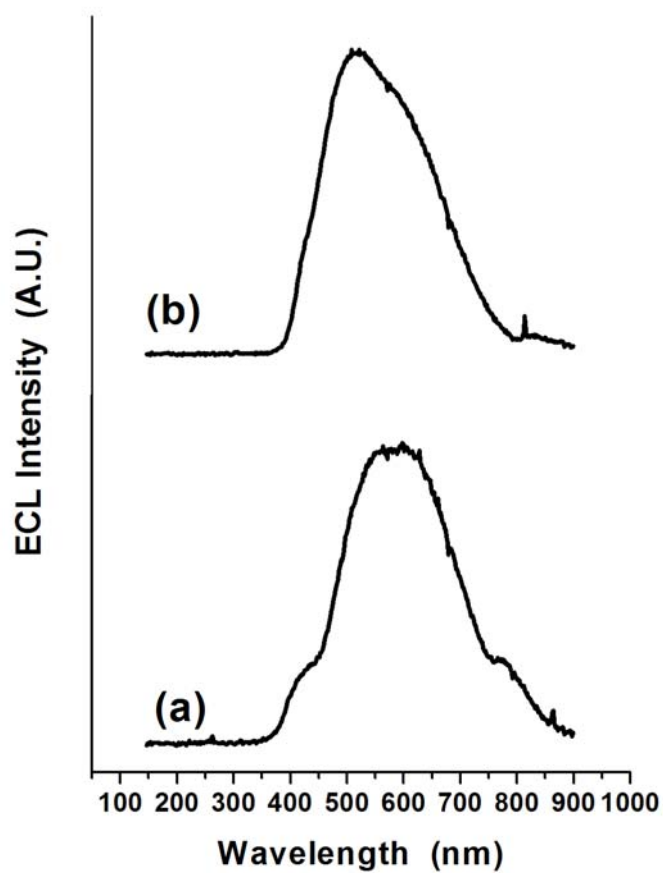
Supporting Information Figure 5.1. *Continued on the next page.*



**Supporting Information Figure 5.1. (Cont.)** UV-Vis Spectra of (a) 10  $\mu$ M and 0.25 mM of TDAF-1 and (b) 10  $\mu$ M and 0.25 mM TDAF-2. In MeCN:Bz (1:1, v:v). 1 cm path cuvette for 10  $\mu$ M and 2 mm path one for 0.25 mM.



**Supporting Information Figure 5.2.** Fluorescence spectra of TDAF-1 (solid line) and TDAF-2 (dashed line) measured after ECL experiments. All solutions were diluted to 10  $\mu$ M.



**Supporting Information Figure 5.3.** (a) Unfiltered and (b) filtered ECL spectra of 0.5 mM TDAF-4 generated by ion annihilation. Long-wavelength pass (LP) filter of 425 nm employed in front of CCD camera for (b).

## Reference

- (1) Wong, K. -T; Chien, Y. -Y; Chen, R. -T; Wang, C. -F; Lin, Y. -T; Chiang, H. -H; Hsieh, P. -Y; Wu, C. -C; Chou, C. H.; Su, Y. O.; Lee, G. -H.; Peng, S. -M. *J. Am. Chem. Soc.* **2002**, *124*, 11576.
- (2) Geng, Y.; Katsis, D.; Culligan, S. W.; Ou, J. J.; Chen, S. H.; Rothberg, L. J. *Chem. Mater.* **2002**, *14*, 463.
- (3) Katsis, D.; Geng, Y. H.; Ou, J. J.; Culligan, S. W.; Trajkovska, A.; Chen, S. H.; Rothberg, L. J. *Chem. Mater.* **2002**, *14*, 1332.
- (4) Belletête, M.; Morin, J. -F.; Beaupré, S.; Ranger, M.; Leclerc, M.; Durocher, G. *Macromolecules* **2001**, *34*, 2288.
- (5) Destri, S.; Pasini, M.; Botta, C.; Porzio, W.; Bertini, F.; Marchiò, L. *J. Mater. Chem.* **2002**, *12*, 924.
- (6) Chang, S. -C.; Yang, Y.; Pei, Q. *Appl. Phys. Lett.* **1999**, *74*, 2081.
- (7) Teetsov, J.; Fox, M. A. *J. Mater. Chem.* **1999**, *9*, 2117.
- (8) Chang, S. -C.; Li, Y.; Yang, Y. *J. Phys. Chem.* **2000**, *104*, 11650.
- (9) Lupton, J. M.; Craig, M. R.; Meijer, E. W. *Appl. Phys. Lett.* **2002**, *80*, 4489.
- (10) Wu, C. -C.; Liu, T. -L.; Hung, W. -Y.; Lin, Y. -T.; Wong, K. -T.; Chen, R. -T; Chen, Y. -M.; Chien, Y. -Y. *J. Am. Chem. Soc.* **2003**, *125*, 3710.
- (11) Faulkner, L. R.; Bard, A. J. In *Electroanalytical Chemistry*; Bard, A. J., Ed; Marcel Dekker: New York, 1977; Vol. 10, p 1-95.
- (12) Noffsinger, J. B.; Danielson, N. D. *Anal. Chem.* **1987**, *59*, 865.
- (13) Leland, J. K.; Powell, M. J. *J. Electrochem. Soc.* **1990**, *137*, 3127.
- (14) Zu, Y.; Bard, A. J. *Anal. Chem.* **2000**, *72*, 3223.
- (15) Kanoufi, F.; Zu, Y.; Bard, A. J. *J. Phys. Chem. B* **2001**, *105*, 210.
- (16) Miao, W.; Choi, J. -P.; Bard, A. J. *J. Am. Chem. Soc.* **2002**, *124*, 14478.
- (17) Chang, M. -M.; Saji, T.; Bard, A. J. *J. Am. Chem. Soc.* **1977**, *99*, 5399.
- (18) Rubinstein, I.; Bard, A. J. *J. Am. Chem. Soc.* **1981**, *103*, 512.

- (19) Kanoufi, F.; Bard, A. J. *J. Phys. Chem. B* **1999**, *103*, 10469.
- (20) White, H. S.; Bard, A. J. *J. Am. Chem. Soc.* **1982**, *104*, 6891.
- (21) Becker, W. G.; Seung, H. S.; Bard, A. J. *J. Electroanal. Chem.* **1984**, *167*, 127.
- (22) Fabrizio, E. F.; Prieto, I.; Bard, A. J. *J. Am. Chem. Soc.* **2000**, *122*, 4996.
- (23) Debad, J. D.; Morris, J. C.; Magnus, P.; Bard, A. J. *J. Org. Chem.* **1997**, *62*, 530.
- (24) McCord, P.; Bard, A. J. *J. Electroanal. Chem.* **1991**, *318*, 91.
- (25) Parker, C. A. In *Photoluminescence of Solutions*, Elsevier Publishing Co.: New York, 1968, Chapter 1, p. 38.
- (26) Prieto, I.; Teetsov, J.; Fox, M. A.; Vanden Bout, D. A.; Bard, A. J. *J. Phys. Chem. A* **2001**, *105*, 520.
- (27) Bard, A. J.; Faulkner, L. R. In *Electrochemical Methods*, 2nd Ed., John Wiley & Sons: New York, 2001, Chapter 12, p 476.
- (28) Chandross, E. A.; Sonntag, F. I. *J. Am. Chem. Soc.* **1966**, *88*, 1089.
- (29) Akins, D. L.; Birke, R. L. *Chem. Phys. Lett.* **1974**, *29*, 428.
- (30) Santa Cruz, T. D.; Akins, D. L.; Birke, R. L. *J. Am. Chem. Soc.* **1976**, *98*, 1677.
- (31) Birks, J. B. In *Photophysics of Aromatic Molecules*, Wiley-Interscience: New York, 1970, Chapter 7.
- (32) Bard, A. J.; Park, S. M. In *The Exciplex*; Gordon, M.; Ware, W. R., Eds.; Academic Press: New York, 1975, p. 305.
- (33) Zachariasse, K. In *The Exciplex*; Gordon, M.; Ware, W. R., Eds.; Academic Press: New York, 1975, p. 275.
- (34) Rothe, C.; Monkman, A. *Phys. Rev. B* **2002**, *65*, 073201.
- (35) Wallace, W. L.; Bard, A. J. *J. Phys. Chem.* **1979**, *83*, 1350.
- (36) Tokel-Takvoryan, N. E.; Hemingway, R. E.; Bard, A. J. *J. Am. Chem. Soc.* **1973**, *95*, 6582.

(37) Taken from  $E_{1/2}$  of  $\text{Ru}(\text{bpy})_3^{2+/3+}$  measured in MeCN:Bz (1:1,v:v)/0.1 M TBAP.

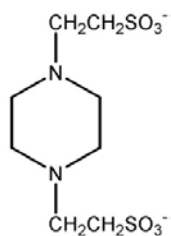
## Chapter 6: Concluding Remarks

Understanding electrogenerated chemiluminescence (ECL) reaction mechanisms is important in designing and selecting the ECL emitter/coreactant system. Moreover, optimizing the conditions to generate ECL is also significant to utilize ECL for practical applications. In the amine coreactant study, a new route involving amine radical cations ( $R_2N^{\bullet+}R'$ ) produced from amine coreactants to generate  $Ru(bpy)_3^{2+}$  ECL was suggested. This route describes  $Ru(bpy)_3^{2+}$  producing luminescence without being oxidized. The first and second ECL wave intensities of  $Ru(bpy)_3^{2+}$  depend on the stability of both radical cations and free radicals produced from amine coreactants. Therefore, the general rules of amine coreactants to enhance the ECL of  $Ru(bpy)_3^{2+}$  are established as follows. (1) Tertiary amine coreactants produce the most intense ECL compared with primary and secondary amines because the stability of the produced radical ions increases in the order of primary < secondary < tertiary amines. (2) ECL increases as alkyl groups of coreactants are longer because the longer alkyl groups provide the better stability of radical ions. (3) In the neutral pH region, monoamine coreactants generate more intense first and second ECL waves than do diamines, because the radical ions of diamines are easily decomposed by the positive charge on protonated nitrogen atoms of diamines. (4) If there are electron-withdrawing

groups on amine coreactants, they reduce the stability of free radicals so that a weak second ECL wave is produced. However, the presence of electron-donating groups enhanced the second ECL wave. (5) Acyclic amine coreactants usually generate more intense first and second ECL waves than do heteroalicyclic amines because of difficulty of rearrangement.

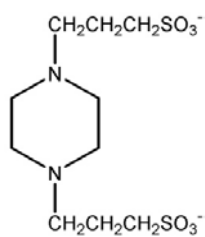
In the coreactant buffer (CB) study, the fact that no additional coreactant is needed to produce ECL may have an advantage for the ECL analysis in immunoassays or DNA-probe assays, especially when a side-reaction of analyte occurs with an added coreactant. The reactivity and ECL reaction mechanism of CBs also follow the general rules of amine coreactants. Besides CBs used in this research, use of PIPES, PIPPS, and PIPBS (see Figure 6.1 for structures and nomenclatures) as CBs may be promising in future study. Among them, PIPES, which provides a useful buffer in the pH range of 6.0 – 7.3<sup>1</sup> may be most promising as a candidate for not only CB, but also a coreactant. Because its second  $pK_a$  value is 6.78,<sup>1</sup> the deprotonated form of PIPES will be predominant at pHs 7.5 – 8.0, so that the stability of produced radical ions will not be affected like protonated diamine coreactants. In fact, some diamine coreactants, such as *N,N,N',N'*-tetraethylethylenediamine (TEDAE) and *N,N,N',N'*-tetraethyl-1,3-diamine (TEDAP), produced a higher second ECL wave intensity at pH 12.5 than did tri-*n*-propylamine (TPrA) at pH 7.5,<sup>2</sup> although the background emission at such high pH also contributed to ECL.

(a) PIPES



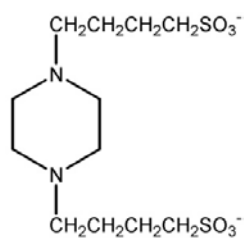
Piperazine-*N,N'*-bis[2-ethanesulfonic acid]

(b) PIPPS



Piperazine-*N,N'*-bis[3-propanesulfonic acid]

(c) PIPBS



Piperazine-*N,N'*-bis[4-buthanesulfonic acid]

**Figure 6.1.** Structures of (a) PIPES, (b) PIPPS, and (c) PIPBS.

Benzoyl peroxide (BPO) produces a strong reducing agent,  $C_6H_5CO_2^\bullet$  upon its reduction. A BPO coreactant generates ECL in the presence of neutral red (NR), ter(9,9-diarylfuorene)s (TDAFs), and  $Ru(bpy)_3^{2+}$ . Because NR produces only a stable radical anion, its ECL is not generated by ion annihilation. Stable radical cation formation of NR may be achieved by converting the  $-NH_2$  group of NR to a tertiary amine group to avoid the faster follow-up decomposition reaction induced from the  $-NH_2$  group. The high concentration of BPO shows effective quenching of  $NR^*$  ( $> 10$  mM compare to 0.5 mM NR), and the quenching reaction may occur by electron transfer from  $NR^*$  to BPO.

In the ECL study of TDAFs, formation of excimers by ion annihilation is an efficient process, even though TDAFs have bulky substituent groups and a solvent having high dielectric constant is used. A significant emission from excimers was prevented by use of BPO coreactant, implying that coreactants can be used to avoid the interference of excimer or exciplex emission.

## References

- (1) Kandegedara, A.; Rorabacher, D. B. *Anal. Chem.* **1999**, *71*, 3140.
- (2) Unpublished Data.

## Appendix A. List of Symbols

### Roman Symbols

$a$	Radius of an UME
$A$	Electron acceptor molecule
${}^1(A^-D^+)$	Exciplex
$d$	Distance of the tip from the substrate in SECM ( $\mu\text{m}$ )
$C$	(1) Constant (2) Local concentration of species (M or $\text{mol}/\text{cm}^3$ )
$C^*$	Bulk concentration of species ( $\text{mol}/\text{cm}^3$ )
$D$	Electron donor molecule
$D$	Diffusion coefficient ( $\text{cm}^2/\text{s}$ )
$E$	Voltage (V)
$E^\circ$	Standard potential (V)
$E_{1/2}$	Half-wave potential (V)
$E_p$	Peak potential (V)
$\Delta E_p$	Peak potential separation
$E_{p,a}$	Anodic peak potential (V)
$E_{p,c}$	Cathodic peak potential (V)
$E_s$	The lowest excited singlet energy (eV)
$E_t$	Triplet energy (eV)
$\Delta E^*$	Energy change in triplet state quenching

$f$	Activity coefficient
$F$	Faraday constant (C)
$\Delta G$	Gibbs free energy change
$h$	Planck constant (Js)
$\Delta H_{\text{ann}}$	Enthalpy change of ion annihilation (eV)
$\Delta H_{\text{co}}$	Enthalpy change of a reaction between ECL emitters and coreactants (eV)
$i$	Current (A)
$i_{\text{cv}}$	Current in CV (A)
$i_{\text{d}}(t)$	Chronoamperometric diffusion current at $t$ (A)
$i_{\text{p}}$	Peak current (A)
$i_{\text{pa}}$	Anodic peak current (A)
$i_{\text{pc}}$	Cathodic peak current (A)
$i_{\text{ss}}$	Steady-state current of an UME
$i_{\text{T}}$	Tip Current in SECM (A)
$I_{\text{ECL}}$	Intensity of ECL
$I_{\text{ECL}}^{\circ}$	ECL intensity of a standard emitter
$I$	Fluorescence intensity
$I_0$	Initial fluorescence intensity without a quencher
$k^{\circ}$	Standard heterogeneous rate constant (cm/s)
$k_{\text{b}}$	Homogeneous rate constant for “backward” reaction
$k_{\text{f}}$	Homogeneous rate constant for “forward” reaction
$k_{\text{q}}$	Quenching rate constant

$k_s$	Standard heterogeneous rate constant (cm/s)
$K_a$	Acid dissociation constant
$K_b$	Base dissociation constant
$K_{SV}$	Stern-Volmer quenching constant
$n$	Number of electrons transferred
$Q_{a,c}$	Total anodic or cathodic charge (C)
$R$	Gas constant ( $\text{Jmol}^{-1}\text{K}^{-1}$ )
$R$	ECL emitter or Chromophore
$R^{\bullet-}$	Radical anion of an ECL emitter
$R^{\bullet+}$	Radical cation of an ECL emitter
$R^*$	Excited state of R
$^1R^*$	The lowest excited singlet state of R
$^3R^*$	Triplet state of R
$(R_2)^*$	Excimer
$\Delta S$	Entropy change
$t$	Time (s)
$T$	Absolute temperature (K)

### Greek Symbols

$\alpha$	Transfer coefficient
$\varepsilon$	Dielectric constant
$\lambda_{em}$	Wavelength for emission

$\lambda_{\text{ex}}$	Wavelength for excitation
$\nu$	(1) Frequency of light ( $\text{s}^{-1}$ ) (2) Scan rate (V/s)
$\tau$	Lifetime of radical ions (s)
$\tau_{1/2}$	Half-lifetime of radical ions (s)
$\tau^{\text{s}}$	Lifetime of the lowest excited singlet state
$\phi_{\text{ECL}}$	ECL efficiency or quantum efficiency of ECL
$\phi^{\circ}_{\text{ECL}}$	ECL efficiency of a standard emitter
$\phi_{\text{F}}$	Quantum efficiency of fluorescence

## Glossary

AN	Anthracene
A.U.	Arbitrary Unit
BES	<i>N,N</i> -Bis[2-hydroxyethyl]-2-aminoethanesulfonic Acid
BICINE	<i>N,N</i> -Bis[2-hydroxyethyl]glycine
BPO	Benzoyl Peroxide
bpy	2,2'-Bipyridine
BTP	1,3-Bis[tris(hydroxymethyl)methylamino]propane
Bz	Benzene
CB	Coreactant Buffer
CCD	Charge-coupled Device
CI	Chemical Ionization
CL	Chemiluminescence
CR	Coreactant
CV	Cyclic Voltammetry or Cyclic Voltammogram
DEPz	1,4-Diethylpiperazine
DIPSO	3-[ <i>N,N</i> -Bis(2-hydroxyethyl)amino]-2-hydroxypropanesulfonic Acid
DMF	<i>N,N</i> -Dimethylformamide
DMSO	Dimethyl sulfoxide
DMPz	1,4-Dimethylpiperazine
DPA	9,10-Diphenylanthracene

DPPz	1,4-Di- <i>n</i> -propylpiperazine
DPV	Differential Pulse Voltammogram
ECE	Electron transfer-Chemical reaction-Electron transfer
ECL	Electrogenerated Chemiluminescence
EDAC	1-Ethyl-3-(3-dimethylaminopropyl) Carbodiimide hydrochlorid
EP	1-Ethylpiperidine
EPPS	<i>N</i> -[2-Hydroxyethyl]piperazine- <i>N'</i> [3-propanesulfonic acid]
ESR	Electron Spin Resonance
ET	Electron Transfer
Fc	Ferrocene
Fc <sup>+</sup>	Ferrocenium Cation
GC	Glassy Carbon
GCE	Glassy Carbon Electrode
GLY-GLY	<i>N</i> -Glycylglycine
HEPBS	<i>N</i> -[2-hydroxyethyl]piperazine- <i>N'</i> [4-butanesulfonic acid]
HEPES	<i>N</i> -[2-Hydroxyethyl]piperazine- <i>N'</i> [2-ethanesulfonic acid]
HEPPSO	<i>N</i> -[2-Hydroxyethyl]piperazine- <i>N'</i> [2-hydroxypropanesulfonic acid]
HPLC	High Performance Liquid Chromatography
ICCD	Intensified Charge Coupled Device
ITO	Indium-Tin Oxide
LP	Long-wavelength Pass
LSV	Linear Sweep Voltammetry
MeCN	Acetonitrile

MOBS	4-[ <i>N</i> -Morpholino]butanesulfonic Acid
MOPS	3-[ <i>N</i> -Morpholino]propanesulfonic Acid
MOPSO	3-[ <i>N</i> -Morpholino]-2-hydroxypropanesulfonic Acid
MP	1-Methylpiperidine
MS	Mass Spectrometry
NHE	Normal Hydrogen Electrode
NMR	Nuclear Magnetic Resonance
NR	Neutral Red
NRH <sup>+</sup>	Protonated Neutral Red
OLED	Organic Light-emitting Device
PBS	Phosphate Buffer Solution
PIPBS	Piperazine- <i>N,N'</i> -bis[4-butanesulfonic acid]
PIPES	Piperazine- <i>N,N'</i> -bis[2-ethanesulfonic acid]
PIPPS	Piperazine- <i>N,N'</i> -bis[3-propanesulfonic acid]
PMT	Photomultiplier Tube
PP	1- <i>n</i> -propylpiperidine
Py	Pyrene
QRE	Quasi-reference Electrode
Ru(bpy) <sub>3</sub> <sup>2+</sup>	Tris(2,2'-bipyridine)ruthenium (II)
SCE	Saturated Calomel Electrode
SECM	Scanning Electrochemical Microscopy
S.R.	Scan Rate
TAPS	<i>N</i> -Tris[hydroxymethyl]methyl-3-aminopropanesulfonic Acid

TAPSO	3-[ <i>N</i> -Tris(hydroxymethyl)methylamino]-2-hydroxypropanesulfonic Acid
TBAP	Tetra- <i>n</i> -butylammonium Perchlorate
TDAF	Ter(9,9-diarylfuorene)s
TEA	Triethanolamine
TEDAE	<i>N,N,N',N'</i> -Tetraethylethylenediamine
TEDAM	<i>N,N,N',N'</i> -Tetraethylmethanediamine
TEDAP	<i>N,N,N',N'</i> -Tetraethyl-1,3-propanediamine
TES	<i>N</i> -Tris[hydroxymethyl]methyl-2-aminoethanesulfonic Acid
TEtA	Triethylamine
TFA	Trifluoroacetic Acid
THF	Tetrahydrofuran
TMPD	<i>N,N,N',N'</i> -Tetramethyl- <i>p</i> -phenylenediamine
TPDAE	<i>N,N,N',N'</i> -Tetra- <i>n</i> -propylethylenediamine
TPDAM	<i>N,N,N',N'</i> -Tetra- <i>n</i> -propylmethanediamine
TPDAP	<i>N,N,N',N'</i> -Tetra- <i>n</i> -propyl-1,3-propanediamine
TPrA	Tri- <i>n</i> -propylamine
TRICINE	<i>N</i> -Tris[hydroxymethyl]methylglycine
TTA	Triplet-triplet Annihilation
UME	Ultramicroelectrode

## References

### Chapter 1

- (1) Dufford, R. T.; Nightingale, D.; Gaddum, L. W. J. *Am. Chem. Soc.* 1927, 49, 1858.
- (2) Harvey, N. J. *Phys. Chem.* 1929, 33, 1456.
- (3) Kuwana, T.; *J. Electroanal. Chem. Interfacial Electrochem.* 1963, 67, 2243.
- (4) Hercules, D. M. *Science* 1964, 145, 808.
- (5) Faulkner, L. R.; Bard, A. J. In *Electroanalytical Chemistry*; Bard, A. J., Ed., Marcel Dekker: New York, 1977; Vol. 10, p1.
- (6) Faulkner, L. R. *Methods Enzymol.* 1978, 57, 494.
- (7) Glass, R. S.; Faulkner, L. R. In *Chemical and Biological Generation of Excited States*; Adam, W.; Cilento, G., Eds., Academic Press, New York, 1982, Chapter 6.
- (8) Knight, A. W.; Greenway, G. M. *Analyst* 1994, 119, 879.
- (9) Lee, W. Y. *Mikrochim. Acta* 1997, 127, 19.
- (10) Bard, A. J.; Debad, J. D.; Leland, J. K.; Sigal, G. B.; Wilbur, J. L.; Wohlstadter, J. N. In *Encyclopedia of Analytical Chemistry: Applications, Theory, and Instrumentation*, Meyer, R. A. Ed.; John Wiley & Sons: New York, 2000, p. 9842.
- (11) Faulkner, L. R.; Tachikawa, H.; Bard, A. J. *J. Am. Chem. Soc.* 1972, 94, 691.
- (12) Bezman, R.; Faulkner, L. R. *J. Am. Chem. Soc.* 1972, 94, 6317.
- (13) Faulkner, L. R.; Bard, A. J. *J. Am. Chem. Soc.* 1969, 91, 209.
- (14) Bezman, R.; Faulkner, L. R. *J. Am. Chem. Soc.* 1973, 95, 3083
- (15) Bezman, R.; Faulkner, L. R. *J. Am. Chem. Soc.* 1972, 94, 6324.
- (16) Bezman, R.; Faulkner, L. R. *J. Am. Chem. Soc.* 1972, 94, 6331.

- (17) Tachikawa, H.; Bard, A. J. *Chem. Phys. Letters* 1974, 26, 246.
- (18) Periasamy, N.; Santhanam, K. S. V. *Proc. Ind. Acad. Sci.* 1974, 80A, 821.
- (19) Pighin, A.; Conway, B. E. *J. Electrochem. Soc.* 1975, 122, 619.
- (20) Chang, M. –M.; Saji, T.; Bard, A. J. *J. Am. Chem. Soc.* 1977, 99, 5399.
- (21) Rubinstein, I.; Bard, A. J. *J. Am. Chem. Soc.* 1981, 103, 512.
- (22) Butler, J.; Hengline, A. *Radiat. Phys. Chem.* 1980, 15, 603.
- (23) Noffsinger, J. B.; Danielson, N. D. *Anal. Chem.* 1987, 59, 865.
- (24) Leland, J. K.; Powell, M. J. *J. Electrochem. Soc.* 1990, 137, 3127.
- (25) Zu, Y.; Bard, A. J. *Anal. Chem.* 2000, 72, 3223.
- (26) Kanoufi, F.; Zu, Y.; Bard, A. J. *J. Phys. Chem. B* 2001, 105, 210.
- (27) White, H. S.; Bard, A. J. *J. Am. Chem. Soc.* 1982, 104, 6891.
- (28) Becker, W. G.; Seung, H. S.; Bard, A. J. *J. Electroanal. Chem.* 1984, 167, 127.
- (29) Fabrizio, E. F.; Prieto, I.; Bard, A. J. *J. Am. Chem. Soc.* 2000, 122, 4996.
- (30) Chandross, E. A.; Longworth, J. W.; Visco, R.E. *J. Am. Chem. Soc.* 1965, 87, 3259.
- (31) Maloy, J. T.; Bard, A. J. *J. Am. Chem. Soc.* 1971, 93, 5968.
- (32) Bard, A. J.; Park, S. M. In *The Exciplex*; Gordon, M.; Ware, W. R., Eds.; Academic Press: New York, 1975, p. 305.
- (33) Keszthelyi, C. P.; Bard, A. J. *Chem. Phys. Letters* 1974, 24, 300.
- (34) Hercules, D. M.; Lansbury, R. C.; Roe, D. K. *J. Am. Chem. Soc.* 1966, 88, 4578.
- (35) Maricle, D. L.; Maurer, A. J. *J. Am. Chem. Soc.* 1967, 89, 188.
- (36) Zweig, A.; Hoffman, A. K.; Maricle, D. L.; Maurer, A. H. *Chem. Commun.* 1967, 106.
- (37) Zweig, A.; Maricle, D. L.; Brinen, J. S.; Maurer, A. H. *J. Am. Chem. Soc.* 1967, 89, 473.
- (38) Egashira, N.; Kumasako, H.; Ohga, K. *Anal. Sci.* 1990, 6, 903.

- (39) Kuhn, L. S.; Weber, A.; Weber, S. G. *Anal. Chem.* 1990, 62, 1613.
- (40) Preston, J.; Nieman, T. A. *Anal. Chem.* 1996, 68, 966.
- (41) Noffsinger, J. B.; Danielson, N. D. *J. Chromatogr.* 1987, 387, 520.
- (42) Uchikura, K.; Kirisawa, M. *Anal.Sci.* 1991, 7, 971.
- (43) Skotty, D. R.; Lee, W. Y.; Nieman, T. A. *Anal. Chem.* 1996, 68, 1530.
- (44) Martin, A. F.; Nieman, T. A. *Anal. Chim. Acta* 1993, 281, 475.
- (45) Yokoyama, K.; Sasaki, S.; Ikebukuro, K.; Takeuchi, T.; Karube, I.; Tokitsu, Y.; Masuda, Y. *Talanta* 1994, 31, 1035.
- (46) Jameison, F.; Sanchez, R. I.; Dong, L.; Leland J. K.; Yost, D.; Martin, M. T. *Anal. Chem.* 1996, 68, 1298.
- (47) Blackburn, G. F.; Shah, H. P.; Kenten, J. H.; Leland, J.; Kamin, R. A.; Link, J.; Peterman, J.; Powell, M. J.; Shah, A.; Talley, D. B.; Tyagi, S. K.; Wilkins, E.; Wu, T. G.; Massey, R. J. *Clin. Chem.* 1991, 37, 1534.
- (48) Kenten, J. H.; Casadei, J.; Link, J.; Lupold, S.; Willey, J.; Powell, M. J.; Rees, A.; Massey, R. J. *Clin. Chem.* 1991, 37, 1626.
- (49) DiCesare, J.; Grossman, B.; Katz, E.; Picozza, E.; Ragusa, R.; Woundenberg, T. *Biotechniques* 1993, 15, 152.

## **Chapter 2**

- (1) Noffsinger, J. B.; Danielson, N. D. *Anal. Chem.* 1987, 59, 865.
- (2) Leland, J. K.; Powell, M. J. *J. Electrochem. Soc.* 1990, 137, 3127.
- (3) Bard, A. J.; Debad, J. D; Leland, J. K.; Sigal, G. B.; Wilbur, J. L.; Wohlstadter, J. N., "Chemiluminescence, Electrogenerated," in *Encyclopedia of Analytical Chemistry: Applications, Theory and Instrumentation*, R. A. Meyers, Ed., John Wiley & Sons: New York, 2000, Vol. 11, p. 9842 and references therein.
- (4) Kanoufi, F.; Zu, Y.; Bard, A. J. *J. Phys. Chem. B* 2001, 105, 210.

- (5) Zu, Y.; Bard, A. J. *Anal. Chem.* 2000, 72, 3223.
- (6) Gross, E. M.; Pastore, P.; Wightman, R. M. *J. Phys. Chem. B* 2001, 105, 8732.
- (7) He, L.; Cox, K. A.; Danielson, N. D. *Anal. Lett.* 1990, 23, 195.
- (8) Rubinstein, I.; Bard, A. J. *J. Am. Chem. Soc.* 1981, 103, 512.
- (9) Zu, Y.; Bard, A. J. *Anal. Chem.* 2001, 73, 3960.
- (10) Sprintschnik, G.; Sprintschnik, H. W.; Kirsch, P. P.; Whitten, D. G. *J. Am. Chem. Soc.* 1977, 99, 4947.
- (11) Murray, R. W. In *Electroanalytical Chemistry*; Bard, A. J., Ed.; Marcel Dekker, Inc.: New York, 1984; Vol. 13, p 191.
- (12) Charkoudian, J. C. *J. Magn. Reson.* 1984, 57, 287.
- (13) Windle, J. J.; Wiersema, A. K. *J. Chem. Phys.* 1963, 39, 1139.
- (14) Pake, G. E.; Townsend, J.; Weissman, S. I. *Phys. Rev.* 1952, 85, 682.
- (15) Duling, D. R. *J. Magn. Reson., Ser. B* 1994, 104, 105.
- (16) Bard, A. J.; Mirkin, M. V., Eds., *Scanning Electrochemical Microscopy*, Marcel Dekker, New York, 2001.
- (17) Chow, Y. L.; Danen, W. C.; Nelsen, S. F.; Rosenblatt, D. H. *Chem. Rev.* 1978, 78, 243.
- (18) Mann, C. K. *Anal. Chem.* 1964, 36, 2424.
- (19) Masui, M.; Sayo, H.; Tsuda, Y. *J. Chem. Soc., B* 1968, 973.
- (20) Portis, L. C.; Bhat, V. V.; Mann, C. K. *J. Org. Chem.* 1970, 35, 2175.
- (21) Ross, S. D. *Tetrahedron Lett.* 1973, 1237.
- (22) Elliott, C. M.; Hershenhart, E. J. *J. Am. Chem. Soc.* 1982, 104, 7519.
- (23) Lai, R., Bard, A. J., *unpublished experiments*.
- (24) Roundhill, D. M. In *Photochemistry and Photophysics of Metal Complexes*; Fackler, J. J. P., Ed.; Plenum Press: New York, 1994, p 165.
- (25) Bard, A. J.; Faulkner, L. R. *Electrochemical Methods*; 2nd ed.; John Wiley & Sons, Inc.: New York, 2000.

- (26) Eastland, G. W.; Rao, D. N. R.; Symons, M. C. R. *J. Chem. Soc., Perkin Trans. 2* 1984, 1551.
- (27) Liu, W.; Yamanaka, S.; Shiotani, M.; Michalik, J.; Lund, A. *Phys. Chem. Chem. Phys.* 2001, 3, 1611.
- (28) Ledney, M.; Dutta, P. K. *J. Am. Chem. Soc.* 1995, 117, 7687.
- (29) Quayle, W. H.; Lunsford, J. H. *Inorg. Chem.* 1982, 21, 97.
- (30) Matsuura, K.; Kevan, L. *J. Phys. Chem.* 1996, 100, 10652.
- (31) Matsuura, K.; Kevan, L. *Radiat. Phys. Chem.* 2001, 62, 399.

### Chapter 3

- (1) Faulkner, L. R.; Bard, A. J. In *Electroanalytical Chemistry*; Bard, A. J., Ed.; Marcel Dekker: New York, 1977; Vol. 10, p. 1.
- (2) Knight, A. W.; Greenway, G. M. *Analyst* **1994**, 119, 879.
- (3) Bard, A. J.; Debad, J. D.; Leland, J. K.; Sigal, G. B.; Wilber, J. L.; Wohlstadter, J. N. In *Encyclopedia of Analytical Chemistry: Applications, Theory, and Instrumentation*; Meyers, R. A., Ed.; John Wiley & Sons: New York, 2000, Vol. 11, p. 9842.
- (4) Leland, J. K.; Powell M. J. *J. Electrochem. Soc.* **1990**, 137, 3127.
- (5) Knight, A. W.; Greenway, G. M. *Analyst* **1996**, 121, 101R.
- (6) Kanoufi, F.; Zu, Y.; Bard, A. J. *J. Phys. Chem. B* **2001**, 105, 210.
- (7) Zu, Y.; Bard, A. J. *Anal. Chem.* **2001**, 73, 3960.
- (8) Gross, E. M.; Pastore, P.; Wightman, R. M. *J. Phys. Chem. B* **2001**, 105, 8732.
- (9) Zu, Y.; Bard, A. J. *Anal. Chem.* **2000**, 72, 3223.
- (10) Miao, W.; Choi, J. -P.; Bard, A. J. *J. Am. Chem. Soc.* **2002**, 124, 14478.
- (11) Noffsinger, J. B.; Danielson, N. D. *Anal. Chem.* **1987**, 59, 865.
- (12) Downey, T. M.; Nieman, T. A. *Anal. Chem.* **1992**, 64, 261.
- (13) Christian, G. D.; Purdy, W. C. *J. Electroanal. Chem.* **1962**, 3, 363.

- (14) Tokel-Takvoryan, N. E.; Hemingway, R. E.; Bard, A. J. *J. Am. Chem. Soc.* **1973**, *95*, 6582.
- (15) Gillard, R. D.; Hughes, C. T.; Williams, P. A. *Transition Met. Chem.* **1976**, *1*, 51.
- (16) Sagüés, J. A. A.; Gillard, R. D.; Lancashire, R. J.; Willaims, P. A. *J. Chem. Soc. Dalton Trans.* **1979**, 193.
- (17) Constable, E. C.; Seddon, E. A. *J. Chem. Soc. Chem. Comm.* **1982**, 34.
- (18) Constable, E. C. *Polyhedron* **1983**, *2*, 551.
- (19) Creutz, C.; Sutin, N. *Proc. Nat. Acad. Sci.* **1975**, *72*, 2858.
- (20) Serpon, N.; Bolletta, F. *Inorg. Chim. Acta.* **1983**, *75*, 189.
- (21) Serpon, N.; Ponterini, G.; Jamieson, M. A.; Bolletta, F.; Maestri, M. *Coord. Chem. Rev.* **1983**, *50*, 209.
- (22) For a general review on an nonaromatic amine oxidation, Chow, Y. L.; Danen, W. C.; Nelsen, S. F.; Rosenblatt, D. H. *Chem. Rev.* **1978**, *78*, 243.
- (23) Mann, C. K. *Anal. Chem.* **1964**, *36*, 2424.
- (24) Masui, M.; Sayo, H.; Tsuda, Y. *J. Chem. Soc. B* **1968**, 973.
- (25) Portis, L. C.; Bhat, V. V.; Mann, C. K. *J. Org. Chem.* **1970**, *35*, 2175.
- (26) Ross, S. D. *Tetrahedron Lett.* **1973**, *14*, 1237.
- (27) Bard, A. J.; Faulkner, L. R. In *Electrochemical Method, 2nd Ed.* Wiley & Sons: New York, 2001, Chapter 6.
- (28) Calculated from an equation:  $E^\circ [\text{R}_3\text{N}/\text{R}_3\text{N}^{*+}] = E_s + E^\circ [\text{Ru}(\text{bpy})_3^{2+/+}] + 0.1$  eV where  $E_s$  is the excited singlet energy of  $\text{Ru}(\text{bpy})_3^{2+}$  and 0.1 eV is the entropy correction term.
- (29) Kalyanasundaram, K. *Coord. Chem. Rev.* **1982**, *46*, 159.
- (30) The first  $pK_a$ 's of most diamines are below 5 and the second  $pK_a$ 's are above 9.
- (31) Hercules, D. M.; Lytle F. E. *J. Am. Chem. Soc.* **1966**, *88*, 4745.

- (32) In *CRC Handbook of Chemistry and Physics, 83rd Ed.*, Lide, D. R. Ed., CRC Press: Boca Raton, FL, 2002/03, Section 8.
- (33) Dean, J. A. In *Lange's Handbook of Chemistry, 15th Ed.*, McGraw-Hill, Inc.: New York, 1999, Section 8.
- (34) Yu, Q.; Kandegedara, A.; Xu, Y.; Rorabacher, D. B. *Anal. Biochem.* **1997**, *253*, 50.
- (35) Gero, A. *J. Am. Chem. Soc.* **1954**, *76*, 5158.
- (36) Perrin, D. D. In *Dissociation Constants of Organic Bases in Aqueous Solution*. Butterworths: London, 1965.
- (37) Dega-Szafran, Z.; Jaskólski, M.; Kurzyca, I.; Barczyński, P.; Szafran, M. *J. Mol. Struct.* **2002**, *614*, 23.
- (38) Brune, S. N.; Bobbitt, D. R. *Anal. Chem.* **1992**, *64*, 166.
- (39) March, J. In *Advanced Organic Chemistry: Reactions, Mechanisms, and Structure, 4th Ed.* Wiley & Sons: New York, 1992, Chapter 9.

#### Chapter 4

- (1) Lamanna, J. C.; McCracken, K. A. *Anal. Biochem.* **1984**, *142*, 117.
- (2) Haumann, M.; Junge, W. *Biochemistry*, **1994**, *33*, 864.
- (3) Osborne, R.; Perkins, M. A. *Food Chem. Toxicol.* **1994**, *32*, 133.
- (4) Gaullier, J. M.; Geze, M.; Santus, R.; Sa e Melo, T.; Maziere, J. C.; Bazin, M.; Morliere, P.; Dubertret, L. *Photochem. Photobiol.* **1995**, *62*, 114.
- (5) Woodburn, K. W.; Vardaxis, N. J.; Hill, J. S.; Kaye, A. H.; Phillips, D. R. *Photochem. Photobiol.* **1991**, *54*, 725.
- (6) Chen, G.; Hanson, C. L.; Ebner, T. J. *J. Neurophysiol.* **1996**, *76*, 4169.
- (7) Okada, D. *J. Neurosci. Methods* **2000**, *101*, 85.
- (8) Walz Jr., F. G.; Terenna, B.; Rolince, D. *Biopolymers*, **1975**, *14*, 825.

- (9) For general reviews, (a) Faulkner, L. R.; Glass, R. S. In *Chemical and Biological Generation of Excited States*, Adam, W.; Cilento, G., Eds.; Academic Press: New York, Chapter 6, 1982, p. 191. (b) Knight, A. W.; Greenway, G. M. *Analyst* **1994**, *119*, 879. (c) Bard, A. J.; Debad, J. D.; Leland, J. K.; Sigal, G. B.; Wilbur, J. L.; Wohlstadter, J. N. In *Encyclopedia of Analytical Chemistry: Applications, Theory, and Instrumentation*, Meyer, R. A. Ed.; John Wiley & Sons: New York, 2000, p. 9842.
- (10) White, H. S.; Bard, A. J. *J. Am. Chem. Soc.* **1982**, *104*, 6891.
- (11) Bolleta, F.; Ciano, M.; Balzani, V.; Serpone, N. *Inorg. Chim. Acta.* **1982**, *62*, 207.
- (12) Becker, W. G.; Seung, H. S.; Bard, A. J. *J. Electroanal. Chem.* **1984**, *167*, 127.
- (13) Bard, A. J.; Whitesides, G. M. *U.S. Patents* 5 221 605, 1993; 5 238 808, 1993; and 5 310 687, 1994.
- (14) Blackburn, G. F.; Shah, H. P.; Kenien, J. H.; Leland, J.; Kamin, R. A.; Link, J.; Peterman, J.; Powell, M. J.; Shah, A.; Talley, D. B.; Tyagi, S. K.; Wilkins, E.; Wu, T. -G.; Massey, R. J. *J. Clin. Chem.* **1991**, *37*, 1534.
- (15) Coetzee, J. F.; Kolthoff, I. M. *J. Am. Chem. Soc.* **1957**, *79*, 6110.
- (16) Debad, J. D.; Morris, J. S.; Magnus, P.; Bard, A. J. *J. Org. Chem.* **1997**, *62*, 530.
- (17) McCord, P.; Bard, A. J. *J. Electroanal. Chem.* **1991**, *318*, 91.
- (18) Kolthoff, I. M.; Bruckenstein, S.; Chantooni, M. K. *J. Am. Chem. Soc.* **1961**, *83*, 3927.
- (19) Halliday, C. S.; Matthews, D. B. *Aust. J. Chem.* **1983**, *36*, 507.
- (20) Bauldrey, J. M.; Archer, M. D. *Electrochim. Acta* **1983**, *28*, 1515.
- (21) Creager, S. E.; Marks, G. T.; Aikens, D. A.; Richtol, H. H. *J. Electroanal. Chem.* **1983**, *152*, 197.
- (22) Witt, E. *Ber. Dtsch. Chem. Ges.* **1878**, *12*, 931.

- (23) Denuault, G.; Mirkin, M. V.; Bard, A. J. *J. Electroanal. Chem.* **1991**, *308*, 27.
- (24) Wightman, R. M.; Wipf, D. O. In *Electroanalytical Chemistry*; Bard, A. J., Ed.; Marcel Dekker: New York, 1988, Vol. 15. p. 267.
- (25) Bard, A. J.; Fan, F. -R.; Kwak, J.; Lev, O. *Anal. Chem.* **1989**, *61*, 132.
- (26) Oldham, K. B. *J. Electroanal. Chem.* **1981**, *122*, 1.
- (27) Oldham, K. B.; Zoski, C. G. *J. Electroanal. Chem.* **1988**, *256*, 11.
- (28) Sawyer, D. T.; Komai, R. Y. *Anal. Chem.* **1972**, *44*, 715.
- (29) Bard, A. J.; Faulkner, L. R. In *Electrochemical Methods*, 2nd Ed., John Wiley & Sons: New York, 2001, Chapter 12, p 476.
- (30) Chandross, E. A.; Sonntag, F. I. *J. Am. Chem. Soc.* **1966**, *88*, 1089.
- (31) Akins, D. L.; Birke, R. L. *Chem. Phys. Lett.* **1974**, *29*, 428.
- (32) Faulkner, L. R.; Bard, A. J. In *Electroanalytical Chemistry*; Bard, A. J., Ed; Marcel Dekker: New York, 1977; Vol. 10, p 1.
- (33) Singh, M. K.; Pal, H.; Bhasikuttan, A. C.; Sapre, A. V. *Photochem. Photobiol.* **1998**, *68*, 32.
- (34) Oishi, S.; Tajime, K.; Shiojima, I. *J. Mol. Catal.* **1982**, *14*, 383.
- (35) Urano, T.; Kitamura, A.; Sakuragi, H.; Tokumaru, K. *J. Photochem.* **1984**, *26*, 69.
- (36) Wilkinson, F. In *Fluorescence: Theory, Instrumentation, and Practice*; Guilbault, G. G., Ed; Marcel Dekker: New York, 1967; Chapter 1.
- (37) Kalyanasundaram, K. *Coor. Chem. Rev.* **1982**, *46*, 159.
- (38) Calculated by eq. (4.14) with  $E^\circ(\text{C}_6\text{H}_5\text{CO}_2^\bullet/\text{C}_6\text{H}_5\text{CO}_2^-) = + 0.8 \text{ V}$  from ref. (31) and  $E^\circ(\text{Ru}(\text{bpy})_3^{2+/+}) = - 1.5 \text{ V}$  from ref. (10)
- (39) Tokel-Takvoryan, N. E.; Hemingway, R. E.; Bard, A. J. *J. Am. Chem. Soc.* **1973**, *95*, 6582.
- (40) Wallace, W. L.; Bard, A. J. *J. Phys. Chem.* **1979**, *83*, 1350.
- (41) Itoh, K.; Honda, K. *Chem. Lett.* **1979**, 99.

(42) Luttmer, J. D.; Bard, A. J. *J. Phys. Chem.* **1981**, *85*, 1155.

## Chapter 5

- (1) Wong, K. -T; Chien, Y. -Y; Chen, R. -T; Wang, C. -F; Lin, Y. -T; Chiang, H. -H; Hsieh, P. -Y; Wu, C. -C; Chou, C. H.; Su, Y. O.; Lee, G. -H.; Peng, S. -M. *J. Am. Chem. Soc.* **2002**, *124*, 11576.
- (2) Geng, Y.; Katsis, D.; Culligan, S. W.; Ou, J. J.; Chen, S. H.; Rothberg, L. J. *J. Chem. Mater.* **2002**, *14*, 463.
- (3) Katsis, D.; Geng, Y. H.; Ou, J. J.; Culligan, S. W.; Trajkovska, A.; Chen, S. H.; Rothberg, L. J. *J. Chem. Mater.* **2002**, *14*, 1332.
- (4) Belletête, M.; Morin, J. -F.; Beaupré, S.; Ranger, M.; Leclerc, M.; Durocher, G. *Macromolecules* **2001**, *34*, 2288.
- (5) Destri, S.; Pasini, M.; Botta, C.; Porzio, W.; Bertini, F.; Marchiò, L. *J. Mater. Chem.* **2002**, *12*, 924.
- (6) Chang, S. -C.; Yang, Y.; Pei, Q. *Appl. Phys. Lett.* **1999**, *74*, 2081.
- (7) Teetsov, J.; Fox, M. A. *J. Mater. Chem.* **1999**, *9*, 2117.
- (8) Chang, S. -C.; Li, Y.; Yang, Y. *J. Phys. Chem.* **2000**, *104*, 11650.
- (9) Lupton, J. M.; Craig, M. R.; Meijer, E. W. *Appl. Phys. Lett.* **2002**, *80*, 4489.
- (10) Wu, C. -C.; Liu, T. -L.; Hung, W. -Y.; Lin, Y. -T.; Wong, K. -T.; Chen, R. -T; Chen, Y. -M.; Chien, Y. -Y. *J. Am. Chem. Soc.* **2003**, *125*, 3710.
- (11) Faulkner, L. R.; Bard, A. J. In *Electroanalytical Chemistry*; Bard, A. J., Ed; Marcel Dekker: New York, 1977; Vol. 10, p 1-95.
- (12) Noffsinger, J. B.; Danielson, N. D. *Anal. Chem.* **1987**, *59*, 865.
- (13) Leland, J. K.; Powell, M. J. *J. Electrochem. Soc.* **1990**, *137*, 3127.
- (14) Zu, Y.; Bard, A. J. *Anal. Chem.* **2000**, *72*, 3223.
- (15) Kanoufi, F.; Zu, Y.; Bard, A. J. *J. Phys. Chem. B* **2001**, *105*, 210.
- (16) Miao, W.; Choi, J. -P.; Bard, A. J. *J. Am. Chem. Soc.* **2002**, *124*, 14478.

- (17) Chang, M. –M.; Saji, T.; Bard, A. J. *J. Am. Chem. Soc.* **1977**, *99*, 5399.
- (18) Rubinstein, I.; Bard, A. J. *J. Am. Chem. Soc.* **1981**, *103*, 512.
- (19) Kanoufi, F.; Bard, A. J. *J. Phys. Chem. B* **1999**, *103*, 10469.
- (20) White, H. S.; Bard, A. J. *J. Am. Chem. Soc.* **1982**, *104*, 6891.
- (21) Becker, W. G.; Seung, H. S.; Bard, A. J. *J. Electroanal. Chem.* **1984**, *167*, 127.
- (22) Fabrizio, E. F.; Prieto, I.; Bard, A. J. *J. Am. Chem. Soc.* **2000**, *122*, 4996.
- (23) Debad, J. D.; Morris, J. C.; Magnus, P.; Bard, A. J. *J. Org. Chem.* **1997**, *62*, 530.
- (24) McCord, P.; Bard, A. J. *J. Electroanal. Chem.* **1991**, *318*, 91.
- (25) Parker, C. A. In *Photoluminescence of Solutions*, Elsevier Publishing Co.: New York, 1968, Chapter 1, p. 38.
- (26) Prieto, I.; Teetsov, J.; Fox, M. A.; Vanden Bout, D. A.; Bard, A. J. *J. Phys. Chem. A* **2001**, *105*, 520.
- (27) Bard, A. J.; Faulkner, L. R. In *Electrochemical Methods*, 2nd Ed., John Wiley & Sons: New York, 2001, Chapter 12, p 476.
- (28) Chandross, E. A.; Sonntag, F. I. *J. Am. Chem. Soc.* **1966**, *88*, 1089.
- (29) Akins, D. L.; Birke, R. L. *Chem. Phys. Lett.* **1974**, *29*, 428.
- (30) Santa Cruz, T. D.; Akins, D. L.; Birke, R. L. *J. Am. Chem. Soc.* **1976**, *98*, 1677.
- (31) Birks, J. B. In *Photophysics of Aromatic Molecules*, Wiley-Interscience:New York, 1970, Chapter 7.
- (32) Bard, A. J.; Park, S. M. In *The Exciplex*; Gordon, M.;Ware, W. R., Eds.; Academic Press: New York, 1975, p. 305.
- (33) Zachariasse, K. In *The Exciplex*; Gordon, M.;Ware, W. R., Eds.; Academic Press: New York, 1975, p. 275.
- (34) Rothe, C.; Monkman, A. *Phys. Rev. B* **2002**, *65*, 073201.
- (35) Wallace, W. L.; Bard, A. J. *J. Phys. Chem.* **1979**, *83*, 1350.

- (36) Tokel-Takvoryan, N. E.; Hemingway, R. E.; Bard, A. J. *J. Am. Chem. Soc.* **1973**, *95*, 6582.
- (37) Taken from  $E_{1/2}$  of  $\text{Ru}(\text{bpy})_3^{2+/3+}$  measured in MeCN:Bz (1:1,v:v)/0.1 M TBAP.

## **Chapter 6**

- (1) Kandegedara, A.; Rorabacher, D. B. *Anal. Chem.* **1999**, *71*, 3140.
- (2) Unpublished Data.

## Vita

Jai-Pil Choi was born in Seoul, Korea, on April 8, 1968 as the first son of Mr. Myoung Hwan Choi and Mrs. Se Ja Moon. He got the B.S. degree in chemistry from Kon-Kuk University in 1992. During the senior year of his undergraduate study, he performed the undergraduate research on *Synthesis of Ferroelectric Liquid Crystals* (Research advisor: Dr. Yong Bae Kim). After trained by R.O.T.C. program during last 2 years of his undergraduate study, he became an intelligence officer of Korean Army. In 1994, he was discharged from the duty of military service as the first lieutenant. He earned the M.S. degree in chemistry from the Wichita State University with a thesis titled *Study on the Electrocatalytic Behavior of Fullerenes* in 1999 (Research advisor: Dr. Francis D'Souza). Then he joined Professor Allen J. Bard's group of the University of Texas at Austin in fall of 1999.

### Publications

1. D'Souza, F.; Choi, J. -P.; Hsieh, Y. Y.; Shriver, K.; Kutner, W. "Electrocatalytic Reduction of  $\alpha,\omega$ -diiodoalkanes,  $I(CH_2)_mI$  ( $m = 1 - 8$ ) by  $C_{60}^{n-}$  ( $n = 1 - 3$ ) Anions in Solution and at the C60 Modified Electrodes." *J. Phys. Chem. B* **1998**, *102*, 212-217.

2. D'Souza, F.; Choi, J. -P.; Kutner, W. "Catalytic Reduction of  $\alpha,\omega$ -dihaloalkane,  $X(CH_2)_mX$  ( $X = Cl, Br, \text{ or } I$  and  $m = 2 - 8$ ), by Electrochemically Generated  $C_{70}^{n-}$  ( $n = 2$  or  $3$ ) in Benzonitrile Solutions." *J. Phys. Chem. B* **1998**, *102*, 4247-4252.
3. D'Souza, F.; Choi, J. -P.; Hsieh, Y. Y.; Shriver, K.; Kutner, W. "Catalytic Reduction of 1,2-Dihaloethanes by Electrochemically Generated  $C_{60}^{n-}$  ( $n = 2$  and  $3$ )." In *Electronic Properties of Novel Materials – Progress in Molecular Nanostructure*; AIP Conference Proceedings 442, American Institute of Physics: College Park, MD, 1998, pp 241-244.
4. D'Souza, F.; Choi, J. -P.; Kutner, W. "Electrocatalytic Reduction of  $\alpha,\omega$ -Dihaloalkanes by  $C_{60}^{n-}$  and  $C_{70}^{n-}$  ( $n = 1$  to  $3$ ) in Benzonitrile Solutions." In *Recent Advances in the Chemistry and Physics of Fullerenes and Related Materials*; Kadish, K. M., Ruoff, R. S., Ed.; The Electrochemical Society Proceedings Series; Pennington, NJ, 1998; Vol. 6, pp 1276-1290.
5. D'Souza, F.; Choi, J. -P.; Kutner, W. "Electrocatalytic Dehalogenation of 1,2-Dihaloethanes by the  $C_{60}$ ,  $C_{70}$ ,  $C_{76}$ ,  $C_{78}$ , and  $C_{84}$  Fullerene Anions: Structure-Reactivity Aspects." *J. Phys. Chem. B* **1999**, *103*, 2892-2896.
6. D'Souza, F.; Deviprasad, G. R.; Rahman, M. S.; Choi, J. -P. "Self-Assembled Porphyrin- $C_{60}$  and Porphycene- $C_{60}$  Complexes via Metal Axial Coordination." *Inorg. Chem.* **1999**, *38*, 2157-2160.
7. Ford, W. T.; Nishioka, T.; Qiu, F.; D'Souza, F.; Choi, J. -P.; Kutner, W. "Structure Determination and Electrochemistry of Products from the Radical Reaction of  $C_{60}$  with Azo(bisisobutyronitrile)." *J. Org. Chem.* **1999**, *64*, 6257-6262.
8. D'Souza, F.; Choi, J. -P.; Kutner, W. "Electrocatalytic Properties of the  $C_{60}$ ,  $C_{70}$ ,  $C_{76}$ ,  $C_{78}$ , and  $C_{84}$  Fullerene Anions." In *Electronic Properties of Novel Materials – Progress in Molecular Nanostructure*; AIP Conference

Proceedings 486, American Institute of Physics: College Park, MD, 1999, pp 452-455.

9. Ford, W. T.; Nishioka, T.; Qiu, F.; D'Souza, F.; Choi, J. -P.; Kutner, W. "Electrochemistry of Adducts of 2-Cyano-2-propyl Radicals to C<sub>60</sub>." In *Recent Advances in the Chemistry and Physics of Fullerenes and Related Materials*; Kamat, P. V.; Guldi, D. M., and Kadish, K. M., Eds. The Electrochemical Society Proceedings Series; Pennington, NJ, 1999; Vol. 7, pp 71.
10. Ford, W. T.; Nishioka, T.; Qiu, F.; D'Souza, F.; Choi, J. -P. "Dimethyl Azo(bisisobutyrate) and C<sub>60</sub> Produce 1,4- and 1,16-Di(2-carbomethoxy-2-propyl)-1,x-dihydro[60]fullerenes." *J. Org. Chem.* **2000**, *65*, 5780-5784.
11. Miao, W.; Choi, J. -P.; Bard, A. J. "Electrogenerated Chemiluminescence 69. The Tris(2,2'-bipyridine)ruthenium(II), (Ru(bpy)<sub>3</sub><sup>2+</sup>)/Tri-*n*-propylamine (TPrA) System Revisited. A New Route Involving TPrA<sup>•+</sup> Cation Radicals. *J. Am. Chem. Soc.* **2002**, *124*, 14478-14485.
12. Choi, J. -P.; Ozer, S.; Fungo, F.; Jenekhe, S. A.; Bard, A. J. "Electrochromic Devices Based on Polymer Films. Electrochemical Characterization and Devices of Benzimidazolebenzophenanthroline (BBL and BBB) and 3,7-[bis(4-phenylquinoline)]10-methylphenothiazine (PPTZPQ) polymers. *Polymer Preprints* **2002**, *43*(1), 40.
13. Choi, J. -P.; Miao, W. In *Electrogenerated Chemiluminescence*. Bard, A. J., Ed. Marcel Dekker: New York, Chapter 5, In press.
14. Choi, J. -P.; Bard, A. J.; Wong, K. "Electrogenerated Chemiluminescence of Ter(9,9-diarylfuorene)s: Excited Singlet Emission vs. Triplet State Emission." Submitted to JPC.
15. Choi, J. -P.; Bard, A. J. "Electrogenerated Chemiluminescence 70. Structure and Reactivity Effects of Various Amine Coreactants and Coreactive Buffers on the Electrogenerated Chemiluminescence of Tris(2,2'-

bipyridine)ruthenium(II) Complex,  $\text{Ru}(\text{bpy})_3^{2+}$ , in Aqueous Media. In preparation for publication.

16. Choi, J. -P.; Bard, A. J. "Electrogenerated Chemiluminescence of Tris(2,2'-bipyridine)ruthenium(II),  $\text{Ru}(\text{bpy})_3^{2+}$ , Using  $\text{H}_2\text{O}_2$  Coreactant." In preparation for publication.
17. Choi, J. -P.; Bard, A. J. "Photophysical Properties, Electrochemistry, and Electrogenerated Chemiluminescence of Neutral Red." In preparation for publication.

### **Presentations**

1. Choi, J. -P.; D'Souza, F.; Kutner, W. "Electrocatalytic Behavior of Fullerenes: Structure-Reactivity Aspects." *33rd ACS Midwest Regional Meeting*, Wichita, KS, November, (1998).
2. Choi, J. -P.; Miao, W.; Bard, A. J. "Electrogenerated Chemiluminescence of  $\text{Ru}(\text{bpy})_3^{2+}$  with a Series of Amine Coreactants." *58th ACS Southwest Regional Meeting*, Austin, TX, November, (2002)

Permanent address: Sun Kyoung APT 1614 – 1001, Sang-dong, Wonmi-gu,  
Buchun-si, Kyoungki-do, Korea

This dissertation was typed by the author.